Title
Understanding the Moonlighting Functions of Glycerol Kinase

Author
Ho, Clark Ki Lok

Publication Date
2015

Peer reviewed|Thesis/dissertation

UNIVERSITY OF CALIFORNIA

Los Angeles

Understanding the Moonlighting Functions of Glycerol Kinase

A dissertation submitted in partial satisfaction of the

requirement for the degree Doctor of Philosophy

in Biomedical Engineering

By

Clark Ki Lok Ho

2015

ABSTRACT OF THE DISSERTATION

Understanding the Moonlighting Functions of Glycerol Kinase

By

Clark Ki Lok Ho

Doctor of Philosophy in Biomedical Engineering

University of California, Los Angeles, 2014

Professor Katrina M. Dipple, Chair

Glycerol kinase (GK in humans, Gyk in mice) is an enzyme that catalyzes the conversion of glycerol to glycerol 3-phosphate, which is an intermediate useful for both glycolysis and lipid synthesis. Like many other enzymes in the same metabolic pathways, GK is a moonlighting protein with abilities to perform many functions unrelated to its phosphorylative properties. Of particular interest, GK is the ATP-stimulated translocation promoter (ASTP) that interacts with glucocorticoid receptor (GR) by assisting the translocation of activated GR complex into the nucleus and promoting the transactivation of GR responsive genes. In this thesis, I investigated the protein-protein interactions of GK/GR and its contribution to the pathogenesis of isolated glycerol kinase deficiency

(GKD), a X-linked inborn error of metabolism due to mutations or deletions of the GK gene.

First of all, we characterized our newly developed *Gyk* liver-specific transgenic mouse strains. Transgenic strains exhibited statistically significant weight gain compared to wild type controls on a high fat diet. Our overall results showed that *Gyk* transgenic mice became obese and were at risk of developing type II diabetes mellitus (T2DM). This data is consistent with the GKD human data, showing alterations in *GK* expression may cause changes in the overall lipid and glucose metabolism in mice.

We sought to develop more study models to facilitate our analysis of GKD pathogenesis. A mathematical model of the insulin signal transduction pathway was engineered for predicting insulin sensitivity in the *Gyk* knock out mice. The model covered all components in the insulin signal transduction pathway and calculated glucose uptake results similar to an actual glucose tolerance test. The model simulations suggested that the knock outs had reduced glucose uptake in response to an insulin stimulation, therefore decreased insulin sensitivity than normal mice.

A new gene targeting technology, called CRISPR/Cas9 recombinase system, was incorporated into our cell culture studies to develop a human *GK* knock out cell line. Preliminary results showed that the knock out cells no longer produced functional GK proteins. Using lentiviral gene transfer, several *GK* mutants, found in individuals with GKD, were made for analysis in cell culture. Initial GKD mutations analyses in cell culture revealed that GKD mutants had reduced mRNA levels of GR direct target genes, also defined as ASTP activity, which suggests that the protein-protein interaction of GK and GR interaction is important for the pathogenesis of iGKD.

We also applied the same strategy to develop site-directed *GK* mutants with variation in its LXXLL motif and demonstrated that the LXXLL motif in GK is critical for the interaction of GK and GR. Similar to the GKD mutants, mutations were generated in the LXXLL functional motif of GK in the knock out cells. While the enzymatic property of GK is unaffected in the LXXLL mutants, the ASTP activities were significantly reduced compared to normal cells. Overall, these experiments demonstrated GK's moonlighting roles are just as critical to the pathogenesis of iGKD as its enzymatic role.

In summary, this thesis examines the role of *GK*'s moonlighting functions in obesity, T2DM, and other phenotypes observed in individuals with GKD. We extensively studied the ASTP activity of GK, specifically the protein-protein interaction of GK and GR. It has become clear that moonlighting functions of GK is just as important as its enzymatic functions in regulating the lipid and carbohydrate metabolism.

The dissertation of Clark Ki Lok Ho is approved.

Harold G. Monbouquette

Esteban Dell'Angelica

Katrina M. Dipple, Committee Chair

University of California, Los Angeles

2015

Table of Contents

List of Tables and Figures

Acknowledgement

I want to take this opportunity to give thanks to everybody who gave me assistance during my graduate school years at UCLA. Special thanks to Dr. Katrina Dipple for all her support and guidance in every meeting in the past five and half years. I also want to thank my committee members, Dr. Harold Monbouquette, Dr. James Liao, and Dr. Esteban Dell'Angelica, for their support and ideas that contributed to my experiments. Thanks to all previous and current Dipple Lab staff members, including Dr. Lilly Parr, Dr. Patrick Wightman, Dr. Carol Brown, Dr. Wan-yin Chan, Johnathan Park, and Amanda Yoon, for providing assistance and creating such a wonderful work environment. I also want to give appreciation to my wonderful undergraduate students, including Anish Badjatiya, Lin Jing, Denisse Barajas, and Binh Pham. I would like to thank the NIH Biotechnology Training Program (T32GM067555) for the support.

I would like to acknowledge Dr.Ganesh Sriram for giving me the opportunity to participate in his mathematical model design project. For the mouse projects, I would like to thank Dr. Zhiqiang Zhou from Dr. Richard Davis lab for his assistance on the NMR experiments and Carmen Volpe from the CHS4V mouse facility for her assistance on the lipid metabolite experiments. I want to thank the UCLA Vector Core for helping me with plasmid designs and cloning experiments. Lastly, I also want to thank Dr. Nam Che from Dr. Jake Lusis lab for introducing me to his CRISPR designs and sharing his expertise in the tissue culture.

VITA

2009	Biomedical Engineering University of California, Davis
2010	Teaching Assistant, CHEM153L Department of Biochemistry University of California, Los Angeles
2011-2013	Research Grant Trainee NIH Biotechnology Training Grant University of California, Los Angeles
2012	Research Internship Genentech, Inc. South San Francisco, California

PUBLICATIONS AND PRESENTATIONS

Publications

1) Grahn et al. Feline mtDNA Control Region Database for Forensic Evidence, Forensic Sci Int Genet.; 5(1):33-42, 2009
2) Stein-Wexler et al. An Interactive Teaching Device Simulating Intussusception Reduction, Pediatr Radiol.; 40(11): 1810–1815, 2010
3) Ho et al. Mice with enhanced Glycerol Kinase Expression have High Risk for Developing Obesity and Type II Diabetes Mellitus (Manuscript In Preparation)
4) Ho et al. Mathematical Modeling of the Insulin Signal Transduction Pathway for Prediction of Insulin Sensitivity from Expression Data, Mol Genet Metab. 114(1):66-72, 2015
5) Ho et al. Insulin Sensitivity predictions in individuals with obesity and type II diabetes mellitus using mathematical model of the insulin signal transduction pathway (Manuscript Under Review)

Poster Presentations

1) Ho, C.K., Badjatiya, A., Dipple, K.M. Glycerol Kinase Transgenic Mice Have Increased Risk for Obesity. Presented at the 63rd Annual Meeting of The American Society of Human Genetics, Boston, MA, October, 2013
2) Ho, C.K., Badjatiya, A., Dipple, K.M. Glycerol Kinase over expression in mouse liver leads to increased fat deposition and obesity. Presented at the International Congress of Inborn Errors of metabolism, Barcelona, Spain, September 2013
3) Ho, C.K., Liao, J.C., Dipple, K.M. Mathematical Modeling of Insulin Signal Transduction Pathway for Prediction of Insulin Sensitivity from Expression Data (Program Number 2238W). Presented at the 62nd Annual Meeting of The American Society of Human Genetics, San Francisco, CA, November 2012

Chapter 1

Introduction

Glycerol Kinase

Glycerol kinase (*GK* in humans, *Gyk* in mice) is a key gene in central carbon and lipid metabolism. The main function of GK is to catalyze the phosphorylation of glycerol to yield glycerol 3-phosphate (G3P) [1]. G3P can be converted to dihydroxyacetone phosphate (DHAP) for glycolysis or gluconeogenesis (Fig 1.1). G3P is also a critical component in making triacylglycerol, or triglyceride, for fat storage. Triglyceride can be hydrolyzed back to glycerol and free fatty acids, which can be recycled back where the conversion to G3P by GK can re-occur.

There are more than six human *GK* genes in the genome, which include two loci on the X chromosome (Xp21.3 and Xq22-q23), three loci on chromosome 4, as well as one on chromosome 1 [1, 2]. Two of the loci on chromosome 4 encode testis-specific *GK*. The loci on chromosomes Xq, 1, and 4 contain no introns. *GK* in the Xp21.3 locus consists of 21 exons. However, alternative splicing of the gene at this particular location can occur, where exon 8A and exon 18 may be spliced out [2, 3]. The different isoforms of *GK* on Xp21.3 have distinct functional properties and subcellular localization in the liver, where GK predominantly exists in humans and mice [4]. The predominant isoform lacks exon 18.

GK is a member of the sugar heat shock 70(HSC70)/actin superfamily of ATPases [5, 6]. In addition to its expression in the liver, GK is also expressed in other tissues and organs in mammals, including adipose tissue, mammary glands, the brain, cardiac and skeletal muscle, and lung tissue [1]. The first crystal structure of GK was performed on *Escherichia coli* (*E. coli*) glycerol kinase [5]. Structural analysis was able to show that *E. coli* GK contains an actin fold made of two alpha/beta domains, flanking

a hinge region that becomes the ATP-binding site. It has been shown that *E. coli* GK can act as both a dimer and tetramer, however, mammalian GK can only act as a dimer [5]. The *E. coli* GK gene is 48% homologous (only 48% overall identity) to human GK [7].

Glycerol Kinase Deficiency

Glycerol kinase deficiency (GKD) is an X-linked inborn error of metabolism due to mutations or deletions of the GK gene on Xp21 [1] . The main features of GKD can be characterized biochemically, which include hyperglycerolemia and hyperglyceroluria. There are two forms of GKD: the complex GKD (cGKD) and the isolated GKD (iGKD) [1]. cGKD is a contiguous gene syndrome involving multiple loci, which includes the *GK* locus, as well as *DAX1* responsible for congenital adrenal hypoplasia congenital (CAH) and *DMD* for Duchenne muscular dystrophy (DMD). The majority of individuals with cGKD have also been diagnosed with AHC and DMD. Some of them only have GKD with AHC, with symptoms corresponding to the affected loci where the mutations are found. For example, a case of brothers with GKD and DMD was reported with progressive muscle weakness but normal adrenal function [1]. In contrast to cGKD, iGKD occurs when mutations or deletions are found only within the *GK* gene. There are two forms of iGKD: the symptomatic (juvenile) form and asymptomatic (adult) form. Interestingly, there are no genotype and phenotype correlations in individuals with iGKD [1]. Family members with the same mutation in the GK gene have different phenotypes, in terms of severity of the disease [8, 9]. For example, an interesting case was observed where only one of the two nonidentical twins with the same nonsense mutation was symptomatic [3]. Moreover, the enzymatic activity of GK between the two subtypes of

iGKD are comparable, implying that there are other factors that contribute to the pathogenesis of iGKD. We hypothesize that many factors, including environmental, multifunctional aspects of the gene, and metabolic fluxes in the crosstalking pathways, can contribute to the severity of the disease. In this dissertation, we will emphasize on the multifunctional aspect, also known as moonlighting functions, of GK.

Mouse Models of GK

A number of *Gyk* mouse strains is available for our GK studies in the laboratory. One of these strains is a *Gyk* knockout (KO) created by Huq et al., using gene targeting techniques [10]. It was produced in attempt to study iGKD in humans, where mutations and deletions are found on the X chromosome. Heterozygous female mice were bred with C57BL/6J males to produce the complete KO male offspring used in our study. Although the heterozygous female have normal blood glycerol and glucose concentrations, the KO males subsequently die at a young age [10, 11]. They are born in normal numbers and sizes, but become growth retarded by day of life 2 and ultimately die on day of life 3-4. It was shown that the KO males have a >80-fold increase in plasma glycerol and a 3-fold increase in free fatty acids compared to the wild type littermates[10]. These mice have significantly lower body weight and smaller brown fat pads when compared to wild type mice of the same age [12]. The cause of death of these mice is unknown but it may be linked to extensive acidosis [13]. A microarray analysis, using brown adipose tissue in a *Gyk* KO males, found genes involved in lipid and carbohydrate metabolism, and insuiln signaling to be altered compared to WT [12].

Since the KO males do not live into adulthood, we have developed an alternative transgenic mouse model overexpressing wild type *Gyk* cDNA without exon 18 specifically in the livers. The transgene was inserted in chromosome 7 within the C57BL/6J contig, between ATP/GTP binding protein-like 1 (*AGBL1*) and neurotrophic tyrosine kinase receptor, type 3 (*NTRK3*) [14]. Both the heterozygous (WT/Tg) and homozygous (Tg/Tg) transgenic mice are confirmed viable. Initial experiments on the founder heterozygous transgenic mice showed a possible trend towards obesity in the transgenic mice, compared to WT [14]. Fascinated by this observation, a diet experiment was designed using these transgenic mice based on the hypothesis that overexpression of *GK* are linked to obesity and type II diabetes mellitus. Additionally, we have also begun the development of a conditional knockout model with *GK* knocked out in the targeted tissues. We anticipate that the conditional knockout mice will avoid the same detrimental complications as the complete knock outs, thereby allowing us to extensively study *Gyk* KO in specific tissues and associate with the pathogenesis of GKD.

Moonlighting Functions of GK

Kinases are known to have many functional properties outside of their regular enzymatic functions [15, 16]. The definition of moonlighting functions for a protein is its ability to perform at least two different functions. These functions can relate to very different functional activities and can occur within or outside of the cell. A list of enzymes and transcription factors have been listed as moonlighting proteins [15]. Many of these enzymes are glycolytic enzymes in the central carbon metabolism, and their moonlighting activities are highly diverse, which includes transcriptional and

translational regulation. Since there is no genotype-phenotype correlation for iGKD, we hypothesized that some moonlighting activities of GK may be one of the important factors contributing to the phenotype of this disorder. Understanding these moonlighting activities will help us further elucidate the pathogenesis of GKD.

One of GK's moonlighting activities, of particular interest in our projects, is the role of GK as a nuclear receptor coactivator. GK was found to be an ATP-stimulated translocation promoter (ASTP) in the liver [17]. As an ASTP protein, it can facilitate the translocation of an activated GR complex to the nucleus, where GR responsive genes are transcribed as a result (Fig 1.2). Also, GK interacts with histones [18] and porins on the outer surface of the outer mitochondrial membrane [19]. We hypothesized that the ASTP activity of GK is the cause of activation of many GR responsive genes, including transcriptional factors for immune response, metabolism and cell development.

Obesity and type II diabetes mellitus (T2DM) are some of the complex traits found in individuals with GKD. Glucose tolerance tests were performed on individuals with GKD, showing that these individuals have impaired glucose tolerance and T2DM [20]. The pathogenesis for these traits are still unclear. We anticipated that understanding ASTP activity and other moonlighting functions will help us explain the role of GK in obesity and type II diabetes mellitus.

Despite the fact that GK is a well studied enzyme in its phosphorylative properties, GK's moonlighting functions are still poorly understood. In this thesis, we investigate the importance of the moonlighting functions, specifically the ASTP activity, and how they contribute to the pathogenesis of GKD.

References

1. Dipple, K.M., Zhang, Y.H., Huang, B.L., McCabe, L.L., Dallongeville, J., Inokuchi, T., Kimura, M., Marx, H.J., Roederer, G.O., Shih, V., Yamaguchi, S., Yoshida, I., McCabe, E.R.(2001). Glycerol kinase deficiency: evidence for complexity in a single gene disorder. Human genetics *109*, 55-62.

2. Sargent, C.A., Young, C., Marsh, S., Ferguson-Smith, M.A., and Affara, N.A. (1994). The glycerol kinase gene family: structure of the Xp gene, and related intronless retroposons. Human molecular genetics *3*, 1317-1324.

3. Sargent, C.A., Kidd, A., Moore, S., Dean, J., Besley, G.T., and Affara, N.A. (2000). Five cases of isolated glycerol kinase deficiency, including two families: failure to find genotype:phenotype correlation. Journal of medical genetics *37*, 434-441.

4. Ohira, R.H., Dipple, K.M., Zhang, Y.H., and McCabe, E.R. (2005). Human and murine glycerol kinase: influence of exon 18 alternative splicing on function. Biochemical and biophysical research communications *331*, 239-246.

5. Hurley, J.H., Faber, H.R., Worthylake, D., Meadow, N.D., Roseman, S., Pettigrew, D.W., and Remington, S.J. (1993). Structure of the regulatory complex of Escherichia coli IIIGlc with glycerol kinase. Science *259*, 673-677.

6. Mao, C., Ozer, Z., Zhou, M., and Uckun, F.M. (1999). X-Ray structure of glycerol kinase complexed with an ATP analog implies a novel mechanism for the ATP-dependent glycerol phosphorylation by glycerol kinase. Biochemical and biophysical research communications *259*, 640-644.

7. Guo, W., Worley, K., Adams, V., Mason, J., Sylvester-Jackson, D., Zhang, Y.H., Towbin, J.A., Fogt, D.D., Madu, S., Wheeler, D.A., *et al.* (1993). Genomic scanning for expressed sequences in Xp21 identifies the glycerol kinase gene. Nature genetics *4*, 367-372.

8. Blomquist, H.K., Dahl, N., Gustafsson, L., Hellerud, C., Holme, E., Holmgren, G., Matsson, L., and von Zweigbergk, M. (1996). Glycerol kinase deficiency in two brothers with and without clinical manifestations. Clinical genetics *50*, 375-379.

9. Sjarif, D.R., Sinke, R.J., Duran, M., Beemer, F.A., Kleijer, W.J., Ploos van Amstel, J.K., and Poll-The, B.T. (1998). Clinical heterogeneity and novel mutations in the glycerol kinase gene in three families with isolated glycerol kinase deficiency. Journal of medical genetics *35*, 650-656.

10. Huq, A.H., Lovell, R.S., Ou, C.N., Beaudet, A.L., and Craigen, W.J. (1997). X-linked glycerol kinase deficiency in the mouse leads to growth retardation, altered fat metabolism, autonomous glucocorticoid secretion and neonatal death. Human molecular genetics *6*, 1803-1809.

11. Kuwada, N., Nagano, K., MacLennan, N., Havens, J., Kumar, M., Dipple, K.M., and McCabe, E.R. (2005). Gene therapy for murine glycerol kinase deficiency: importance of murine ortholog. Biochemical and biophysical research communications *335*, 247-255.

12. Rahib, L., MacLennan, N.K., Horvath, S., Liao, J.C., and Dipple, K.M. (2007). Glycerol kinase deficiency alters expression of genes involved in lipid metabolism, carbohydrate metabolism, and insulin signaling. European journal of human genetics : EJHG *15*, 646-657.

13. MacLennan, N.K., Rahib, L., Shin, C., Fang, Z., Horvath, S., Dean, J., Liao, J.C., McCabe, E.R., and Dipple, K.M. (2006). Targeted disruption of glycerol kinase gene in mice: expression analysis in liver shows alterations in network partners related to glycerol kinase activity. Human molecular genetics *15*, 405-415.

14. Parr, L.(2010), *The role of glycerol kinase in adipogenesis*, in Department of Human Genetics. University of California, Los Angeles: Los Angeles

15. Jeffery, C.J. (1999). Moonlighting proteins. Trends in biochemical sciences *24*, 8-11.

16. Jeffery, C.J. (2009). Moonlighting proteins--an update. Molecular bioSystems *5*, 345-350.

17. Okamoto, K., Isohashi, F., Ueda, K., and Sakamoto, Y. (1989). Properties of an adenosine triphosphate-stimulated factor that enhances the nuclear binding of activated glucocorticoid-receptor complex: binding to histone-agarose. Endocrinology *124*, 675-680.

18. Okamoto, K., Isohashi, F., Horiuchi, M., and Sakamoto, Y. (1984). An ATP-stimulated factor that enhances the nuclear binding of "activated" receptor-glucocorticoid complex. Biochemical and biophysical research communications *121*, 940-945.

19. Ostlund, A.K., Gohring, U., Krause, J., and Brdiczka, D. (1983). The binding of glycerol kinase to the outer membrane of rat liver mitochondria: its importance in metabolic regulation. Biochemical medicine *30*, 231-245.

20. Gaudet, D., Arsenault, S., Perusse, L., Vohl, M.C., St-Pierre, J., Bergeron, J., Despres, J.P., Dewar, K., Daly, M.J., Hudson, T., Rioux, J.D. (2000). Glycerol as a correlate of impaired glucose tolerance: dissection of a complex system by use of a simple genetic trait. American journal of human genetics *66*, 1558-1568.

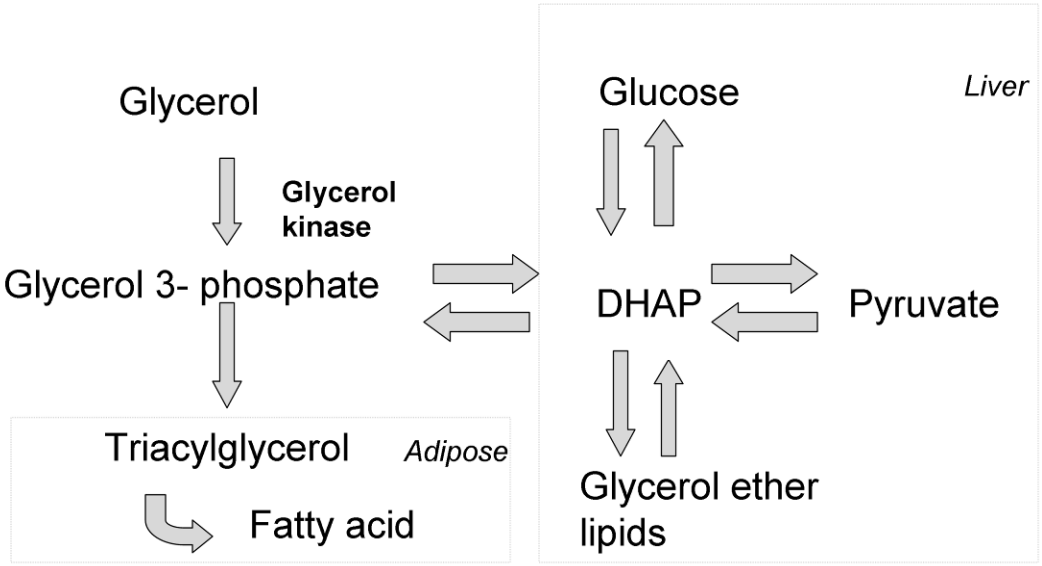

Figure 1.1 Glycerol kinase metabolic pathway

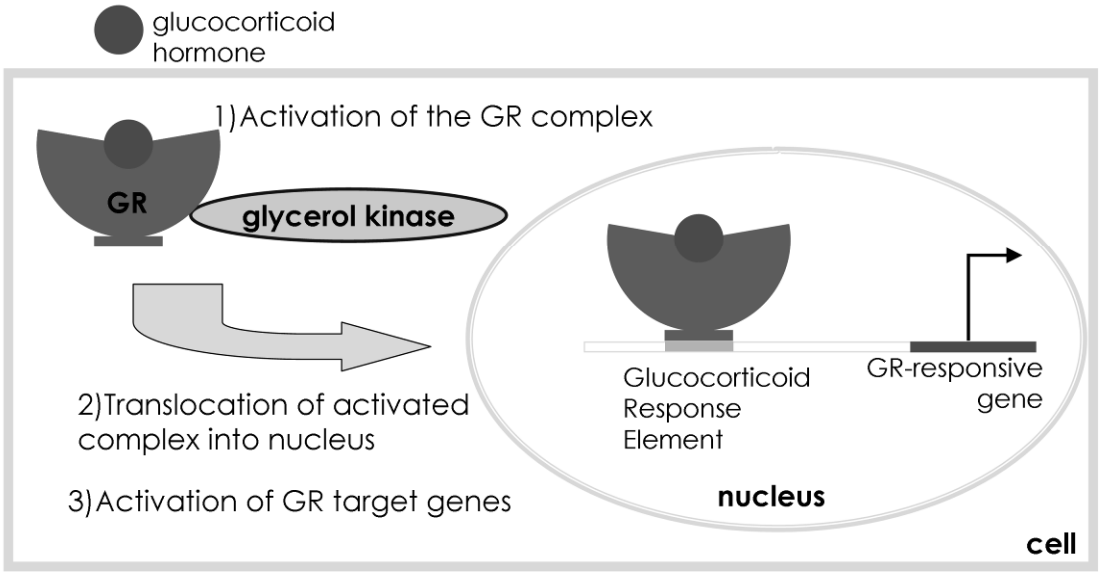

Figure 1.2 The protein-protein interaction of glycerol kinase and the glucocorticoid receptor. An illustration of glucocorticoid receptor (GR)-responsive gene activation as a result of GR complex activation followed by GK-GR complex translocation into the nucleus.

Chapter 2

Characterization of a *Gyk* Liver Specific Transgenic Mouse Model

Abstract

Liver-specific *gyk* transgenic mouse strains were developed in our laboratory to study the alternative functions of GK and examine its role in adipogenesis and obesity. Male wildtype (WT/WT), heterozygous (WT/Tg) and homozygous (Tg/Tg) transgenic mice were placed on regular chow or high fat (HF) diet for 12 weeks and monitored for weight gain and percentage body fat. Fasting glucose and cholesterol levels were measured from plasma of each mouse to assess their risk for obesity and type II diabetes mellitus (T2DM). Nuclear magnetic resonance analysis revealed both wildtype and transgenic mice had at least two-fold increase in percentage body fat as a result of consuming the HF diet. WT/Tg and Tg/Tg mice on HF diet gained more weight than WT/WT mice ($p<0.05$). The elevated body weight in transgenic mice was also validated based on weighing of various tissues, including the mass of liver, visceral fat, perirenal fat and subcutaneous fat pads. Tg/Tg mice on chow diet had significantly greater mass in the liver tissue (25.8%), visceral fat pads (53.3%), and perirenal fat pads (40.2%) compared to the WT/WT mice ($p<0.05$), suggesting that *Gyk* overexpression is associated with abdominal obesity. Blood glucose and cholesterol tests showed that Tg/Tg mice on HF diet had higher triglycerides levels (16.4%), total cholesterol levels (41.3%), and fasting glucose levels (45.4%) relative to WT/WT, also implying high risk for obesity and T2DM ($p<0.05$). mRNA levels of fatty acid oxidation genes were lower in transgenic mice, suggesting that their energy expenditure rate was slowed down, which corresponds with more lipid accumulation in their bodies. This study demonstrates that GK is involved in fat deposition and adipogenesis, and its overexpression increases risk of

obesity and T2DM in mice. In addition, we propose that our *Gyk* transgenic mouse strains may serve as a useful model for obesity and T2DM research.

Introduction

Glycerol kinase (GK in humans, Gyk in mice) is a key enzyme in carbohydrate and lipid metabolism. Previous studies of GK suggested a possible link between GK and obesity/type II diabetes mellitus (T2DM). Gaudet *et al.* performed glucose tolerance tests on 18 individuals with glycerol kinase deficiency (GKD) and many of them met the criteria for either T2DM or impaired glucose tolerance [1]. In addition, a protein-protein interaction between GK and glucocorticoid receptor (GR) was identified by Okamoto *et al*. [2], implying that GK may have an alternative function of leading to transcriptional activation of GR-responsive genes. Some of the direct target genes include insulin-like growth factor binding protein 1(*Igfbp1*) and adipose differentiation related protein (*Adfp*) [3], which play important roles in the development of metabolic disorders such as obesity and T2DM.

Two transgenic mouse strains (heterozygous WT/Tg and homozygous Tg/Tg) were generated to study the effect of *GK* expression on fat deposition. Since *Gyk* is predominantly expressed in liver, our transgenic mouse strains were designed to have enhanced *Gyk* expression specifically in the liver tissue. Previous GK experiments demonstrated that *GK* overexpression alters metabolic fluxes through central carbon metabolism [4]. Also, a mathematical tool, called Network Component Analysis (NCA) that is used to quantitatively predict hidden transcription factor activities, estimated that at least nine transcriptional factors were altered by *GK* overexpression [5, 6]. Unlike the

complete knock out mice, the transgenic mice live into adulthood, allowing for extensive experimental analyses. Preliminary observations of the transgenic mice showed that the transgenic mice became obese naturally as they grew older [7], which led to our hypothesis that *GK* overexpression is associated with increased adiposity. In this particular study, male wild type and transgenic mice were placed on either regular chow or high fat (HF) diet for 12 weeks. We monitored their weekly weight gain, their overall weight gain, and their selected tissue weights. Lipid metabolites in plasma were measured in order to evaluate their risk of developing obesity and T2DM. Quantitative real time PCR analysis (qRT-PCR) was performed using mouse livers and adipose tissues to investigate the adipogenesis and fat accumulation as a result of *Gyk* overexpression. To complement the results from diet studies, we developed a tissue culture model was incorporated by using mouse embryonic fibroblasts (MEFs) from the mouse strains. Mature adipocytes were differentiated from the MEFs and were stained with Oil red O staining to determine the amount of fat storage. Triglyceride content was quantitatively measured in these cells.

Materials and Methods

Generation of the Mouse Strains

Gyk transgenic strains were developed by microinjecting a 1.6kb fragment, corresponding to the *Gyk* cDNA without exon 18, into a B6D2F1/J male pronuclei. The transgenic mice, with *Gyk* overexpression specifically in liver, were created by the UCLA Transgenic Core. Founder mice were screened and their offspring were rederived as generation F0. These mice were backcrossed to the C57BL/6J line to create the inbred

strain. The transgene was inserted in chromosome 7 within the C57BL/6J contig, between the *AGBL1* and *NTRK3* gene. The transgenic mice were obtained by pairing of two heterozygous transgenic mice. Polymerase chain reaction genotyping was done on each mouse to confirm the presence of the transgene [7]. The WT controls used in this study were littermates of heterozygous transgenic mice.

Animal Care

All mice were housed on a 12 hour light/dark cycle. During diet experiment, WT/WT, WT/Tg, and Tg/Tg mice were maintained on either normal chow diet (Harlan-Teklad 7013; 4.07Kcal/g, 24.7% calories from protein, 13.2% from fat, and 62.1% carbohydrate) or a high fat Western diet (Research Diet D12492i; 5.24Kcal/g, 20% calories from protein, 60% from fat, and 20 % carbohydrate) for 12 weeks. All mice in the study started their diet at 6 to 8 weeks of age and were sacrificed by cervical dislocation at the end of the 12^{th} dietary week. Experiments were per our UCLA Chancellor's Animal Research Committee approved protocol.

Body Fat Composition Analysis

At the end of the 12 week diet, prior to euthanasia, mice were measured for total body fat mass and lean mass by nuclear magnetic resonance (NMR) using the Bruker Minispec with software from Echo Medical Systems (Houston, TX) [8]. Body fat composition of each mouse was calculated based on fat mass relative to lean mass.

Plasma Lipid and Metabolic Analysis

Blood plasma samples were collected from mice fasted overnight (at least 8 hours) and bled from the retro-orbital plexus under isoflurane anesthesia. Lipid metabolites enzymatic assays were performed by the UCLA Lipid Core. Total cholesterol, HDL cholesterol, free cholesterol, triglycerides, and FFA concentrations were determined in triplicate as previously described[9, 10]. Serum insulin levels were measured with an ultra-sensitive mouse insulin ELISA kit (Alpco Diagnostics).

Body and Tissue Weight Determination

Body weights of each mouse were recorded weekly. Animals were weighed at the end of the 12^{th} week prior to euthanasia. Liver and adipose tissues (e.g. visceral fat, perirenal fat, and subcutaneous fat) were collected, weighed, and stored at -80°C).

MEF Isolation and Cell Culture

Primary MEFs were isolated from 14-day post coitus embryos of transgenic and WT *Gyk* mice. Female mice were first sacrificed by cervical dislocation before embryos were surgically removed. The bodies were minced finely and incubated in 0.25% trypsin solution in a shaking 37°C incubator for 60 minutes. The solution was centrifuged aftere the incubation for 3 minutes at 1000 x g. The supernatant was decanted and pellet was resuspended in DMEM in 10 % FBS. Cells were mained for at least 2 passages before used for cell differentiation into adipocytes.

Adipocyte differentation were performed by incubating MEFs cells with DMEM growth medium supplemented with PPARγ ligand, rosiglitazone. Media was removed

after 2 days and was replaced with DMEM containing 10% FBS with insulin and rosiglitazone [7]. Cells were harvested on day 6 where they were either re-plated on a 6-well plate for Oil Red O staining, or homogenized for triglyceride determination.

Oil Red O Staining

Cells were grown to confluence on a 6 well plate and fixed with 4% paraformaldehyde or 10% formalin, and stained with 0.7% Oil Red O solution (Sigma, St. Louis, MO). Staining was quantified by extracting the dye with isopropanol and measured by absorbances at 510nm [7]. Absorbances were normalized to total cell number in each well.

Triglyceride Assay

Cells were homogenized in buffer containing 10mM Tris-HCL, 1mM EDTA, 10mM NaCl, and 0.5% Triton X-100. Supernatant was collected and used in an L-Type Triglyceride M assay (Wako Diagnostics, Richmond, VA), per manufacturer's instructions. Cellular triglyceride levels were normalized to total protein content in the sample.

RNA Isolation and cDNA Synthesis

Total RNA was isolated from cell lines using the GeneJET RNA purification kit (Thermo Scientific, Pittsburgh, PA) per manufacturer's instructions. RNA was further purified using Turbo DNA-free DNase treatment (Life Technologies, Grand Island, NY). Purified RNA was visualized on agarose gel and its concentration was quantified using a

NanoDrop specctrophotometer (NanoDrop Technologies, Wilmington, DE). cDNA was synthesized using Superscript III First-Strand systems (Life Technologies, Grand Island, NY) per manufacturer's instructions with random hexamers primers. cDNA samples were diluted to an optimized concentration of 1ng/uL.

Quantitative Real Time PCR (qRT-PCR)

All assays were carried out using PerfeCTa SYBR Green FastMix (Quanta Biosciences, Gaithersburg, MD) with QuantiTect (Qiagen, Valencia, CA) primer assays. Cells were treated with 100nM dexamethasone [11] for 24 hours, after which RNA was isolated. Genes assayed included acyl-CoA oxidase 1 (*AOX1*), Carnitine palmitoyltransferase 1 (*Cpt1a*), fatty acid binding protein 4 (*Fabp4*), PR domain containing 16 (*Prdm16*), uncoupled protein 1 (*UCP1*), Peroxisome proliferator-activated receptor gamma (*PPAR gamma*), peroxisome proliferator-activated receptor gamma, coactivator 1 alpha (*PGC1-alpha*). Primer pairs for real-time PCR were designed using the mouse primer depot database (http://mouseprimerdepot.nci.nih.gov/). 1ng of cDNA was loaded into each reaction, which was detected using ABI prism 7500 Sequence detection system. Each sample was assayed in duplicate and each reaction was replicated as least once. Fold differences for each of the genes were determined using the $2^{(-\text{Delta Delta CT})}$ method [12].

Statistical Analysis

Power calculation analysis (PASS12 software, NCSS statistical software) was employed to estimate the sample size needed for each experimental group [13]. All values were presented as mean ± SEM. A two-tailed Student's t test was used to calculate p values for all assays.

Results

Enhanced glycerol kinase expression in liver tissue leads to increased fat deposition

To investigate the role of GK in fat deposition, male transgenic mice (both homozygous and heterozygous transgenics; n=10 for each group) were placed on either a chow or HF diet for 12 weeks. The effect of feeding HF diet to these mice was pronounced, demonstrated by the overall weight gain in all mice on HF diet (24.26-26.23 g) compared to mice on chow diet (9.2-10.0 g) (Fig.2.1A and B). All mice consistently gained weight throughout the diet study.

On a chow diet, the WT/Tg showed a slightly higher weight gain (49.3%) as a result of the 12 weeks diet, compared to WT controls (43.5%). When fed on a HF diet, both WT/Tg and Tg/Tg showed accelerated weight gain by increasing their body weight by 136.9% and 151.8%, respectively, since the start of diet. On the other hand, WT mice on high fat diet only gained 112% body weight due to the HF diet. The overall weight gain of our transgenic strains was quantified at the end of the experiment, showing that WT/Tg and Tg/Tg had a significantly greater weight gain relative to wild types (13% and 2%, respectively) on chow diet and (22% and 35%, respectively) on HF diet (Fig.2.1C and D).

Increased liver and abdominal fat mass observed in the *Gyk* transgenic mice

The evidence of increased overall weight in the *Gyk* transgenic mice was supported by their greater body fat percentage (Fig. 2.2A). To address where the fat was stored due to *Gyk* over expression in liver, the liver and the white fat pads (e.g. visceral, perirenal, subcutaneous fat tissues) were collected and weighed(Fig. 2.2B). There was statistical difference between the WT/Tg and Tg/Tg when we compared the liver, visceral fat, and subcutaneous fat. The tissue weight was normalized to the total body weight. Tg/Tg and WT/Tg had more fat accumulation in the abdominal region (Fig. 2.2C). The appearance of the liver in the transgenic mice looked more bright and fatty, suggesting these mice had developed hepatic steatosis and possibly other defects in fatty acid metabolism. To confirm whether the increased liver mass was due to fat deposition, triglyceride assays were performed on liver. Results confirmed that triglyceride levels of the transgenic mice were increased by two-fold compared to the WT controls (Fig. 2.2D). Adipogenic markers, including *Fabp4*, *Prdm16*, and *UCP1*, were overexpressed in the adipose tissues of the transgenic mice compared to WT/WT, on the HF diet (Fig 2.3). Two adipogenic genes upstream of *Gyk*, *PPAR(gamma)* and *PGC1-(alpha)*, were not overexpressed in the WT/Tg, and Tg/Tg.

Instead of expending the excess fat content into energy, the transgenic mice seemed to be storing them primarily in the abdominal region. To demonstrate whether fatty acid oxidation is affected in transgenic mice, qRT-PCR analysis was done on mRNA from livers for fatty acid oxidation direct target genes, including acyl-CoA oxidase 1 (*AOX1*) and Carnitine palmitoyltransferase 1 (*Cpt1a*). The qRT-PCR results showed that these genes were under-expressed in the transgenic mice compared to

wildtype, which was consistent for both diets (Fig. 2.4A and B). On the high fat diet, *AOX1* expression is also down-regulated by 1.6-fold in the WT/Tg and 2.2-fold in the Tg/Tg. *Cpt1a* expression is down-regulated by 1.6-fold in the WT/Tg and 2.4-fold in the Tg/Tg.

Quantitative Plasma Analysis Suggested Increased Risk in Type II Diabetes Mellitus in *Gyk* Transgenic Mice

To explore the effect of *Gyk* overexpression on metabolites, plasma was purified from each mouse at the end of the diet experiment. Plasma metabolites, including triglyceride, cholesterol, free fatty acids, fasting glucose, and insulin, were compared among the study groups. Our results showed that the WT/Tg and Tg/Tg had higher lipid and glucose profiles on both diet, with more significant differences when they were on HF diet (Table 2.1). For example, both WT/Tg and Tg/Tg had evidently higher total cholesterol levels (43.5% and 41.3%, respectively) compared to the wild type. They also had elevated fasting glucose (72.0% and 45.4%, respectively) and insulin levels (49.5% and 456%, respectively). These results not only demonstrated that *Gyk* overexpression led to elevated metabolites levels in plasma, it also suggested that the transgenic strains were more likely to develop obesity and T2DM.

Cell Culture Experiments Confirmed Greater Adiposity in Transgenic Mature Adipocytes

MEFs from Tg/Tg mice were isolated and differentiated into mature adipocytes. The cells were fixed and stained with Oil Red O dye, allowing the visualization of

triglycerides and other lipid content. The amount of lipid content was quantified by a spectrophotometer based on the intensity of the red stains. The adipocytes from Tg/Tg contained greater lipid content than normal cells (Fig.2.5). Triglyceride testing results of these adipocytes and the liver samples collected from mice in the diet study were consistent to other assessments, showing that the Tg/Tg had greater lipid content than normal mice (Fig.2.6). Overall, this diet study shows that liver specific *Gyk* leads to increased weight gain, increased fat storage and increased triglyceride and low fasting blood sugar, which increase their risk of developing obesity and T2DM.

Discussion

We studied the effect of liver specific *Gyk* overexpression in mouse using our new transgenic mouse model. Although *Gyk* KO mice may serve as more suitable model for GKD pathogenesis studies, our KO mice do not live long enough and therefore not suitable for long-term diet experiment. The *Gyk* KO mice become growth retarded by the day of life (dol) two and die of extensive acidosis by dol three[14]. Initial experiments on the heterozygous transgenic mice, using qRT-PCR, showed an approximately 1.4-fold increase in *Gyk* expression in the Tg/Tg mouse liver and 1.3 fold increase in *Gyk* expression in the WT/Tg mouse liver [7].

The diet experiment showed that the transgenic mice became obese and were at risk of developing T2DM. The *Gyk* transgenic mice gained more weight and stored more fat compared to the WT controls. We observed significant differences in adipose tissue masses in the abdomenal region as a result of differential expression of adipogenic genes of liver and adipose, which suggested that the abnormal expression levels in *Gyk* in liver tissue cause changes in the overall lipid and glucose metabolism in mice. The quantitative

assays, including triglyceride and blood tests, also showed that the transgenic mice had higher cholesterol and fasting blood glucose levels, supporting our claims that they were at higher risk of developing obesity and T2DM. We observed in many instances that there were significant differences in the results between the homozygous and heterozygous transgenic mice, suggesting that an extra transgenic allele, or extra doses of *Gyk*, leads to significant overall differences in lipid and carbohydrate metabolism. To further our analysis on the association of GK and obesity and T2DM, it may be interesting to investigate its effect on other related tissues, such as cardiac and skeletal muscle tissues.

A major cause of obesity is an energy imbalance between intake and expenditure. The outcome of the energy imbalance leads to accumulation of excess lipid deposits. Fatty acid oxidation (FAO) and energy imbalance towards obesity are closely associated. Short-term genetic studies that increased FAO in liver showed reduction in hepatic triacylglyceride levels [15] and insulin resistance in obese rodents [16, 17]. Based on their appearance of fatty livers and their elevated weight gain in surrounding adipose tissues, we expected that the *Gyk* transgenic mice also exhibit signs of energy imbalance. Since FAO is one of the main mechanisms that would explain the particular phenotypes observed in our mice, we studied the expression of direct target genes in FAO. *Cpt1a*, and *AOX1* are the rate-limiting steps in fatty-acid β-oxidation that would provide good indication of energy imbalance in our transgenic mice. Quantitative RT-PCR results confirmed that both strains of transgenic mice have reduced FAO activity in liver. This data also correlates with our blood metabolite results, for example the elevated triglyceride and cholesterol levels of our transgenic strains on HF diet. It is a consistent

with the appearance of hepatic steatosis observed in the transgenic liver. Results suggested that FAO activity is impeded in the liver, leading to accumulation of metabolites. It is likely that the transgenic mice are struggled to expend the energy provided from high fat diet, leading to lipid accumulation in abdominal tissues and high risk for insulin resistance.

In summary, our transgenic mice were characterized with a series of experiments following their dietary conditioning. The transgenic mice have elevated weight gain, due to increased fat deposition in both liver and adipose tissues, compared to control mice. Increased triglyceride levels and increased fasting blood glucose levels were observed in the transgenic mice, confirming our hypothesis that *Gyk* is associated with obesity and T2DM.

References

1. Gaudet, D., Arsenault, S., Perusse, L., Vohl, M.C., St-Pierre, J., Bergeron, J., Despres, J.P., Dewar, K., Daly, M.J., Hudson, T. Rioux, J.D. (2000). Glycerol as a correlate of impaired glucose tolerance: dissection of a complex system by use of a simple genetic trait. American Journal of Human Genetics *66*, 1558-1568.

2. Okamoto, K., Isohashi, F., Horiuchi, M., and Sakamoto, Y. (1984). An ATP-stimulated factor that enhances the nuclear binding of "activated" receptor-glucocorticoid complex. Biochemical and Biophysical Research Communications *121*, 940-945.

3. Le, P.P., Friedman, J.R., Schug, J., Brestelli, J.E., Parker, J.B., Bochkis, I.M., and Kaestner, K.H. (2005). Glucocorticoid receptor-dependent gene regulatory networks. PLoS Genetics *1*, 159-170.

4. Sriram, G., Rahib, L., He, J.S., Campos, A.E., Parr, L.S., Liao, J.C., and Dipple, K.M. (2008). Global metabolic effects of glycerol kinase overexpression in rat hepatoma cells. Molecular Genetics and Metabolism *93*, 145-159.

5. Galbraith, S.J., Tran, L.M., and Liao, J.C. (2006). Transcriptome network component analysis with limited microarray data. Bioinformatics *22*, 1886-1894.

6. Liao, J.C., Boscolo, R., Yang, Y.L., Tran, L.M., Sabatti, C., and Roychowdhury, V.P. (2003). Network component analysis: Reconstruction of regulatory signals in biological systems. Proceedings of the National Academy of Sciences of the United States of America *100*, 15522-15527.

7. Parr, L. (2010). The role of glycerol kinase in adipogenesis, in Department of Human Genetics. 2010, University of California, Los Angeles: Los Angeles

8. Taicher, G.Z., Tinsley, F.C., Reiderman, A., and Heiman, M.L. (2003). Quantitative magnetic resonance (QMR) method for bone and whole-body-composition analysis. Analytical and Bioanalytical Chemistry *377*, 990-1002.

9. Davis, R.C., van Nas, A., Castellani, L.W., Zhao, Y., Zhou, Z., Wen, P., Yu, S., Qi, H., Rosales, M., Schadt, E.E., Broman, K.W. Peterfy, M., Lusis, A.J. (2012). Systems genetics of susceptibility to obesity-induced diabetes in mice. Physiological Genomics *44*, 1-13.

10. Hedrick, C.C., Castellani, L.W., Warden, C.H., Puppione, D.L., and Lusis, A.J. (1993). Influence of mouse apolipoprotein A-II on plasma lipoproteins in transgenic mice. The Journal of Biological Chemistry *268*, 20676-20682.

11. Rubin, C.T., Capilla, E., Luu, Y.K., Busa, B., Crawford, H., Nolan, D.J., Mittal, V., Rosen, C.J., Pessin, J.E., and Judex, S. (2007). Adipogenesis is inhibited by brief, daily exposure to high-frequency, extremely low-magnitude mechanical

signals. Proceedings of the National Academy of Sciences of the United States of America *104*, 17879-17884.

12. Livak, K.J., and Schmittgen, T.D. (2001). Analysis of relative gene expression data using real-time quantitative PCR and the 2(-Delta Delta C(T)) Method. Methods *25*, 402-408.

13. Zhou, X., Obuchowski, N., McClish, D (2002). *Statistical Methods in Diagnostic Medicine*. John Wiley & Sons, Inc. New York, New York.

14. Huq, A.H., Lovell, R.S., Ou, C.N., Beaudet, A.L., and Craigen, W.J. (1997). X-linked glycerol kinase deficiency in the mouse leads to growth retardation, altered fat metabolism, autonomous glucocorticoid secretion and neonatal death. Human Molecular Genetics *6*, 1803-1809.

15. Stefanovic-Racic, M., Perdomo, G., Mantell, B.S., Sipula, I.J., Brown, N.F., and O'Doherty, R.M. (2008). A moderate increase in carnitine palmitoyltransferase 1a activity is sufficient to substantially reduce hepatic triglyceride levels. American Journal of Physiology Endocrinology and Metabolism *294*, E969-977.

16. An, J., Muoio, D.M., Shiota, M., Fujimoto, Y., Cline, G.W., Shulman, G.I., Koves, T.R., Stevens, R., Millington, D., and Newgard, C.B. (2004). Hepatic expression of malonyl-CoA decarboxylase reverses muscle, liver and whole-animal insulin resistance. Nature Medicine *10*, 268-274.

17. Savage, D.B., Choi, C.S., Samuel, V.T., Liu, Z.X., Zhang, D.Y., Wang, A., Zhang, X.M., Cline, G.W., Yu, X.X., Geisler, J.G., Bhanot, S., Monia, B.P., Shulman, G.I. (2006). Reversal of diet-induced hepatic steatosis and hepatic insulin resistance by antisense oligonucleotide inhibitors of acetyl-CoA carboxylases 1 and 2. Journal of Clinical Investigation *116*, 817-824.

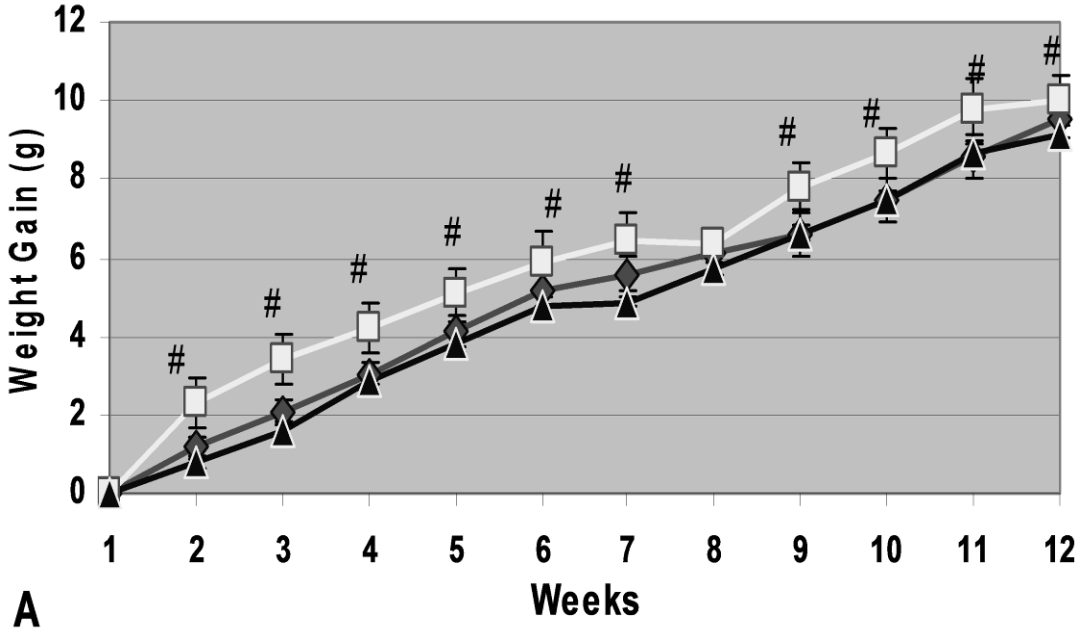

Figure 2.1A Weight gain of male mice on a 12-week diet

Weekly weight gain of male mice (n=10 for each category) on chow diet. ♦ data point represents wildtype (WT/WT), □ data points represent heterozygous transgenic (WT/Tg), and▲ data points represent homozygous transgenic (Tg/Tg). Bars represent mean ± SEM. * represent $p<0.05$ for both Tg/Tg & Tg compared to WT. # represent $p<0.05$ for only WT/Tg compared to WT.

Author Contribution: Weekly weights were done by DLAM staff. Clark Ho (C.H,) received the data from them and did all the analysis and the statistics.

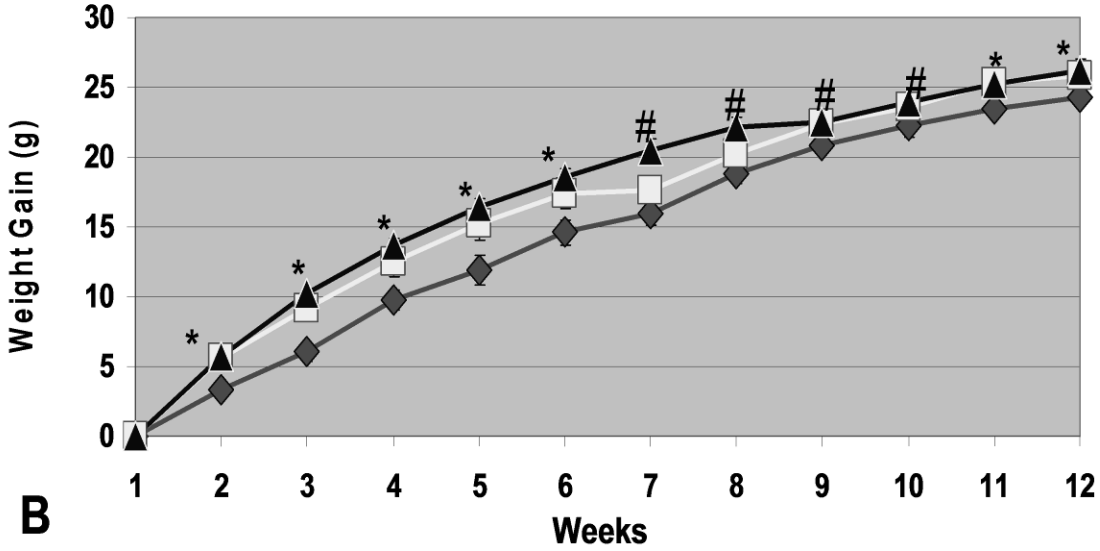

Figure 2.1B Weight gain of male mice on a 12-week diet

Weight gain of male mice (n=10 for each category) on high fat diet. ♦ data point represents wild type (WT/WT), □ data points represent heterozygous transgenic (WT/Tg), and▲ data points represent homozygous transgenic (Tg/Tg). Bars represent mean ± SEM. * represent $p<0.05$ for both Tg/Tg & WT/Tg vs WT. # represent $p<0.05$ for only Tg/Tg compared to WT/WT.

Author Contribution: Weekly weights were done by DLAM staff. C.H. received the data from them and did all the analysis and the statistics.

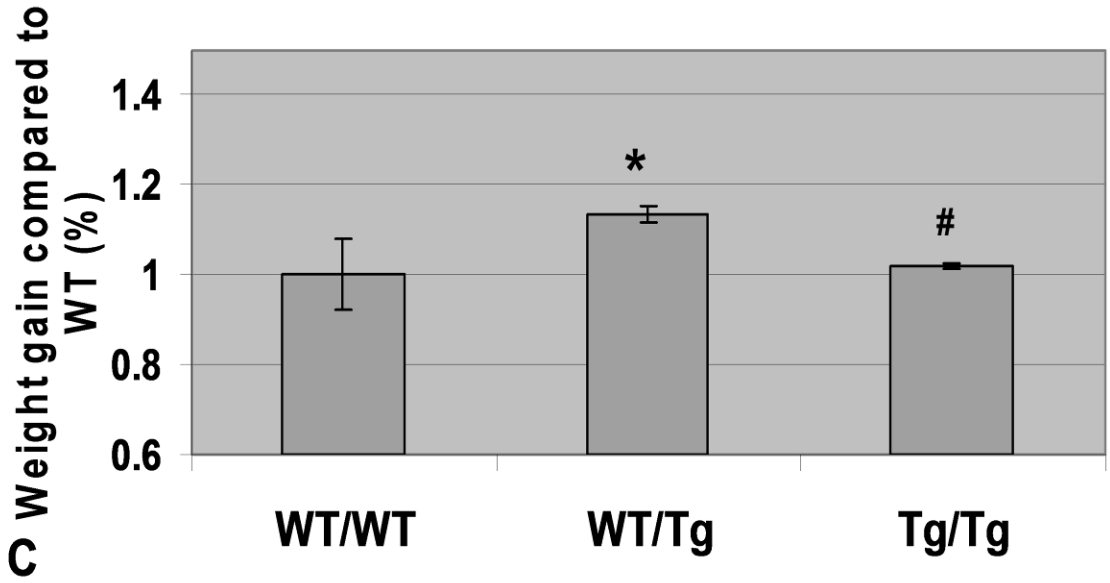

Figure 2.1C Weight gain of male mice on a 12-week diet

Overall weight gain at the conclusion of the 12 week chow diet, normalized to wild type. Bars represent mean ± SEM. * represent $p<0.05$ compared to WT. # represent $p<0.05$ for Tg/Tg vs WT/Tg

Author Contribution: Weekly weights were done by DLAM staff. C.H. received the data from them and did all the analysis and the statistics.

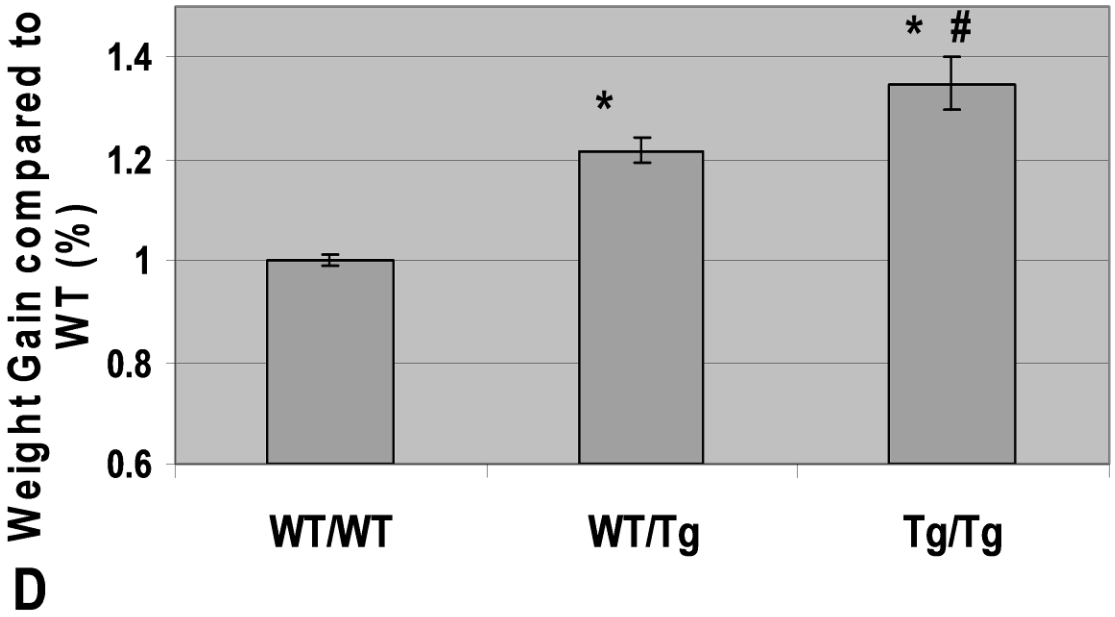

Figure 2.1D Weight gain of male mice on a 12-week diet

Overall weight gain at the conclusion of the 12 week on high fat diet, normalized to wild type. Bars represent mean ± SEM. * represent $p<0.05$ compared to WT. # represent $p<0.05$ for Tg/Tg vs WT/Tg

Author Contribution: Weekly weights were done by DLAM staff. C.H. received the data from them and did all the analysis and the statistics.

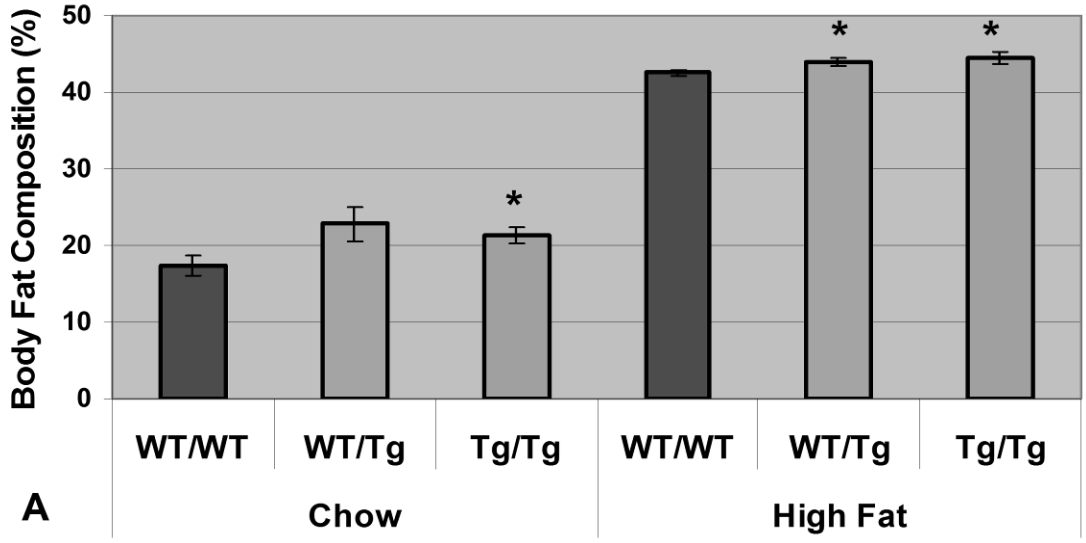

Figure 2.2A Body fat and tissue weight comparison

Percent body fat as determined by Nuclear Magnetic Resonance. Chow diet on the left panel and high fat diet on the right panel. Bars represent mean ± SEM. * represent $p<0.05$ compared to WT/WT in their respective diets.

Author Contribution for Figure 2.2: C.H. performed NMR analysis, anesthesized the animals, disserted the tissues and analyzed the data. Zhiqiang Zhou helped with the NMR experiments while Johnathan Park (technician) and Anish Badjatiya (undergraduate studdent) helped with weighing and freezing tissues.

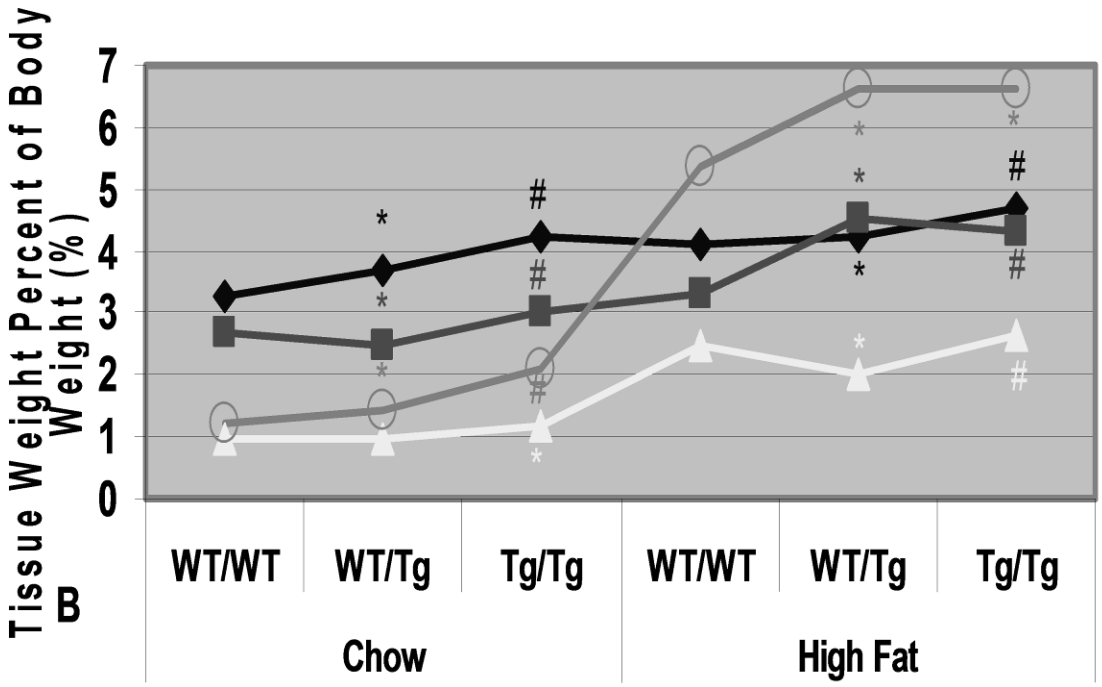

Figure 2.2B Body fat and tissue weight comparison

Tissue weight comparison between all diet groups. Chow diet on the left panel and high fat diet on the right panel. ♦ data points represent liver weights, ■ data points represent visceral fat pad weights, and Δ data points represent perirenal fat pad weights. ○ represent subcutaneous fat pad weights. * represent $p<0.05$ compared to WT/WT in their respective diets. # represent $p<0.05$ WT/Tg vs Tg/Tg.

Author Contribution for Figure 2.2: C.H. performed NMR analysis, anesthesized the animals, disserted the tissues and analyzed the data. Zhiqiang Zhou helped with the NMR experiments while Johnathan Park (technician) and Anish Badjatiya (undergraduate studdent) helped with weighing and freezing tissues.

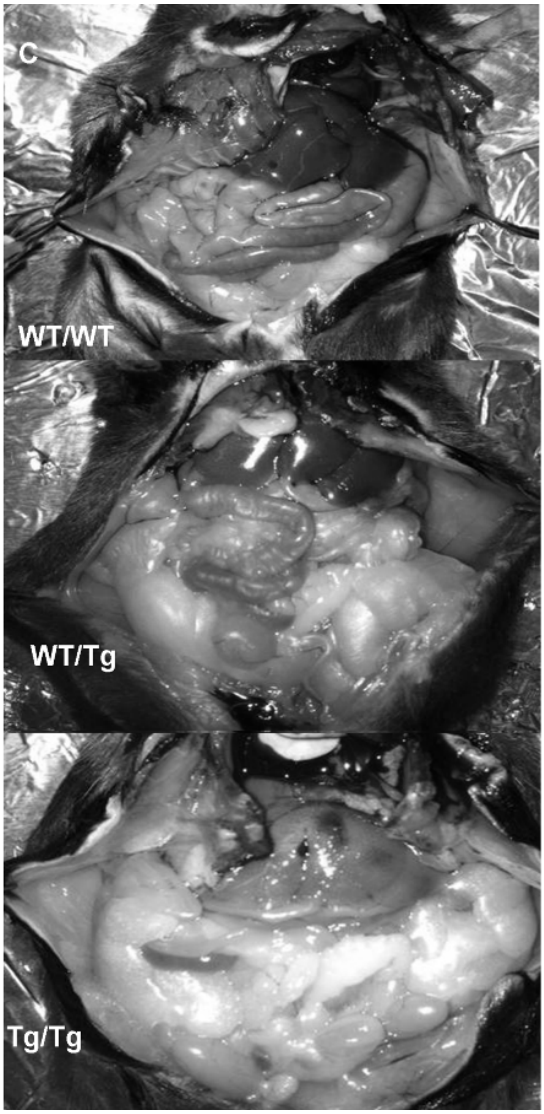

Figure 2.2C Body fat and tissue weight comparison

Visualization of the abdominal cavity of wild type (top), heterozygous transgenic (middle), and homozygous transgenic (bottom) mice

Author Contribution for Figure 2.2: C.H. performed NMR analysis, anesthesized the animals, disserted the tissues and analyzed the data. Zhiqiang Zhou helped with the NMR experiments while Johnathan Park (technician) and Anish Badjatiya (undergraduate studdent) helped with weighing and freezing tissues.

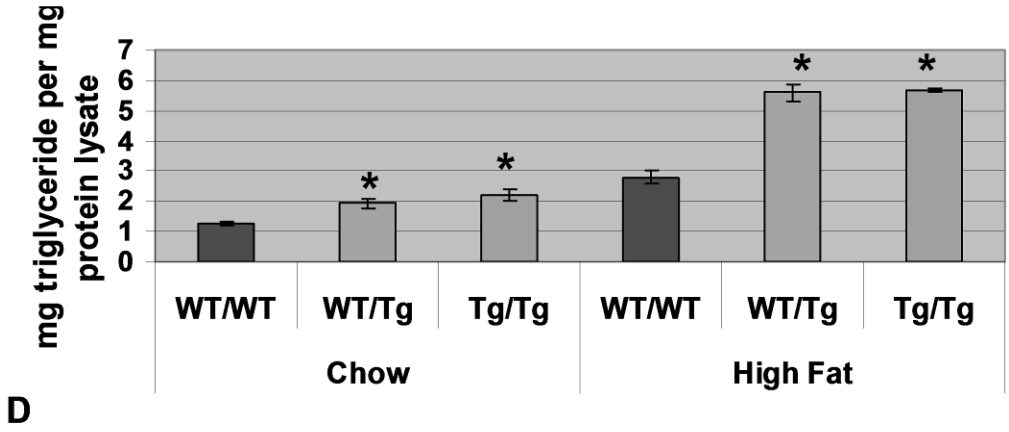

Figure 2.2D Body fat and tissue weight comparison

Liver triglyceride levels. * represent $p<0.05$ compared to WT in their respective diets.

Author Contribution for Figure 2.2: C.H. performed NMR analysis, anesthesized the animals, disserted the tissues and analyzed the data. Zhiqiang Zhou helped with the NMR experiments while Johnathan Park (technician) and Anish Badjatiya (undergraduate studdent) helped with weighing and freezing tissues.

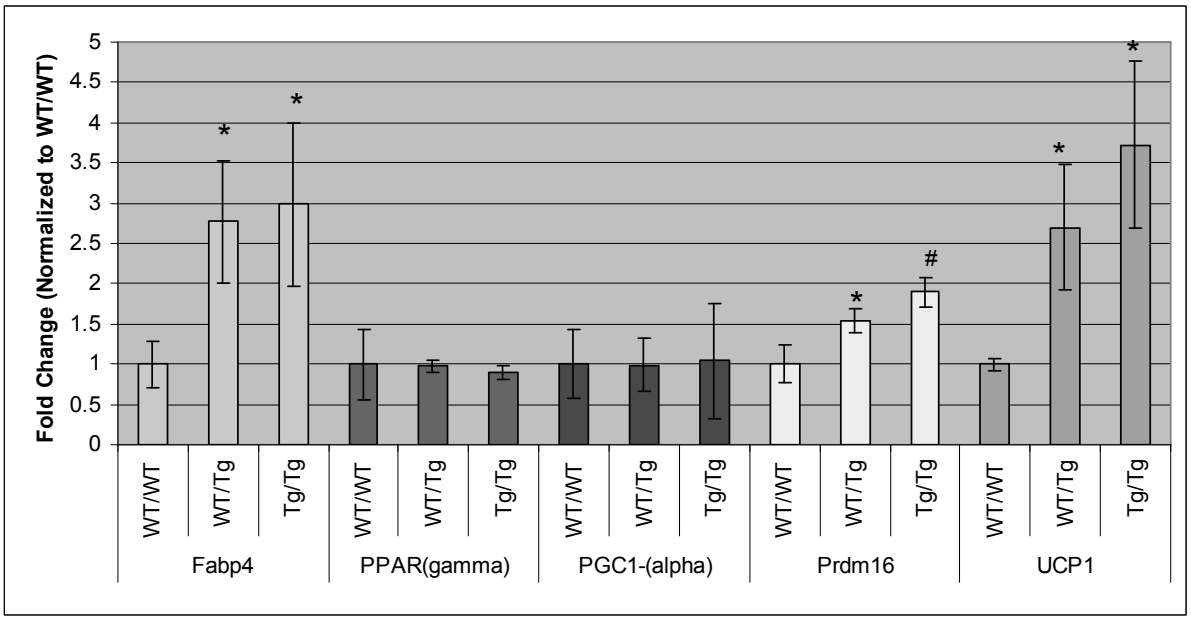

Figure 2.3 mRNA levels of adipogenic genes (*Fabp4, PPAR(gamma), PGC-1(alpha), Prdm16, UCP1*) in adipose tissues of diet mice on a high fat diet.
Comparisons between wildtype (WT/WT) with heterozygous (WT/Tg) and homozygous (Tg/Tg) *Gyk* transgenic mice n=5 for each study group. Bars represent mean ± SEM. * represent $p<0.05$ compared to WT/WT. # represents $p<0.05$ WT/Tg vs Tg/Tg.
Author Contribution: C.H. performed the quantitative RT-PCR experiments and the analysis

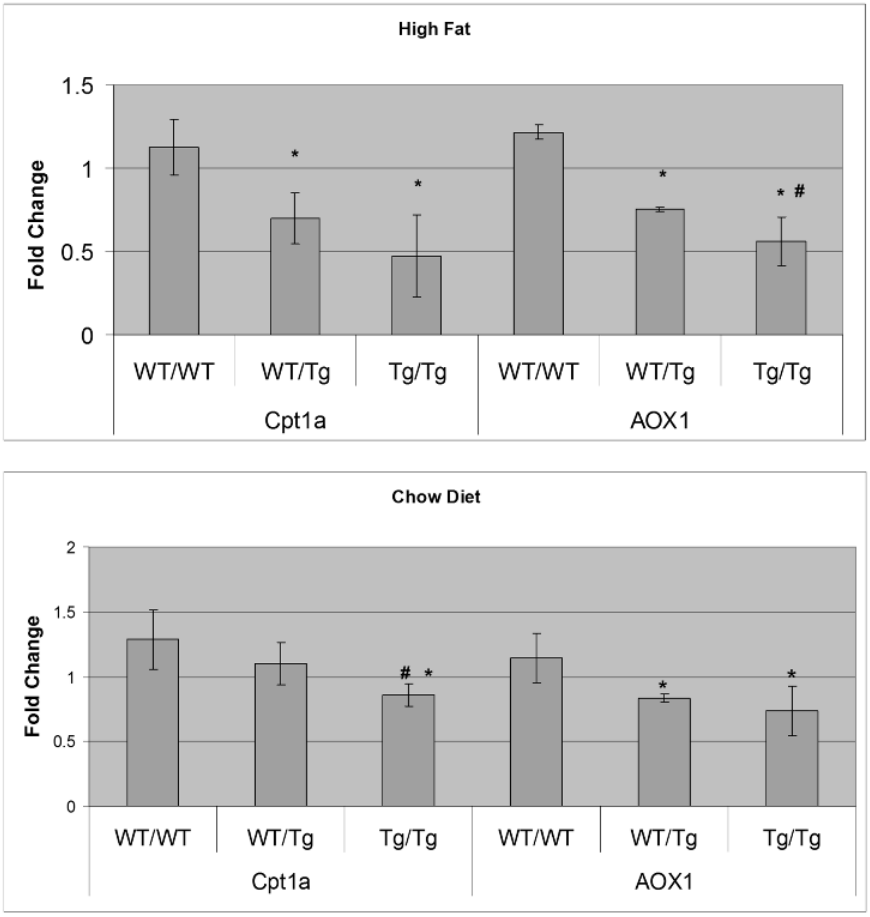

Figure 2.4 Quantitative RT-PCR analysis of fatty acid oxidation genes

A) Fatty acid oxidation gene expressions are reduced in transgenic mouse livers on chow diet. Bars represent mean ± SEM. * represent $p<0.05$ compared to WT/WT, # represent $p<0.05$ for Tg/Tg compared to WT/Tg

B) Fatty acid oxidation gene expressions are also reduced in transgenic mouse livers on high fat diet. Bars represent mean ± SEM. * represent $p<0.05$ compared to WT/WT, # represent $p<0.05$ for Tg/Tg compared to WT/Tg

Author Contribution: C.H. performed the quantitative RT-PCR experiments and the analysis

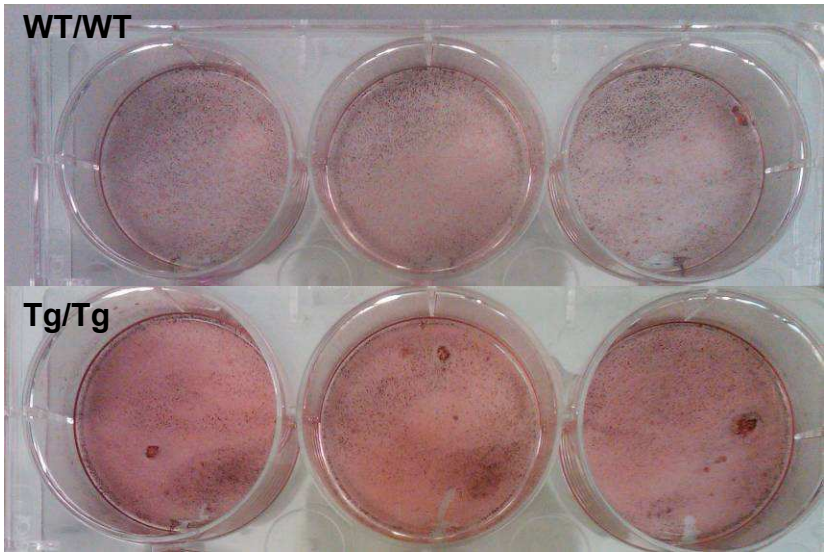

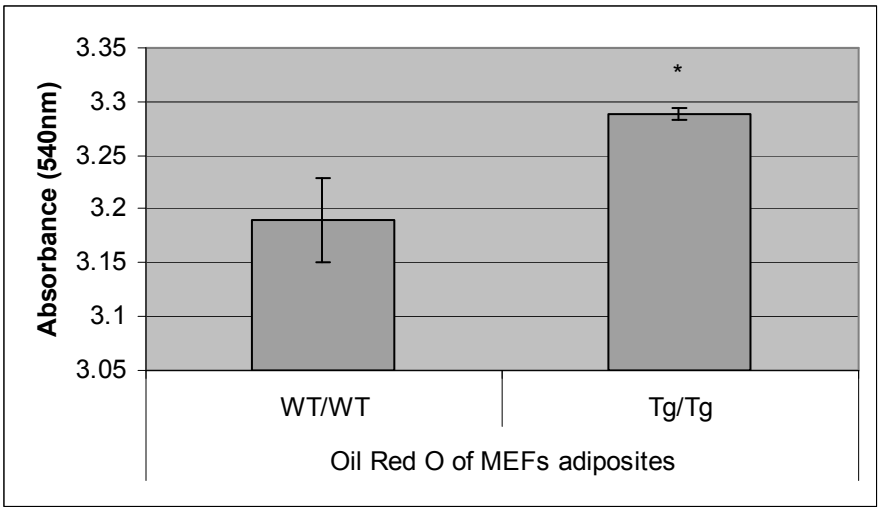

Figure 2.5 Oil red O staining of adipocytes differentiated from mouse embryonic fibroblast

A) Visualization of the Oil Red O staining. Comparison of wildtype MEFs (WT/WT) and homozygous transgenic MEFs (Tg/Tg)

B) Quantitation of lipid content in MEFs. Bars represent mean ± SEM. * represent $p<0.05$ compared to WT/WT. Absorbance is presented as an average of three measurements.

Author Contribution: C.H. performed all staining procedures and the analysis.

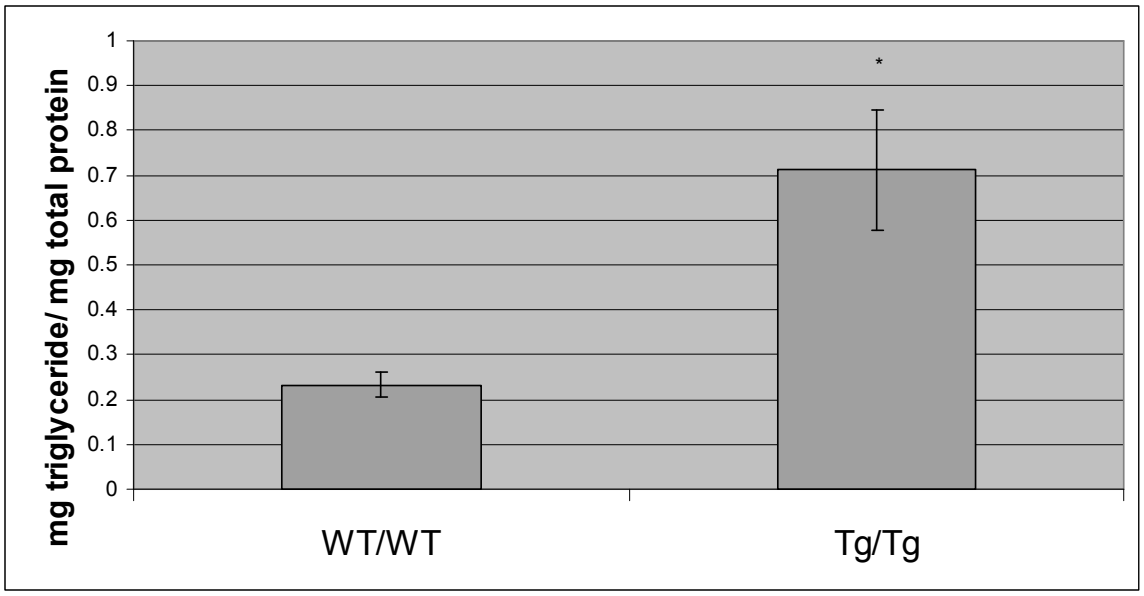

Figure 2.6 Triglyceride levels in mature adipocytes differentiated from mouse embryonic fibroblast

Data represents an average of measurements from five trials. * represent $p<0.05$ compared to WT.

Author Contribution: C.H. performed the triglyceride assays and the analysis.

Table 1	Lipid and glucose analysis of blood plasma					
	Chow			High Fat		
	WT/WT	WT/Tg	Tg/Tg	WT/WT	WT/Tg	Tg/Tg
Triglyceride	50.3±8.1	47.5±5.6	39.4±4.4	38±7	52±3.8*	44.3±4.9
Total Cholesterol	79.3±4.8	108.5±18.6*	87.5±2.7*	147.7±20.6	212±14.3*	208.7±15.6*
HDL Cholesterol	62.4±2.5	80.3±9.3*	71.2±2.0*	119.6±17.8	155.7±12.5*	158.7±14.9*
Unesterified Cholesterol	18.7±1.4	23.4±4.0*	17.6±0.6	32.8±4.0	47.8±3.1*	42.2±5.0*
Free Fatty Acids	31±2.8	29.2±2.0	31.2±2.2	32.4±2.3	28.1±1.8	32.3±2.3
Fasting Glucose	132.3±7.4	141.7±17.7*	157.6±10.5*	116.8±29.9	200.9±12.6*	169.8±12.3*
Insulin	263.0±37.6	401.3±138.4*	396.2±73.5*	394.7±69.4	590.2±128.0*	2194.6±740.5 #

Table 2.1 Lipid and glucose analysis of blood plasma from diet mice.

Comparisons between wildtype (WT/WT) with heterozygous (WT/Tg) and homozygous (Tg/Tg) Gyk transgenic mice. (n=10 from each study group) * $p<0.05$ statistical significance compared to WT in their respective diets; # $p<0.05$ Tg/Tg compared to WT/Tg

Author Contribution: UCLA DLAM staff Carmen Volpe performed the blood collection. UCLA metabolic core performed the lipid metabolic assays. C.H. analyzed the data results.

Chapter Three

Mathematical Model of Insulin Signal Transduction Pathway to Predict Insulin Sensitivity in Glycerol Kinase Knock Out Mice

Molecular Genetics and Metabolism 114 (2015) 66–72

Contents lists available at ScienceDirect

Molecular Genetics and Metabolism

journal homepage: www.elsevier.com/locate/ymgme

Mathematical modeling of the insulin signal transduction pathway for prediction of insulin sensitivity from expression data

Clark K. Ho [a], Lola Rahib [a], James C. Liao [a,b], Ganesh Sriram [b,c,1], Katrina M. Dipple [a,c,d,e,*]

[a] Biomedical Engineering Interdepartmental Program, Henry Samueli School of Engineering and Applied Science at UCLA, USA
[b] Department of Chemical and Biomolecular Engineering, Henry Samueli School of Engineering and Applied Science at UCLA, USA
[c] Department of Human Genetics, David Geffen School of Medicine at UCLA, USA
[d] Department of Pediatrics, David Geffen School of Medicine at UCLA, USA
[e] Mattel Children's Hospital at UCLA, USA

ARTICLE INFO

Article history:
Received 5 August 2014
Received in revised form 29 October 2014
Accepted 2 November 2014
Available online 8 November 2014

Keywords:
Insulin sensitivity
Insulin signal transduction pathway
Mathematical modeling

ABSTRACT

Mathematical models of biological pathways facilitate a systems biology approach to medicine. However, these models need to be updated to reflect the latest available knowledge of the underlying pathways. We developed a mathematical model of the insulin signal transduction pathway by expanding the last major previously reported model and incorporating pathway components elucidated since the original model was reported. Furthermore, we show that inputting gene expression data of key components of the insulin signal transduction pathway leads to sensible predictions of glucose clearance rates in agreement with reported clinical measurements. In one set of simulations, our model predicted that glycerol kinase knockout mice have reduced GLUT4 translocation, and consequently, reduced glucose uptake. Additionally, a comparison of our extended model with the original model showed that the added pathway components improve simulations of glucose clearance rates. We anticipate this expanded model to be a useful tool for predicting insulin sensitivity in mammalian tissues with altered expression protein phosphorylation or mRNA levels of insulin signal transduction pathway components.

1. Introduction

Insulin mediates glucose clearance from blood into tissues by triggering a cascade of interactions collectively known as the insulin signal transduction pathway [1]. Given the widespread, epidemic nature of obesity and type II diabetes mellitus (T2DM) [2], understanding and monitoring insulin sensitivity are critical to providing early and accurate diagnosis and treatment. Therefore, there is currently immense motivation in developing a comprehensive mathematical model of the insulin pathway. A few mathematical models have been developed that simulate mechanisms in this pathway [3,4]. The highly cited model reported by Sedaghat et al. (Sedaghat's model) was one of the first comprehensive models of the insulin signal transduction pathway [3]. However, not all components of the insulin signal transduction pathway were known at the time of publication of Sedaghat's model. Since then, researchers have made significant progress toward elucidating components in this pathway. More recent models emphasize on the insulin–insulin receptor dynamics and whole body glucose homeostasis of the pathway [5–8], but took significantly different mathematical approaches from Sedaghat's model. We, however, chose to develop a comprehensive model based on Sedaghat's model that incorporates elements of the pathway that have been elucidated since 2002. The proposed model of this study is therefore a modification of Sedaghat's model.

In the insulin signal transduction pathway, the activation of insulin receptors leads to phosphorylation events of many, if not all, downstream components [9,10]. The insulin-stimulated phosphorylation of phosphatidyl inositol-3-kinase (PI3K) stimulates the phosphorylation of two downstream proteins—protein kinase C (PKC)-ζ and protein kinase B (Akt) [11,12]. Phosphorylated PKC-ζ and Akt initiate two separate pathway branches, both of which ultimately lead to the translocation of glucose transporter 4 (GLUT4) from the cytoplasm to the plasma membrane. Once at the plasma membrane, GLUT4 facilitates the uptake of glucose into skeletal muscle and adipose cells. The pathway steps elucidated since the introduction of Sedaghat's model in 2002 include crucial downstream signaling steps between PKC-ζ/Akt and GLUT4 translocation [13–15]. These downstream steps have been implicated in insulin resistance and T2DM. For example, AS160, which is an intermediate between Akt and GLUT4, is overexpressed or

Abbreviations: T2DM, type II diabetes mellitus; PI3K, phosphatidyl inositol-3-kinase; (PKC)-ζ, protein kinase C zeta; Akt, protein kinase B; GLUT4, glucose transporter 4; GK/Gyk, glycerol kinase (GK in humans and Gyk in mice); WT, wild type; KO, knockout; PTP, protein tyrosine phosphatase; [i], The concentration of species i; didt, The change in concentration of species i over time; k_A, rate constant of the forward reaction including reacting species A; k_{rxB}, rate constant of the reverse reaction including reacting species B.

* Corresponding author at: David Geffen School of Medicine at UCLA, Departments of Human Genetics and Pediatrics, Gonda 5506B, 695 Charles E. Young Dr. South, Los Angeles, CA 90095-7088, USA. Fax: +1 310 794 5446.
E-mail address: kdipple@ucla.edu (K.M. Dipple).
[1] Currently at the Department of Chemical and Biomolecular Engineering at the University of Maryland.

http://dx.doi.org/10.1016/j.ymgme.2014.11.003
1096-7192/

phosphorylated during exercise [16]. Because of the significance of these newly elucidated pathway steps, we developed an extension of Sedaghat's model incorporating these steps. Our model is also able to simulate both GLUT4 translocation and (clinically relevant) glucose clearance. We validated our expanded model using gene expression data from our knockout mouse model.

1.1. Glycerol kinase and insulin sensitivity

We used our expanded model to predict insulin sensitivity from gene expression data using a glycerol kinase (*GK* in humans, *Gyk* in mice) knockout mouse model in our lab. Glycerol kinase deficiency (GKD; MIM 307030) is an inherited inborn error of metabolism caused by mutations, deletions, or insertions in the glycerol kinase gene on Xp21 [17]. The association between the GKD and insulin sensitivity has been observed in several studies [18–21]. For example, Gaudet et al. [18] reported that 12 out of 18 individuals carrying a particular GKD missense mutation, N288D, met the criteria for either impaired glucose tolerance or diabetes mellitus. Such results suggest the hypothesis that the underexpression or deletion of GK may decrease insulin sensitivity.

We used our expanded model to simulate the translocation of GLUT4 to the plasma membrane and subsequently predict glucose uptake rates, in response to a given dose of insulin. The extent of this translocation is a measure of insulin sensitivity. We evaluated our expanded model by inputting differential gene expression levels in mice [22]. Our model simulations aimed to show the significance of adding new key components of the insulin signal transduction into the previous model.

2. Methods

2.1. Insulin signaling pathway and mathematical model

In the insulin signal transduction pathway, insulin binds to the insulin receptor and initiates a complex signal transduction cascade, ultimately leading to the transport of the glucose transporter GLUT4 to the plasma membrane and subsequent glucose uptake into the cell [3,10]. Fig. 1A depicts Sedaghat's model and the dotted lines shown in the figure symbolize mechanisms that were poorly understood at that time. Fig. 1B depicts our expanded model that incorporates the additional pathway steps elucidated and characterized since the publication of Sedaghat's model. All signaling steps used in Sedaghat's model are included in our expanded model. To improve the level of uncertainty in Sedaghat's model, we have added steps downstream of PKC/AKT components crucial for GLUT4 translocation events.

Our current mathematical model of the insulin signal transduction pathway comprises a set of ordinary differential equations (ODEs) describing all known events in this signal transduction pathway. Each step is modeled as a chemical reaction, whose rate is in first order with respect to each reactant. Additionally, each reaction rate is dependent on the extent of a previous reaction (see Table 1). Table 1 lists the signal transduction events and rate constants in the original model by Sedaghat et al. (Eqs. (1)–(12)) [3], and those that were added in this work (Eqs. (13)–(19)). We added newly elucidated steps that account for the connections between both the PKC-ζ phosphorylation event and the GLUT4 translocation as well as between Akt phosphorylation and GLUT4 translocation. We modeled the steps downstream of PKC based on published studies that confirmed that phosphorylated PKC displaces munc18c from the plasma membrane, thereby facilitating increased GLUT4 translocation to the plasma membrane [13]. We modeled the steps downstream of Akt on the basis of recent investigations, that have shown that Akt phosphorylates AS160, which in turn activates the GTP activity of Rab, triggering movements of GLUT4-containing vesicles to the plasma membrane [14,15].

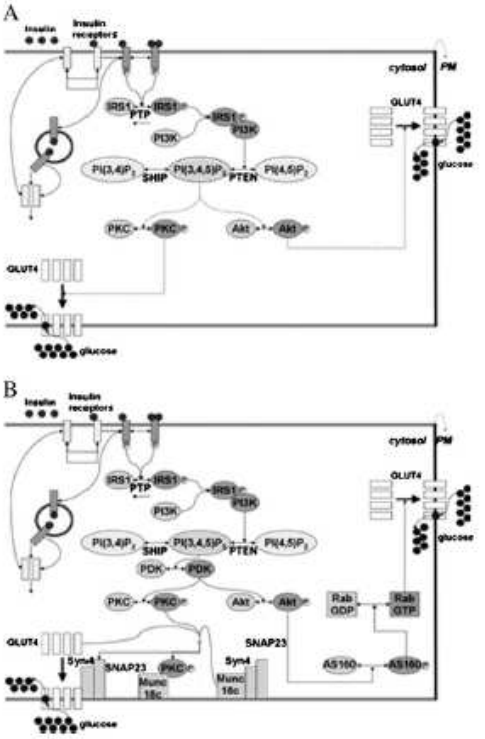

Fig. 1. Insulin signal transduction pathway. Unphosphorylated proteins and inactive molecules are shown in light gray, and phosphorylated proteins and active molecules are shown in dark gray. A. Insulin signal transduction pathway modeled by Sedaghat et al. [3]. Incompletely elucidated pathway steps are shown as dashed lines. B. Our expanded insulin signaling pathway that is simulated in this study. AS160, RabGDP, and Munc18c–Syn4–SNAP23 complex are the new components introduced to this model.

We modified some of the mathematical equations in Sedaghat's model, including the differential equations of Akt and PKC, due to the addition of new downstream components (e.g. AS160, Munc18c). To incorporate the new components into our model, we re-formulated the first order differential equations that simulate the formation and depletion of each component using new rate constants. For example, the transfer of a phosphate group from phosphorylated Akt to AS160 subsequently triggering RabGTP formation, from RabGDP, can be represented by:

$$\frac{d[AS160]}{dt} = -k_{AS160}[Akt\text{-}P][AS160] + k_{toAS160}[AS160\text{-}P]$$

$$\frac{d[AS160\text{-}P]}{dt} = k_{AS160}[Akt\text{-}P][AS160] - k_{toAS160}[AS160\text{-}P] - k_{RabGTP}[AS160\text{-}P][RabGTP] + k_{toAS160}[RabGDP][AS160].$$

Supplementary Table 1 lists the values of rate constants and boundary conditions. The set of ODEs representing the entire model (30 ODEs, including forward and reverse reactions of each step) was solved by using a ode15s ODE solver in MATLAB (The Mathworks, Natick, MA). We have retained all variable and parameter names common to both models. Our newly added pathway components downstream of the

Table 1
Signal transduction events, state variables, and model parameters in the insulin signal transduction pathway.
Reactions 1–12 are original equations included in Sedaghat's model [3]. Reactions 13–19 are new events incorporated into this expanded model.

Reaction			
	Remarks	Rate constants Forward reactions.	Rate constants Reverse reactions.
1	IR + I ↔ IR-I	k1	k_m1
2	IR-I + I ↔ IR-I2	k2	k_m2
3	IR-I, IR-I2 → IR-I-P, IR-I2-P	k3	k_m3 [PTP]
4	IR-I-P + I ↔ IR-I2-P	k2	k_m2
5	IR ↔ IRintracellular	k4	k_m4
6	→ IRintracellular →	k5	k_m5
7	IR-I, IR-I2 → IRintracellular	k4′	
8	IR-I-P, IR-I2-P ↔ IR-I-P intracellular, IR-I2-P intracellular	k4′	k_m4'
9	IRS1 ↔ IRS1-P	k7	k_m7[PTP]
10	IRS1-P + PI3K ↔ IRS1-P-PI3K	k8	k_m8
11	PI(4,5)P2 ↔ PI(3,4,5)P3	k9	k_m9[PTEN]
12	PI(3,4)P2 ↔ PI(3,4,5)P3	k10	k_m10[SHIP]
13	IRS1 ↔ IRS1-P	k113	k_m113
14	Akt ↔ Akt-P	k113	k_m11
15	Akt-P + AS160 ↔ AS160-P	k14a	k_m14a
16	AS160P + RabGDP ↔ RabGTP	k15	k_m15
17	PKC-P + Munc18c-Syn4-SNAP ↔ PKC-P − Munc18c + Syn4–SNAP	k16	k_m16
18	RabGTP + Glut4 → Glut4 translocation	k13p	k_m13
19	PKC-P–Munc18c + Glut4 → Glut4 translocation	k13pp	k_m13

PKC/Akt replaced Eq. 25 of Sedaghat's model [3], which empirically models all the metabolic effects that take place between the PKC/Akt subsystem and the translocation event. Particularly, our expanded model assumes that the formations of RabGTP and the PKC–Munc18c complex are the last reactions of the pathway that directly activate the translocation of GLUT4 to the plasma membrane. In order to account for the metabolic effects of the Sedaghat's model, we created new rate constants, k13p and k13pp, which are designated for the translocation of GLUT4 in response to the RabGTP component and the PKC–Munc18c complex, respectively.

2.2. Determination of the new rate constants and initial conditions

We estimated the rate constants and initial conditions corresponding to the newly added model components by fitting our expanded model to data from the literature. We determined a limited range for each rate constant, tested different combinations of the rate constant values corresponding to the new model components, and ultimately chose the optimal set of parameters that would best fit published in-vivo data, e.g. Baus et al. [23]. The ranges of each rate constant were selected to match the scaling factors of the published data. For experimental data from the literature, see the Results section.

2.3. Output conversion to glucose uptake rate

Instead of using the percentage of Glut4 translocated to plasma membrane, we have simulated the more clinically relevant glucose uptake rate as the ultimate output of our expanded model. We employed the Michaelis–Menten kinetics model in this output conversion. Important parameters of the kinetics model, such as Km and Vmax, are from Chew et al. [4].

2.4. Experimental animals and animal care

Gyk deficient mice were courtesy of W. J. Craigen (Baylor College of Medicine) [24] and our breeding strategy is as previously described [22]. All mice were kept on a normal diet (Harlan Tekland) and all procedures and experiments were performed as per a protocol approved by the UCLA Chancellor's Animal Research Committee. RNA isolation, cDNA hybridization, and microarray analysis are as previously described [22]. The fold differences in selected genes, including *PTP*, *PKC*, and *PI3K*, between wild type mice and knockout mice, reported in Rahib et al. [22], were inserted into the appropriate boundary equations to generate the simulated response curves.

2.5. Statistical analysis

Statistical analysis on the predicted insulin responses was performed by employing a Bootstrap Monte Carlo algorithm [25] to transform the errors illustrated in published data to standard deviations or confidence intervals of the predicted GLUT4 translocation and glucose uptake rate. The statistical significance of the predictions ('p' values) were determined by using Student's t test.

3. Results

Our model of the insulin signal transduction pathway extends the previously published Sedaghat model by capturing mechanisms that have been elucidated since its publication (Figs. 1A, B) [3]. In our model, PKC-ζ is mechanistically linked to the GLUT4 translocation event through the reaction of PKC-P with Munc18c, which is a component of the Munc18c–Syn4–SNAP23 complex. A second route leading to GLUT4 translocation involves Akt, in which Akt phosphorylates AS160, triggers activation of Rab GTP, and subsequently affects GLUT4 movement to the plasma membrane.

We took care to ensure that the changes made in our expanded model did not cause significant deviations in the dynamics of GLUT4 translocation and glucose uptake response in the physiological systems. To test our expanded model, we compared how closely our simulations compared with the simulations from Sedaghat's model. The time response curves of the GLUT4 translocation and the glucose uptake response of our expanded compared to original Sedaghat's model upon administration of an insulin dose of 0.1 nM for 60 min ($t = 0$ to 60 min) are seen in Figs. 2A and B. The GLUT4 translocation and glucose uptake dynamics simulated by our expanded model qualitatively agrees with those simulated by Sedaghat's model (Figs. 2A, B).

To determine the rate constants of the newly added components, we gathered experimental data from published literature that implicates the components' chemical kinetics. For example, we used data presented in Baus et al. to determine the rate constant k14a, which corresponds to the kinetics of the AS160 phosphorylation reaction [23]. In their study, Baus et al. examined insulin-stimulated glucose uptake of skeletal muscle cells expressing the AS160 splice variant, in which the expression of the AS160 transcript variant expression was approximately five fold less than that of the full length AS160 (Fig. 1B of Baus et al.). They showed that cells expressing the variant have increased glucose uptake, approximately 2.3 fold higher than the control, when stimulated with 50 nM insulin. We revised their bar plot results (Fig. 3A of Baus et al.) into scatterplot format to facilitate our determination of the proper rate constant value k14a [23]. By using the chosen rate constant values, we simulated the AS160–glucose uptake fold change relationship observed in the scatterplot (Fig. 2C). Insulin dosage response curves were simulated in the insulin dose range of 10^{-14} to 10^{-7} M (exposure time of 60 min) for two concentrations (e.g. one with baseline expression of AS160 and one with 5-fold increase in expression of AS160). The basal glucose uptake rate under minimum insulin stimulation was approximately 15 μM/min. The dosage response curves matched reasonably well, particularly at low insulin concentrations (0.1 nM) and high concentrations at 50 nM. There was slight deviation at the hillslope of the response curve. Based on the comparison, we concluded that our current model was optimized for the input

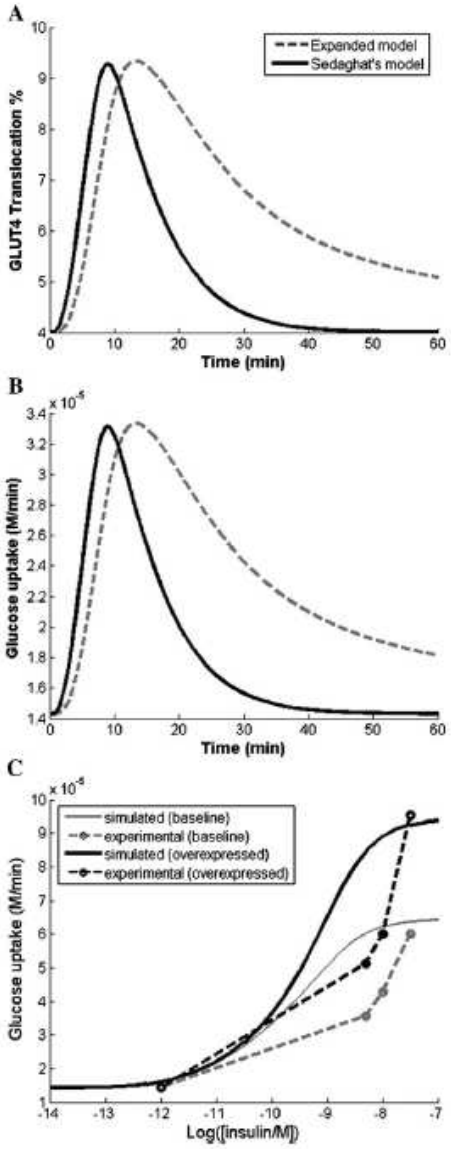

Fig. 2. Comparison of our expanded model (dashed line) and Sedaghat's original model (solid line). A. GLUT4 translocation time–response curve comparing the two models with a single insulin dose input of 0.1 nM and a run time of 60 min. B. Glucose uptake rates with a single insulin dose of 0.1 nM and a run time of 60 min. C. Insulin dosage–response curve showing expected glucose uptake rates from an insulin dose of 10^{-12} M to 10^{-6} M. Comparison of simulated glucose uptake (solid lines) and experimental glucose uptake (dotted lines) as a result of *AS160* overexpression. Experimental results were based on data from the Baus et al. study and data points were presented as hollow circles in the figure.

insulin dose of 0.1 nM. All single dose simulations for the remainder of this study were done using that particular dose.

3.1. Model predicts decreased insulin sensitivity in brown fat of Gyk knockout mice

Microarray analysis of brown fat from *Gyk* knockout (KO) mice revealed that a number of genes in the insulin signal transduction pathway were under- or over-expressed relative to wild type (WT) mice (Table 3 of Rahib et al.) [22]. Two principal genes in the pathway: *PTP* (protein tyrosine phosphatase, 1.51-fold) and *PKC* (protein kinase C, 1.42-fold) were overexpressed in the *Gyk* KO mice. Whereas, *PI3K* was underexpressed 1.48-fold. Other insulin-related genes that were differentially expressed in the *Gyk* knockout mice, but were not in the insulin signal transduction pathway, include *c-fun N-terminal kinase* (overexpressed 1.45-fold), *insulin growth factor 1* (overexpressed 2.1-fold), and *insulin growth factor binding protein* (underexpressed 3.7-fold) [22].

Using our expanded mathematical model of the insulin signal transduction pathway, we simulated the effect of these altered gene expressions on glucose uptake rates using the dataset from Rahib et al. [22]. The translocation of GLUT4 to the plasma membrane for an insulin dose of 0.1 nM for 60 min, was used as a measure of insulin sensitivity. The raw data of all GLUT4 simulations can be found in Supplementary Table 2. Fig. 3 depicts the comparison of GLUT 4 translocation (Fig. 3A) and glucose uptake rates (Fig. 3B) in the *Gyk* KO (dotted line) and WT mice (solid line) due to *PI3K* underexpression accompanied with *PIP* and *PKC* overexpression. The reduction of GLUT4 translocation in *Gyk* KO mice, compared to WT, is 7.4% ($p < 0.05$), and the glucose clearance, the total amount of glucose uptake into cell, is 2.2% less than that of *Gyk* WT mice.

We also simulated the responses of the *Gyk* WT and KO mice to various doses of insulin from 10^{-12} M to 10^{-7} M (Figs. 3B, C). The WT mice exhibit a higher glucose uptake throughout the entire insulin dosage range, with the most pronounced difference at the highest insulin concentration.

4. Discussion

We successfully modified a previously published mathematical model of the insulin signaling pathway (Sedaghat's model) by incorporating recently elucidated pathway components. Our expanded model is able to analyze the effect of insulin sensitivity from altered gene expression of the new components. We used this model to assess insulin sensitivity comparing WT and *Gyk* KO mice. Our results are consistent with the hypothesis that knockout *Gyk* mice have reduced insulin sensitivity.

Although we observed minor differences in the shape of the insulin-stimulated time response curves of our model compared to that of Sedaghat's model (Fig. 2), we believe that our model better suits the physiological system than the original, in terms of the insulin-stimulated GLUT4 translocation response. A recent in-vivo project studying differentiated myotubes showed that the GLUT4 translocation level was peaked at 10 min after stimulation and continued to degrade past 60 min, Fig. 4C of Yuasa et al. [26], further supporting the trend of our model. We noted that the GLUT4 translocation response returns to basal level when simulation time goes past 150 min. Our expanded model reflects that the amount of GLUT4 translocation and glucose uptake, the outputs of our design, are dependent on the amount of insulin input, the level of gene expressions of key players, and the rate of each reversible reactions.

The analysis using *Gyk* KO mice microarray data further strengthens GKD's association with insulin sensitivity. Our model predicted that *Gyk* KO mice were insulin resistant compared to WT mice. Subsequently, our current *Gyk* KO mice model became growth retarded soon after birth and did not survive past day three of life, which does not allow

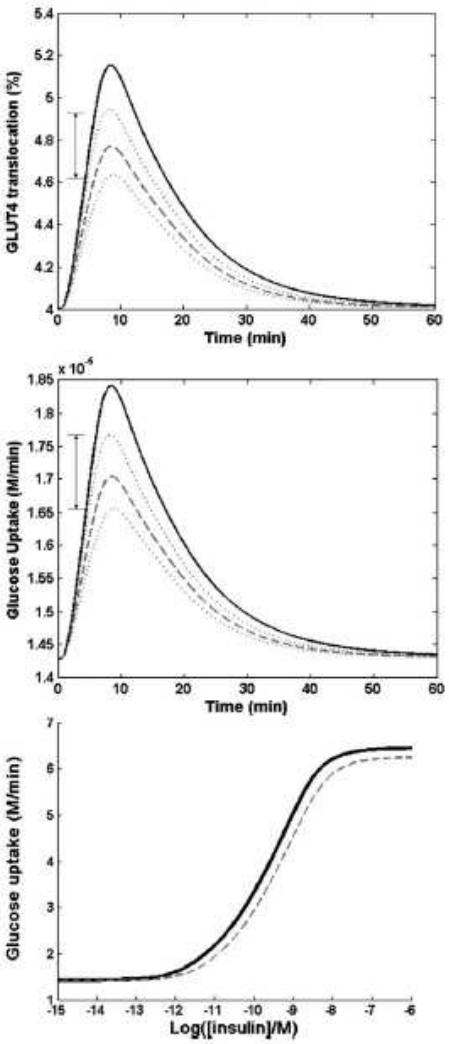

Fig. 3. Simulation of the effect of overexpression of *PTP* (2.8-fold) and *PKC* (3.0-fold), and underexpression of *PBK* (2.8-fold). Recorded from our previous microarray data of *Gyk* KO with respect to *Gyk* WT mice. A. GLUT4 translocation time response curves, *Gyk* KO (dashed and dotted lines) vs WT (solid line), with a single insulin dose input of 0.1 nM and a run time of 60 min ($p < 0.05$). Dotted lines represent the range of outputs for GLUT4 translocation % of *Gyk* KO, accounting for the standard error of the data reported in Rahib et al. [22]. B. Glucose uptake level, *Gyk* KO (dashed and dotted lines vs WT solid line), with a single insulin dose of 0.1 nM and a run time of 60 min ($p < 0.05$). Dotted lines represent the range of outputs for GLUT4 translocation % of *Gyk* KO, accounting for the standard error of the data reported in Rahib et al. [22]. C. Insulin dosage–response curves (*Gyk* KO vs WT) showing expected glucose uptake levels from insulin dose inputs from 10^{-12} M to 10^{-6} M ($p < 0.05$).

for proper insulin sensitivity assessment [24]. However, the model prediction of insulin resistance in *Gyk* KO mice is consistent with the symptoms of isolated GKD in humans [18]. The model simulation results using *Gyk* microarray data also show the trend that *GK* underexpression accompanied by differential expressions of other genes results in a reduction of insulin sensitivity. We suggest two possible reasons why *GK* underexpression is likely contributing to reduced insulin sensitivity. Firstly, GK lies at the interface of carbohydrate and lipid metabolism [27]. In addition, it was reported that the thiazolidinediones, which are agonists for peroxisome *proliferator–activated receptor* γ (PPARγ) and a common drug to treat T2DM, increase *GK* expression in adipocytes [20,21]. GK maintains futile cycling between lipids and carbohydrates, thus perhaps preventing free fatty acid accumulation and insulin desensitization. It is logical to advocate that its deficiency can be expected to have an impact on insulin sensitivity. Secondly, GK is a 'moonlighting enzyme', which has alternative non-enzymatic functions, having at least four functions apart from its enzymatic function [28,29]. Of particular importance is its role as ATP-stimulated translocation factor (ASTP). ASTP is an ATP-stimulated factor that enhances the nuclear binding of the activated glucocorticoid-receptor (GR) complex, an important transcription factor. In fact, GR complex activation is known to activate genes related to obesity/T2DM. A particular study confirmed that white adipose tissues of mice treated with synthetic glucocorticoid have increased triglyceride synthesis [30]. GK may be indirectly responsible for the activation or suppression of other genes, some of which may be involved in insulin response. Therefore, GK deficiency is expected to reduce insulin sensitivity.

Our extended model has shown great potential in simulating GLUT4 translocation and glucose uptake in other applications as well. For example, we can potentially apply the model to an existing study of glucose sensitivity in human patients with obesity or T2DM in response to exercising. Exercise has been shown to prevent or improve obesity and insulin sensitivity in T2DM [16,31–33]. Short-term exercise increases the concentration of active insulin receptors as well as insulin receptor substrate-1 (IRS1) phosphorylation in both obese and T2DM patients [31]. Exercise training has also been shown to increase overall insulin signaling transduction and glucose uptake rates in skeletal muscles of rodents [32]. We will make small changes to the current model by determining a new set of model parameters to fit expression data of human subjects and apply the model with obesity and T2DM datasets.

In order to test our expanded model with datasets of gene expression, we emphasize the subsets of reactions where the forward and reverse kinetic constants are not dependent on each other. If the enzyme product of the differentially expressed gene catalyzes both directions of a reversible reaction, we need to alter both forward and reverse kinetic constants. Some of these reactions are catalyzed irreversibly. For example, PTP de-phosphorylates IRS1-P into IRS1, but it does not participate in the forward reaction. In this case, the forward kinetic constant is independent of the reverse reaction. Another subset of reactions includes differentially expressed genes or proteins that undergo post-translational modification in the insulin signal transduction pathway. The phosphorylation of the protein AS160 is reversible. When the gene or protein expression level of AS160 equals the sum of the unphosphorylated and phosphorylated moieties, we can assume that an increase in the gene expression level will result in increased total availability of the protein. To test whether gene expression data and protein activity data can be used interchangeably, we found published data by Yu et al. [34], showing both gene expression and protein activity level of key insulin signaling gene, PTEN, in diabetic mice. Using their data, we performed our model simulations, generated by using either the published mRNA or protein data, and confirmed that the difference in using gene or protein data is insignificant (Supplementary Fig. 1).

A potential weakness of simulating such a complex signaling system, such as the insulin signal transduction pathway, using a mathematical model is that the selection of appropriate rate constants and boundary conditions can be somewhat arbitrary. Our attempts to strengthen the power of our model include adapting strategies and model parameters that were presented in the established Sedaghat's model and similar

models based on Sedaghat's model. We incorporated some key components between the insulin signaling pathway and GLUT4 trafficking to lower the degree of uncertainty in the model. We also validated our complete model by comparing dosage and time response curves to the selected study (e.g. Rahib et al.). This model could be applied to other datasets [16,35–37] that emphasize exploring the relationship of exercising and key components in the insulin signal transduction pathway to strengthen our current model.

We could also incorporate the current model with elements from other recently developed models that cover other aspects of the insulin signal transduction pathway, such as Dalla Man's model of whole-body glucose homeostasis and Brannmark's dynamic model of receptor mechanisms [7,8]. However, those models took significantly different approaches from the original Sedaghat model, therefore did not fit into the comparisons performed in this study.

5. Conclusions

In this study, we developed an expanded mathematical model of the insulin signal transduction pathway based on Sedaghat's model, which allows for prediction of insulin sensitivity and glucose uptake from microarray data. Our expanded model can simulate the translocation events of the insulin signal transduction pathway more comprehensively with the added key components and present a more clinically relevant model output, glucose uptake. Our model predictions are consistent with our published results that the differential gene expression shown in *Gyk* KO mice contribute to decreased insulin sensitivity. Such predictions, in turn, will be valuable in investigating the relationship between GKD and insulin resistance. The expanded mathematical model developed here can be applied to many biological systems with minimal changes, and will be a useful tool to study insulin resistance for the insulin signal transduction and diabetes research community.

Supplementary data to this article can be found online at http://dx.doi.org/10.1016/j.ymgme.2014.11.003.

Competing interests

The author(s) declare that they have no competing interests.

Author contributions

C.H. and G.S. developed the expanded mathematical model, wrote MATLAB scripts, determined parameter values, and performed the simulations. L.R. performed the microarray analyses. G.S., J.C.L. and K.D. conceived this study. C.H. wrote the manuscript with inputs from G.S., J.C.L., and K.D.

Acknowledgments

This work was supported by NIH Biotechnology Training Program (T32GM067555).

References

[1] D. Leto, A.R. Saltiel, Regulation of glucose transport by insulin: traffic control of GLUT4, Nat. Rev. Mol. Cell Biol. 13 (2012) 383–396.
[2] L. Chen, D.J. Magliano, P.Z. Zimmet, The worldwide epidemiology of type 2 diabetes mellitus—present and future perspectives, Nat. Rev. Endocrinol. 8 (2012) 228–236.
[3] A.R. Sedaghat, A. Sherman, M.J. Quon, A mathematical model of metabolic insulin signaling pathways, Am. J. Physiol. Endocrinol. Metab. 283 (2002) E1084–E1101.
[4] Y.H. Chew, Y.L. Shia, C.T. Lee, F.A. Majid, L.S. Chua, M.R. Sarmidi, R.A. Aziz, Modeling of glucose regulation and insulin-signaling pathways, Mol. Cell. Endocrinol. 303 (2009) 13–24.
[5] V.V. Kiselyov, S. Versteyhe, L. Gauguin, P. De Meyts, Harmonic oscillator model of the insulin and IGF1 receptors' allosteric binding and activation, Mol. Syst. Biol. 5 (2009) 243.
[6] E. Nyman, E.C. Brännmark, R. Palmér, J. Brugård, F.H. Nyström, P. Strålfors, G. Cedersund, A hierarchical whole-body modeling approach elucidates the link between in vitro insulin signaling and in vivo glucose homeostasis, J. Biol. Chem. 286 (2011) 26028–26041.
[7] C. Brännmark, R. Palmér, S.T. Glad, G. Cedersund, P. Strålfors, Mass and information feedbacks through receptor endocytosis govern insulin signaling as revealed using a parameter-free modeling framework, J. Biol. Chem. 285 (2010) 20171–20179.
[8] C. Dalla Man, R.A. Rizza, C. Cobelli, Meal simulation model of the glucose–insulin system, IEEE Trans. Biomed. Eng. 54 (2007) 1740–1749.
[9] M.J. Saad, F. Folli, J.A. Kahn, C.R. Kahn, Modulation of insulin receptor, insulin receptor substrate-1, and phosphatidylinositol 3-kinase in liver and muscle of dexamethasone-treated rats, J. Clin. Invest. 92 (1993) 2065–2072.
[10] M. Kasuga, Y. Zick, D.L. Blithe, M. Crettaz, C.R. Kahn, Insulin stimulates tyrosine phosphorylation of the insulin receptor in a cell-free system, Nature 298 (1982) 667–669.
[11] C.M. Taniguchi, B. Emanuelli, C.R. Kahn, Critical nodes in signalling pathways: insights into insulin action, Nat. Rev. Mol. Cell Biol. 7 (2006) 85–96 (C.P.).
[12] L.C. Cantley, The phosphoinositide 3-kinase pathway, Science 296 (2002) 1655–1657.
[13] C.P. Hodgkinson, A. Mander, G.J. Sale, Protein kinase-zeta interacts with munc18c: role in GLUT4 trafficking, Diabetologia 48 (2005) 1627–1636.
[14] L. Jiang, J. Fan, L. Bai, Y. Wang, Y. Chen, L. Yang, L. Chen, T. Xu, Direct quantification of fusion rate reveals a distal role for AS160 in insulin-stimulated fusion of GLUT4 storage vesicles, J. Biol. Chem. 283 (2008) 8508–8516.
[15] M. Larance, G. Ramm, J. Stöckli, E.M. van Dam, S. Winata, V. Wasinger, F. Simpson, M. Graham, J.R. Junutula, M. Guilhaus, D.E. James, Characterization of the role of the Rab GTPase-activating protein AS160 in insulin-regulated trafficking, J. Biol. Chem. 280 (2005) 37803–37813.
[16] D.J. O'Gorman, H.K. Karlsson, S. McQuaid, O. Yousif, Y. Rahman, D. Gasparro, S. Glund, A.V. Chibalin, J.R. Zierath, J.J. Nolan, Exercise training increases insulin-stimulated glucose disposal and GLUT4 (SLC2A4) protein content in patients with type 2 diabetes, Diabetologia 49 (2006) 2983–2992.
[17] K.M. Dipple, Y.H. Zhang, B.L. Huang, L.L. McCabe, J. Dallongeville, T. Inokuchi, M. Kimura, H.J. Marx, G.O. Roederer, V. Shih, S. Yamaguchi, I. Yoshida, E.R. McCabe, Glycerol kinase deficiency: evidence for complexity in a single gene disorder, Hum. Genet. 109 (2001) 55–62.
[18] D. Gaudet, S. Arsenault, L. Perusse, M.C. Vohl, J. St-Pierre, J. Illergeron, J.P. Despres, K. Dewar, M.J. Daly, T. Hudson, J.D. Rioux, Glycerol as a correlate of impaired glucose tolerance: dissection of a complex system by use of a simple genetic trait, Am. J. Hum. Genet. 66 (2000) 1558–1568.
[19] H.P. Guan, Y. Li, M.V. Jensen, C.B. Newgard, C.M. Steppan, M.A. Lazar, A futile metabolic cycle activated in adipocytes by antidiabetic agents, Nat. Med. 8 (2002) 1122–1128.
[20] J. Tordjman, G. Chauvet, J. Quette, E.G. Beale, C. Forest, B. Antoine, Thiazolidinediones block fatty acid release by inducing glyceroneogenesis in fat cells, J. Biol. Chem. 278 (2003) 18785–18790.
[21] D.H. Lee, D.B. Park, Y.K. Lee, C.S. An, Y.S. Oh, J.S. Kang, S.H. Kang, M.Y. Chung, The effects of thiazolidinedione treatment on the regulations of aquaglyceroporins and glycerol kinase in OLETF rats, Metabolism 54 (2005) 1282–1289.
[22] L. Rahib, N.K. MacLennan, S. Horvath, J.C. Liao, K.M. Dipple, Glycerol kinase deficiency alters expression of genes involved in lipid metabolism, carbohydrate metabolism, and insulin signaling, Eur. J. Hum. Genet. 15 (2007) 646–657.
[23] D. Baus, K. Heermeier, M. De Hoop, C. Metz-Weidmann, J. Gassenhuber, W. Dittrich, S. Welte, N. Tennagels, Identification of a novel AS160 splice variant that regulates GLUT4 translocation and glucose uptake in rat muscle cells, Cell. Signal. 20 (2008) 2237–2246.
[24] A.H. Huq, R.S. Lovell, C.N. Ou, A.L. Beaudet, W.J. Craigen, X-linked glycerol kinase deficiency in the mouse leads to growth retardation, altered fat metabolism, autonomous glucocorticoid secretion and neonatal death, Hum. Mol. Genet. 6 (1997) 1803–1809.
[25] W.H. Press, S.A. Teukolsky, W.T. Vetterling, B.P. Flannery, Numerical Recipes in C: The Art of Scientific Computing, second ed. Cambridge University Press, Cambridge, UK, 1992. (Edited by).
[26] T. Yuasa, K. Uchiyama, Y. Ogura, M. Kimura, K. Teshigawara, T. Hosaka, Y. Tanaka, T. Obata, H. Sano, K. Kishi, Y. Ebina, The Rab GTPase-activating protein AS160 as a common regulator of insulin- and Galphaq-mediated intracellular GLUT4 vesicle distribution, Endocr. J. 56 (2009) 345–359.
[27] L. Rahib, G. Sriram, M.K. Harada, J.C. Liao, K.M. Dipple, Transcriptomic and network component analysis of glycerol kinase in skeletal muscle using a mouse model of glycerol kinase deficiency, Mol. Genet. Metab. 96 (2009) 106–112.
[28] G. Sriram, J.A. Martinez, E.R. McCabe, J.C. Liao, K.M. Dipple, Single-gene disorders: what role could moonlighting enzymes play? Am. J. Hum. Genet. 76 (2005) 911–924.
[29] C.J. Jeffery, Multifunctional proteins: examples of gene sharing, Ann. Med. 35 (2003) 28–35.
[30] C.Y. Yu, O. Mayba, J.V. Lee, J. Tran, C. Harris, T.P. Speed, J.C. Wang, Genome-wide analysis of glucocorticoid receptor binding regions in adipocytes reveal gene network involved in triglyceride homeostasis, PLoS ONE 5 (2010) e15188.
[31] K. Cusi, K. Maezono, A. Osman, M. Pendergrass, M.E. Patti, T. Pratipanawatr, R.A. DeFronzo, C.R. Kahn, L.J. Mandarino, Insulin resistance differentially affects the PI3-kinase- and MAP kinase-mediated signalling in human muscle, J. Clin. Invest. 105 (2000) 311–320.
[32] J.A. Houmard, C.D. Shaw, M.S. Hickey, C.J. Tanner, Effect of short-term exercise training on insulin-stimulated PI3-kinase activity in human skeletal muscle, Am. J. Physiol. 277 (1999) E1055–E1060.
[33] C.J. Tanner, T.R. Koves, R.L. Cortright, W.J. Pories, Y.B. Kim, B.B. Kahn, G.L. Dohm, J.A. Houmard, Effect of short-term exercise training on insulin-stimulated PI 3-kinase

activity in middle-aged men, Am. J. Physiol. Endocrinol. Metab. 282 (2002) E147–E153.
[34] X. Yu, N. Shen, M. Zhang, F. Pan, C. Wang, W. Jia, C. Liu, Q. Gao, X. Gao, B. Xue, C. Li, Egr-1 decreases adipocyte insulin sensitivity by tilting PI3K/Akt and MAPK signal balance in mice, EMBO J. 30 (2011) 3754–3765.
[35] H.K. Karlsson, J.R. Zierath, S. Kane, A. Krook, G.E. Lienhard, H. Wallberg-Henriksson, Insulin-stimulated phosphorylation of the Akt substrate AS160 is impaired in skeletal muscle of type 2 diabetic subjects, Diabetes 54 (2005) 1692–1697.
[36] C. Prats, A.J. Rose, J.T. Treebak, B. Kiens, E.A. Richter, J.F.P. Wojtaszewski, Effects of endurance exercise training on insulin signaling in human skeletal muscle interactions at the level of phosphatidylinositol 3-kinase, Akt, and AS160, Diabetes 8 (2007) 2093–2102.
[37] A. Deshmukh, V.G. Coffey, Z. Zhong, A.V. Chibalin, J.A. Hawley, J.R. Zierath, Exercise-induced phosphorylation of the novel Akt substrates AS160 and filamin A in human skeletal muscle, Diabetes 55 (2006) 1776–1782.

Supplementary Data

Table 3.S1	Description
	state variables, initial conditions, and differential equations are defined

Table 1
Variables Designations
x2: Concentration of unbound surface insulin receptors
x3: Concentration of unphosphorylated once-bound surface receptors
x4: Concentration of phosphorylated twice-bound surface receptors
x5: Concentration of phosphorylated once-bound surface receptors
x6: Concentration of unbound unphosphorylated intracellular receptors
x7: Concentration of phosphorylated twice-bound intracellular receptors
x8: Concentration of phosphorylated once-bound intracellular receptors
x9: Concentration of unphosphorylated IRS-1
x10: Concentration of tyrosine-phosphorylated IRS-1
x11: Concentration of unactivated PI 3-kinase
x12: Concentration of tyrosine-phosphorylated IRS-1/activated PI 3-kinase complex
x13: Percentage of PI(3,4,5)P3 out of the total lipid population
x14: Percentage of PI(4,5)P2 out of the total lipid population
x15: Percentage of PI(3,4)P2 out of the total lipid population
x16: Percentage of unactivated Akt
x17: Percentage of activated Akt
x18: Percentage of unactivated PKC- ζ
x19: Percentage of activated PKC- ζ
x20: Percentage of intracellular GLUT4
x21: Percentage of cell surface GLUT4
x22: Concentration of Munc18c-syr-SNAP complex
x22a: Concentration of PKC-Munc18c complex
x23: Concentration of Syr-SNAP complex
x24: Concentration of unphosphorylated AS 160
x25: Concentration of phosphorylated AS160
x26: Concentration of RabGDP
x27: Concentration of RabGTP

Initial conditions are as follows:

$x1(0) = 0$

$x2(0) = 9 \cdot 10^{-13}\,\mathrm{M}$

$x3(0) = 0$

$x4(0) = 0$

$x5(0) = 0$

$x6(0) = 1 \cdot 10^{-13}\,\mathrm{M}$

$x7(0) = 0$

$x8(0) = 0$

$x9(0) = 1 \cdot 10^{-12}\,\mathrm{M}$

$x10(0) = 0$

$x11(0) = 1 \cdot 10^{-13}\,\mathrm{M}$

$x12(0) = 0$

$x13(0) = 0.31\%$

$x14(0) = 99.40\%$

$x15(0)$ 0.29%

$x16(0) = 100\%$

$x17(0) = 0$

$x18(0) = 100\%$

$x19(0) = 0$

$x20(0) = 96\%$

$x21(0) = 4\%$

$x22(0) = 100\%$

$x22a(0) = 0$

$x23(0) = 0$

$x24(0) = 100\%$

$x25(0) = 0$

$x26(0) = 100\%$

$x27(0) = 0$

Differential equations are as follows
(note: k are rate constants of forward reaction and km are rate constants of reverse reactions)

x1= insulin input

$$dx2dt = k_m1 \cdot x3 + k_m3 \cdot PTP \cdot x5 - k1 \cdot x1 \cdot x2 + k_m4 \cdot x6 - k4 \cdot x2$$
$$dx3dt = k1 \cdot x1 \cdot x2 - k_m1 \cdot x3 - k3 \cdot x3$$
$$dx4dt = k2 \cdot x1 \cdot x5 - k_m2 \cdot x4 + k_m4p \cdot x7 - k4p \cdot x4$$
$$dx5dt = k3 \cdot x3 + k_m2 \cdot x4 - k2 \cdot x1 \cdot x5 - k_m3 \cdot PTP \cdot x5 + k_m4p \cdot x8 - k4p \cdot x5$$
$$dx6dt = k5 - k_m5 \cdot x6 + k6 \cdot PTP \cdot (x7 + x8) + k4 \cdot x2 + k_m4 \cdot x6$$
$$dx7dt = k4p \cdot x4 - k_m4p \cdot x7 - k6 \cdot PTP \cdot x7$$
$$dx8dt = k4p \cdot x5 - k_m4p \cdot x8 - k6 \cdot PTP \cdot x8$$
$$dx9dt = k_m7 \cdot PTP \cdot x10 - k7 \cdot x9 \cdot (x4 + x5) / IRp + k_m7p \cdot x10a - k7p \cdot PKC \cdot x9$$
$$dx10dt = k7 \cdot x9 \cdot (x4 + x5) / IRp + k_m8 \cdot x12 - (k_m7 \cdot PTP + k8 \cdot x11) \cdot x10$$
$$dx11dt = k_m8 \cdot x12 - k8 \cdot x10 \cdot x11$$
$$dx12dt = k8 \cdot x10 \cdot x11 - k_m8 \cdot x12$$
$$dx13dt = k9 \cdot x14 + k10 \cdot x15 - (k_m9 \cdot PTEN + k_m10 \cdot SHIP) \cdot x13$$
$$dx14dt = k_m9 \cdot PTEN \cdot x13 - k9 \cdot x14$$
$$dx15dt = k_m10 \cdot SHIP \cdot x13 - k10 \cdot x15$$
$$dx16dt = k_m11 \cdot x17 - k11 \cdot x16$$
$$dx17dt = k11 \cdot x16 - k_m11 \cdot x17 - (k14a \cdot x17 \cdot x24) + (k_m14a \cdot x25 \cdot x16)$$
$$dx18dt = k_m12 \cdot x19 - k12 \cdot x18$$
$$dx19dt = k12 \cdot x18 - k_m12 \cdot x19 - (k16 \cdot x19 \cdot x22) + (k_m16 \cdot x23 \cdot x22a)$$
$$dx22dt = -(k16 \cdot x19 \cdot x22) + (k_m16 \cdot x23 \cdot x22a)$$
$$dx22adt = (k16 \cdot x19 \cdot x22) - (k_m16 \cdot x23 \cdot x22a)$$
$$dx23dt = (k16 \cdot x19 \cdot x22) - (k_m16 \cdot x23 \cdot x22a)$$
$$dx10adt = (k7p \cdot PKC \cdot x9) - (k_m7p \cdot x10a)$$
$$dx24dt = -(k14a \cdot x17 \cdot x24) + (k_m14a \cdot x25 \cdot x16)$$
$$dx25dt = (k14a \cdot x17 \cdot x24) - (k_m14a \cdot x25 \cdot x16) - (k15 \cdot x25 \cdot x26) + (k_m15 \cdot x27 \cdot x24)$$
$$dx26dt = -(k15 \cdot x25 \cdot x26) + (k_m15 \cdot x27 \cdot x24)$$
$$dx27dt = (k15 \cdot x25 \cdot x26) - (k_m15 \cdot x27 \cdot x24)$$
$$dx20dt = k_m13 \cdot x21 - k13p \cdot x20 + k14 - k_m14 \cdot x20 - (k13 + k13pp) \cdot x20$$
$$dx21dt = (k13 + k13p) \cdot x20 - k_m13 \cdot x21 + k13pp \cdot x20$$

Kinetic rate constants (k)

$k1 = 6 \cdot 10^{7}\ M^{-1}min^{-1}$

$k_m1 = 0.2\ min^{-1}$

$k2 = k1$

$k_m2 = 100km1$

$k3 = 2500min^{-1}$

$k_m3 = k1$

$k4 = k_m4/9$

$k_m4 = 0.003min^{-1}$

$k4' = 2.1E\text{-}3min^{-1}$

$k5 = 10k_m5M \cdot min^{-1}$ for $(x6+x7+x8) > 10^{-13}$

otherwise $60k_m5M \cdot min^{-1}$

$k6 = 0.461min^{-1}$

$k7 = 4.16min^{-1}$

$k_m7 = 2.5/\ 7.45 \cdot k7$

$k8 = k_m8 \cdot (5/70.775) \cdot 10^{12}$

$k_m8 = 10min^{-1}$

$k9 = (k9_{stimulated} - k9_{basal}) \cdot (x12/PI3K) + k9_{basal}$

$k9_{stimulated} = 1.39min^{-1}$

$k_m9 = (94/3.1) \cdot k9_{stimulated}$

$k9_{basal} = (0.31/99.4) \cdot k_m9$

$k10 = (3.1/2.9) \cdot k_m10$

$k_m10 = 2.77min^{-1}$

$k11 = (0.1k_m11) \cdot (x13\text{-}0.31)/\ (3.1\text{-}0.31)$

$k_m11 = 10 \cdot \ln(2)min^{-1}$

$k12 = (0.1k_m12) \cdot (x13\text{-}0.31)/\ (3.1\text{-}0.31)$

$k_m12 = 10 \cdot \ln(2)\ min^{-1}$

$k13 = (4/96) \cdot k_m13$

$k_m13 = 0.167min^{-1}$

$k_m14 = 0.001155min^{-1}$

$k13p = (40/60 - 4/96) \cdot 0.08 \cdot 10^{-2} \cdot x27$

$k13pp = (40/60 - 4/96) \cdot 0.07 \cdot 10^{-2} \cdot x22a$

$Irp = 8.97E\text{-}13M$

[SHIP] = 1.00

[PTEN] = 1.00

[PTP] =1.00

$PI3K = 5 \cdot 10^{-15}\ M$

k14a=2.5

$k_m14a=10$

k15=0.4

$k_m15=0.2$

k16=5

$k_m16=100$

Figure 3.S1

Simulations showing the interchangeable use of mRNA and protein activity data in the proposed model

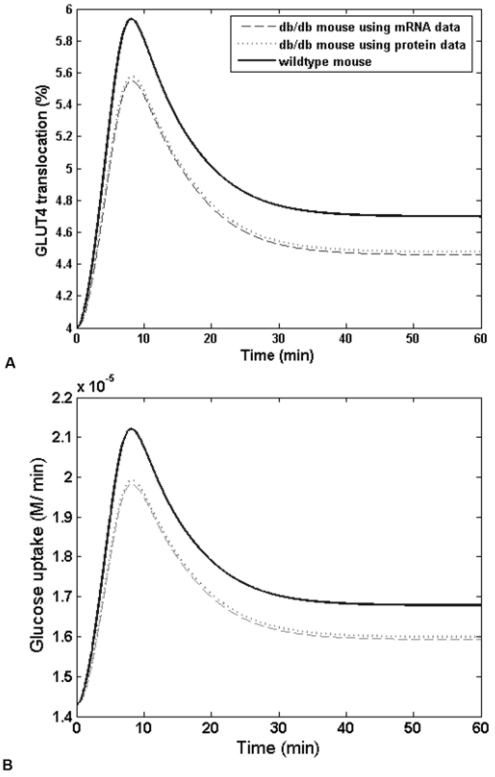

Supplementary Figure 1
Simulation of key insulin signaling gene PTEN expression in diabetic mice. Protein and mRNA data are recorded from Fig. 4Bc of Yu et al. [34]

A. GLUT4 translocation time response curves, db/db mouse (dashed and dotted lines) vs WT mouse (solid line), with a single insulin dose input of 0.1nM and run time of 60 min. ($p<0.05$). Dotted line represents response curve generated using protein activity data of Yu *et al.* Dashed lines represents response curve generated using mRNA data of Yu *et al.*

B. Glucose uptake level time response curves, db/db mouse (dashed and dotted lines) vs WT mouse (solid line), with a single insulin dose input of 0.1nM and run time of 60 min. ($p<0.05$). Dotted line represents response curve generated using protein activity data of Yu *et al.* Dashed lines represents response curve generated using mRNA data of Yu *et al.*

Author Contribution: C.H. performed the simulations and the analysis.

Chapter 4

The Study of Glycerol Kinase Deficiency Mutations in Glycerol Kinase Knock Out Cells

Abstract

A new glycerol kinase knockout model was developed in the cell culture. Using CRISPR/Cas9 recombinase technology, we eliminated *GK* gene expression in human kidney cells. Preliminary data confirmed that over seventy thousand base pairs were truncated from genome of the kidney cells, resulting in the establishment of the *GK* knock out cell line. Gene transfer using lentiviruses was applied to the cell line to develop mutant cells carrying different mutations found in GKD patients. Results show enzymatic activities are reduced in cells with mutations causing GKD, which is consistent with a previous study performed on fibroblasts from the patients with same GKD mutations. Quantitative real-time PCR analysis showed that glucocorticoid receptor responsive genes were differentially expressed in the cells carrying GKD mutations, suggesting that GK's moonlighting activities are critical for the pathogenesis of GKD. In conclusion, we developed a new cell culture design using *GK* knock out cell line complemented with lentiviruses and studied GKD mutations in cells. Our future goals include further studying GKD mutations using the knock out cells, evaluating the functions of the mutant cells, and comparing with phenotypes observed in individuals carrying the same mutations.

Introduction

Glycerol kinase (*GK* in human, *Gyk* in mouse) functions in many tissues such as the skeletal muscles and brain, but it is predominantly expressed in liver and kidney [1]. We aimed to develop more cell culture and mouse models to facilitate the study of GK's

moonlighting functions. Several bioengineering techniques were incorporated into our laboratory practices to inactivate genes in cell culture.

In terms of cell culture technologies, genetic engineering has been developed with custom-designed nucleases. Zinc-finger nucleases (ZFNs) and transcription activator-like effector nucleases (TALEN) are common proteins that recognize DNA genomic sequence [2,3]. By customizing DNA-binding domain of these proteins, it is possible to target any sequence in the genome of a cell. The target sequence is cleaved by the nucleases, introducing a double strand DNA break. When cell repairs the DNA damage, there is a high chance that mutations (e.g. frameshift mutations) are generated to render the protein nonfunctional. In recent years, CRISPR/CAS9 system has emerged to be an efficient alternative to ZFNs and TALENs for targeted genetic alterations. CRISPR, which is short for clustered regularly interspaced short palindromic repeats, is originated from prokaryotic organisms, specifically functions in the immune response system of *Streptococcus pyogenes* [4, 5]. This is a microbial nuclease that acts as a self defense system against invading phages and plasmids. The nuclease generates a guide RNA that targets the foreign invader. Cas9, a recombinase protein, recognizes the guide RNA and cleaves of the foreign DNA. For CRISPR/Cas9 systems, a short noncoding guide RNA, called clustered regularly interspaced short palindromic repeat (CRISPR) RNAs or sgRNA, is made to direct Cas9 protein to sequence-specifically cleave target DNA sequence [6]. CRISPR/CAS9 technology is incorporated into our designs to generate a *GK* knock out cell line.

Our goal for developing new GK study models was to study the alternative roles of *GK*, for which the current GK study models may not achieve. To test our knockout cell

line, we employed a site-directed mutagenesis approach, which allows for generation of different DNA variants of *GK* (e.g. cells with GKD mutations) and study the functions of these variants in cells.

Materials and Methods

HEK293T Cell Culture

HEK-293T were grown at 37 ˚C in a humidified atmosphere containing 5% CO2 in Dulbecco's modified Eagle's medium (DMEM), containing 10% Fetal Bovine Serum (FBS) and 1% Penicillin-Streptomycin Solution (PS) [6]. Prior to stable transfection on day 0, cells were seeded at one hundred thousand cells in a 12-well plate. For lentiviral transfection, cells are seeded at five million cells in a 10cm plate. Transfection can be performed above 75% confluency.

Construction of the Human GK Knockout Cell Line

The knockout cell line is generated using the type II CRISPR nuclease system developed by Cong *et al.* [7]. There are many Cas9 targets sites in human *GK*, but two Cas9 target sites located in exon 1 & exon 17 are chosen to maximize truncation extents. A pX330-GK expression vector was constructed by ligating the cDNA encoding one of the target sequences between the two BbsI sites of the pX330 vector. Consequently, two expression vectors were made to allow for two Cas9 cleaving events in exon 1 and exon 17 of GK. The expression vectors (pX330-GKex1 and pX330GKex17) (1ug of each vector) are co-transfected with 100ng of puromycin into the HEK-293T cells using Lipofectamine 200 transfection reagent as per the manufacturer's protocol (Life Technologies, Grand Island,

NY). Screening of transfected cells were performed by dilution screening technique of single cell clone assisted by incubating cells in puromycin at working concentration of 5ug/ml [8]. PCR and Sanger sequencing were performed to verify the cleaving/ repair sites for each clone. Sequencing data was analyzed using Sequencher DNA sequence analysis software (Gene Codes Corp, Ann Arbor, MI).

Generation of the GKD Mutants

The pRRL.CMV.IRES.GFP lentiviral expression vector was used as the backbone for infection of mutant *GK* constructs into the *GK* KO cells. The pRRL-GK lentiviral expression vector was constructed by ligating the cDNA encoding *hGK* into the BamHI and XmaI sites of the lentiviral vector. Mutant constructs are created using site directed mutagenesis using pRRL-GK as the starting product (Stratagene, Santa Clara, CA). The mutants had the same mutations as individuals with GKD reported in Dipple et al.[9]. We have chosen to study the mutation (N288D [altering the asparagine at codon 288 to aspartic acid], A305V[Alanine to Valine at codon 305], Q438R[Glutamine to Arginine at codon 438, and Q403X[Glutamine to Stop at codon 403]). Lentiviruses, with the ability to introduce GKD mutations to cells, were made co-transfecting GK constructs with 2 packaging plasmids (pMDLg/pRRE and pRSV-Rev) and one envelope plasmid (pMD2.G). These three plasmids, along with our pRRL-GK constructs, termed the 3rd generation lentiviral packaging systems, were co-transfected into HEK-293T human kidney cells to generate lentiviruses. Viral supernatant were harvested 72 hr after transfection. Transfection efficiency was assessed quantitatively using QuickTiter Lentivirus Titer Kit (Cell Biolabs, inc., San Diego, CA) per manufacturer's instructions

and visually by GFP expression using a fluorescent microscope. Lentiviruses were either used for infection directly following harvest or stored in -80˚c.

Lentiviral Transfection of *GK* Mutants

hGK knock out cells were seeded in 6 well plates and were infected at 50% confluence using Multiplicity of infection (MOI) of 10 for each well. Virus supernatants were applied to cells in Dulbecco's modified Eagle's medium DMEM containing 10% FBS and 10ug/ml polybrene in a final volume of 1ml. Cells were incubated with viral supernatant overnight and virus-containing media was replaced with DMEM containing 10% FBS on the following day. Flow cytometry was used at initial testings to access the efficiency of infection. Cells were grown to confluence before harvesting for experiments.

RNA Isolation and cDNA Synthesis

Total RNA was isolated from cell lines using the GeneJET RNA purification kit (Thermo Scientific, Pittsburgh, PA) per manufacturer's instructions. RNA was further purified using Turbo DNA-free DNase treatment (Life Technologies, Grand Island, NY). Purified RNA was visualized on agarose gel and its concentration was quantified using a NanoDrop spectrophotometer (NanoDrop Technologies, Wilmington, DE). cDNA was synthesized using Superscript III First-Strand systems (Life Technologies, Grand Island, NY) per manufacturer's instructions with random hexamers as primers. cDNA samples were diluted to an optimized concentration of 1ng/uL.

Western Blotting

Cells were collected by scraping in 1% KCl/EDTA buffer supplemented with protease inhibitor. Proteins were extracted from cells by sonication. And protein concentration was determined by BCA assay [10]. 100ug of protein were separated on a 4-12% Bis-Tris NuPage gel (Life Technologies, Grand Island, NY) and electroblotted onto a polyvinylidene difluoride (PVDF) membranes at 100 volts for an hour. The membranes were blocked in 0.01M PBS, 0.05% Tween 20 buffer (PBST) containing 10% blotto overnight at 4 °C. Primary antibodies, including anti-GK (ab70029, Abcam, Cambridge, MA) and anti-GR (sc-8992, Santa Cruz Biotechnology, Dallas, Texas) were incubated overnight at 4°C at a concentration 1:1000 dilution, followed by secondary antibodies for 1 hour at room temperature. Immunoreactive bands were visualized by ECL plus kit (Amersham Biosciences, Piscataway, NJ), per manufacturer's protocol. All membranes were subjected to stripping using 1M NaOH for 10 min at room temperature, reblocked, and reprobed for B-actin (Life Technologies, Grand Island, NY) at a concentration of 1:3000 overnight at 4°C, and secondary antibody, goat anti-rabbit HRP, at a concentration of 1:5000 for 1 hour at room temperature and developed using Amersham ECL Plus Westeren Blotting Detection Kit (GE Healthcare Bio-Sciences, Pittsburgh, PA).

Quantitative Real Time PCR (qRT-PCR)

All assays were carried out using PerfeCTa SYBR Green FastMix (Quanta Biosciences, Gaithersburg, MD) with QuantiTect (Qiagen, Valencia, CA) primer assays. Cells were treated with 100nM dexamethasone for 24 hours, after which RNA was isolated. Genes assayed included glucocorticoid receptor (GR) responsive genes [tyrosine

aminotransferase (*TAT*), and phosphoenolpyruvate carboxykinase (*PEPCK*)], adipogenic genes (fatty acid binding protein 4 (*FABP4/aP2*) and CCAAT enhancer-binding protein (*C/EBPα*), non-GR responsive gene Cadherin-15 (*CDH15*), and lastly endogenous control beta-actin (*ACTB*). Primer pairs for real-time PCR were designed using the human primer depot database (http://primerdepot.nci.nih.gov/). 1ng of cDNA was loaded into each reaction, which was detected using ABI prism 7500 Sequence detection system. Each sample was assayed in duplicate and each reaction was replicated as least once. Fold changes for each of the genes were determined using the $2^{(-\text{Delta Delta CT})}$ method [11].

GK Enzymatic Assay.

A radiochemical assay described previously [12] was used to determine the GK enzymatic activity. Each mutant was assayed in duplicate with 4ug of total cellular protein (for HEK-293T cells) for 20 minutes. For each assay, the scintillation count was plotted against the amount of protein, and the counts per minute (CPM) was proportional to relative GK enzymatic activity.

Results

Generation of the *GK* Knock Out Cell Line using CRISPR/CAS9 Technology

CRISPR/ Cas9 nuclease system was introduced to HEK-293T human kidney cells to generate a knock out cell line. Amino acids coding exons 1-17 of *GK* have been eliminated from the genomic DNA of the HEK-293T cells, resulting in the creation of a *hGK* KO liver cell line. The truncation sites for each individual clone were verified using Sanger sequencing. The cut sites were consistently located at the intended target site.

However, the repair sites for each clone varied among clones. The basis of using the CRISPR technology in a mammalian system was to take advantage of mammalian cells that were capable of repairing DNA break and removing a small snip of DNA. The self repair system in mammalian cells allowed the cells to recover, but ultimately rendered the gene nonfunctional. For one particular clone (Fig. 4.1), a cut was made after the 10^{th} codon of the gene, between the first and second codon position of Proline 11. A frameshift was observed on the 12^{th} codon, in which the next codon after Proline turned out to be Serine 510 of GK. The estimated amount of truncated genomic DNA material for this particular clone was seventy thousand base pairs. Western blot analysis of the KO cells using an anti-GK antibody showed no signals (lane 6 in Fig. 4.2A and Fig. 4.2B), indicating that no fully translated GK proteins was made and the KO was successful. We infected these KO cells with lentiviruses containing GKD mutations seen in human GKD patients (lane 2-5 in Fig. 4.2). Using lentiviruses that can infect cells with normal GK proteins, the production of rescue hGK proteins was rescued in KO cells (lane 1 in Fig. 4.2).

The GKD mutant variants were characterized based on enzymatic activity and ASTP activity levels. GK enzymatic assay was used to characterize the enzymatic activity of GKD mutants (e.g. N288D, A305V, Q403X, Q438R) generated from KO cells. As done previously by our group [9], however the cell types used in that particular experiment were lymphocytes collected from actual GKD patients. Dipple *et al.* reported that individuals with the N288D mutation had 5.53% of GK activity compared to normal individuals [9]. This analysis also yielded similar results to the data published by Dipple *et al*., showing that N288D mutants had 4.32% of GK activity of the wild type (Table 1).

Other mutants showed reduced enzymatic activity as well. GKD mutants A305V, Q403X, and Q438R had reduced GK enzymatic activity of 7.34%, 6.04%, and 5.44% , respectively. These results were comparable to those reported in Dipple *et al.,* which provide supporting evidence that this combination of the knockout and the lentivirus designs can be used to study GKD mutations.

To assess the ASTP activity of these GKD mutants, quantitative real time PCR analysis of GR responsive genes (e.g. *TAT* and *PEPCK*) were assayed. Cells were incubated in media with or without dexamethasone (DEX) prior to harvest. The change in mRNA levels of GR responsive genes *TAT* and *PEPCK* in response to DEX activation was our means of determining ASTP activity. qRT-PCR analysis showed that HEK293T cells normally had 1.6 fold increase *TAT* expression in response to DEX activation (Fig. 4.3A). However, GK knockout cells completely lost the effect of *TAT* upregulation in response to DEX activation, confirming that GK knock outs lacked ASTP activity (Fig. 4.3A). When the GK knockout cells were infected with hGK-infecting lentiviruses, the *TAT* expression pattern was rescued (Fig. 4.3A). These results also supported that our cell culture design can be used to characterize GKD variants. In the same analysis, rescue had 1.6-fold increase *TAT* expression in response to DEX activation. On the other hand, *TAT* is upregulated in KO cells by only 1.1-fold in response to DEX activation, suggesting that there is a reduction in *TAT* activity in KO cells (Fig. 4.3B and Table 4.1). Similar to KO, *TAT* is only upregulated in A305V and N288D by 1.1 fold and 1.3-fold, respectively, in responsive to DEX. Q403X and Q438R both had an increased *TAT* expression of 1.0-fold in response to DEX (Fig. 4.3B and Table 4.1). These results suggested that GKD mutants have reduced ASTP activity due to the GKD mutations. To verify the finding, another

GR-responsive gene *PEPCK* was used to test ASTP activity of these mutants. Rescue had 1.8-fold upregulation in response to DEX (Fig. 4.3C and Table 4.1). Both A305V and N288D both had a 1.2-fold upregulation of *PEPCK* in response to DEX, significantly less than the response of the rescue. Similarly, Q438R had 1.4-fold upregulation and Q403X only had residual amount of ASTP. This test demonstrated that the GKD mutants have significant reduced ASTP compare to the rescue.

To investigate the downstream effects upon glucocorticoid receptor activation, qRT-PCR analysis was performed using a set of genes that are direct functional targets of GR in hepatocytes. The chosen set of genes are particularly important for metabolic functions, including adipose differentiation, insulin signaling and mitochondrial activity. We first examined the change of mRNA level in response to GR activation within each mutants, then compared the fold differences to that of the wild type rescue. Insulin-like growth factor binding proteins (*Igfbp1*) is normally upregulated by 1.4-fold in response to GR activation, but the upregulation is significantly reduced to 1.2 to 1.3-fold in the GKD mutants (Fig.4.4A and Table 4.1); lipase (*Lipc*) is normally upregulated by 2.0-fold in response to GR activation, but the upregulation is also significantly reduced to 1.5 to 1.6-fold in the GKD mutants (Fig.4.4C and Table 4.1). In contrast, adipose differentiation related protein (*Adfp*) is normally upregulated by 1.6-fold, but we observed high gene regulation of up to 1.8 to 2.1-fold in the GKD mutants (Fig. 4.4B and Table 4.1). Our results demonstrate that many GR direct gene targets are differentially regulated in response to GR activation as a result of GK mutations.

Discussion

The recombinase technology, specifically CRISPR/Cas9, provided an efficient knock out model that would be easy to use in the cell culture setting. In short, CRISPR/Cas9 target sequence starts with a guanine then 20 random nucleotides ,and ends with 2 guanine. This target sequence is called the PAM domain. Recently, Zhang lab from MIT implemented this recombinase system to be useful in mammalian cells, by showing that the efficiency of site specific DNA cleavage using CRISPR/CAS9 is much higher than existing technology, TALEN and Zinc finger nucleases [13]. They engineered a plasmid that expresses both human CAS9 and the noncoding RNA with cloning site so that we can design a target site, allowing for DNA cleavage of our favorite gene. When the DNA breaks are created in the mammalian cells, the cells will repair the damage and create a frameshift mutation in the gene if one target site is incorporated. In addition, a large truncation in the gene can be generated if two target sites are used instead of one. In the proposed design, two target sites located in exon 1 and 17 of *GK* were designed into the expression plasmid in order to cleave out a total of seventy thousand base pairs of genomic material in the human cells.

CRISPR/CAS9 system coupled with the use of lentiviruses enable gene manipulated in human cells, whether one wants to knock out or rescue the expression, showed promising results shown in this study. Both enzymatic activity and ASTP activity were affected by the mutations causing GKD. Enzymatic activity of all GKD mutants is minimal, and the data is comparable and is consistent with the human studies [14]. The ASTP analysis showed that GKD individuals have either reduced or even lack of ASTP activity. Based on the qRT-PCR analysis, Q403X nonsense mutation completely lacked

ASTP because GR responsive genes, *TAT and PEPCK*, in the Q403X mutant cells did not respond to the GR activation. The change in amino acids, causing GKD, may have caused a conformational change of the glycerol kinase protein and hindering its interaction with GR.

Since we observed reduced ASTP activity in GKD mutants, all downstream genes in response to glucocorticoid receptor activation should be affected. We sought to use qRT-PCR to determine which downstream mechanisms are affected by GK-GR interactions. qRT-PCR data showed that only some genes were affected by the GK mediated GR transcriptional activation. adipose differentiation gene (*ADFP*) and insulin signal transduction gene (*IGFBP1*)were differentially regulated in the mutants due to GK-mediated GR transcriptional activation. For example, the data suggested that lower regulation of insulin signaling gene *IGFBP1* due to GKD mutations affecting ASTP activity. *ADFP* was significantly upregulated due to GKD mutations affecting ASTP activity. The changes in gene regulation due to GKD mutations observed in this study correlates with other studies. In the mathematical modeling study reported in the previous chapter, the simulations of our model predicted that GK knockout mice have reduced insulin signal transduction activity. In the diet study of the transgenic animals, we also demonstrated that the transgenic mice become obese with elevated levels of cholesterol and fasting insulin. The results reported using the proposed strategy have been consistent with previous studies. Future experiments will be to use next generation sequencing to determine all genes and pathways affected in each individual GKD mutations.

CRISPR/Cas9 for genome engineering is evolving quickly towards *in vivo* studies. It has been shown that mutant mice can be generated *in vivo* by injecting Cas9 RNA and

guide RNA (sgRNA) into mouse ES cells [7, 15, 16]. Also, simultaneous targeting of multiplexed genes can be achieved by cotransfecting multiple sgRNAs with the Cas9 expressing plasmid [7]. By incorporating a tissue specific promoter that drives Cas9 expression in the Cas9-expressing adenoviral plasmid, one can inject vectors directly to any tissue of interests [16]. This allows for *in vivo* studies of gene function in specific tissue. Future goal is to generate a conditional knock out mouse model using one of these new CRISPR designs. As we continue to reveal the association between GK and obesity/T2DM, it may be interesting to knock out the gene expression in other tissues such as liver, skeletal muscle, and heart.

References

1. MacLennan, N.K., Rahib, L., Shin, C., Fang, Z., Horvath, S., Dean, J., Liao, J.C., McCabe, E.R., and Dipple, K.M. (2006). Targeted disruption of glycerol kinase gene in mice: expression analysis in liver shows alterations in network partners related to glycerol kinase activity. Human molecular genetics *15*, 405-415.

2. Urnov, F.D., Rebar, E.J., Holmes, M.C., Zhang, H.S., and Gregory, P.D. (2010). Genome editing with engineered zinc finger nucleases. Nature reviews Genetics *11*, 636-646.

3. Christian, M., Cermak, T., Doyle, E.L., Schmidt, C., Zhang, F., Hummel, A., Bogdanove, A.J., and Voytas, D.F. (2010). Targeting DNA double-strand breaks with TAL effector nucleases. Genetics *186*, 757-761.

4. Horvath, P., and Barrangou, R. (2010). CRISPR/Cas, the immune system of bacteria and archaea. Science *327*, 167-170.

5. Marraffini, L.A., and Sontheimer, E.J. (2010). CRISPR interference: RNA-directed adaptive immunity in bacteria and archaea. Nature reviews Genetics *11*, 181-190.

6. Zhu, X., Xu, Y., Yu, S., Lu, L., Ding, M., Cheng, J., Song, G., Gao, X., Yao, L., Fan, D., Meng, S., Zhang, X., Hu, S., Tian, Y. (2014). An efficient genotyping method for genome-modified animals and human cells generated with CRISPR/Cas9 system. Scientific reports *4*, 6420.

7. Cong, L., Ran, F.A., Cox, D., Lin, S., Barretto, R., Habib, N., Hsu, P.D., Wu, X., Jiang, W., Marraffini, L.A., Zhang, F. (2013). Multiplex genome engineering using CRISPR/Cas systems. Science *339*, 819-823.

8. Lacalle, R.A., Pulido, D., Vara, J., Zalacain, M., and Jimenez, A. (1989). Molecular analysis of the pac gene encoding a puromycin N-acetyl transferase from Streptomyces alboniger. Gene *79*, 375-380.

9. Dipple, K.M., Zhang, Y.H., Huang, B.L., McCabe, L.L., Dallongeville, J., Inokuchi, T., Kimura, M., Marx, H.J., Roederer, G.O., Shih, V., Yamaguchi, S., Yoshida, I., McCabe, E.R.(2001). Glycerol kinase deficiency: evidence for complexity in a single gene disorder. Human genetics *109*, 55-62.

10. Bradford, M.M. (1976). A rapid and sensitive method for the quantitation of microgram quantities of protein utilizing the principle of protein-dye binding. Analytical biochemistry *72*, 248-254.

11. Livak, K.J., and Schmittgen, T.D. (2001). Analysis of relative gene expression data using real-time quantitative PCR and the 2(-Delta Delta C(T)) Method. Methods *25*, 402-408

12. McCabe, E.R., Fennessey, P.V., Guggenheim, M.A., Miles, B.S., Bullen, W.W., Sceats, D.J., and Goodman, S.I. (1977). Human glycerol kinase deficiency with hyperglycerolemia and glyceroluria. Biochemical and biophysical research communications *78*, 1327-1333.

13. Zhang, Q., Rho, M., Tang, H., Doak, T.G., and Ye, Y. (2013). CRISPR-Cas systems target a diverse collection of invasive mobile genetic elements in human microbiomes. Genome biology *14*, R40.

14. Wang, H., Yang, H., Shivalila, C.S., Dawlaty, M.M., Cheng, A.W., Zhang, F., and Jaenisch, R. (2013). One-step generation of mice carrying mutations in multiple genes by CRISPR/Cas-mediated genome engineering. Cell *153*, 910-918.

15. Mali, P., Yang, L.H., Esvelt, K.M., Aach, J., Guell, M., DiCarlo, J.E., Norville, J.E., and Church, G.M. (2013). RNA-Guided Human Genome Engineering via Cas9. Science *339*, 823-826.

16. Swiech, L., Heidenreich, M., Banerjee, A., Habib, N., Li, Y., Trombetta, J., Sur, M., and Zhang, F. (2015). In vivo interrogation of gene function in the mammalian brain using CRISPR-Cas9. Nature biotechnology *33*, 102-106.

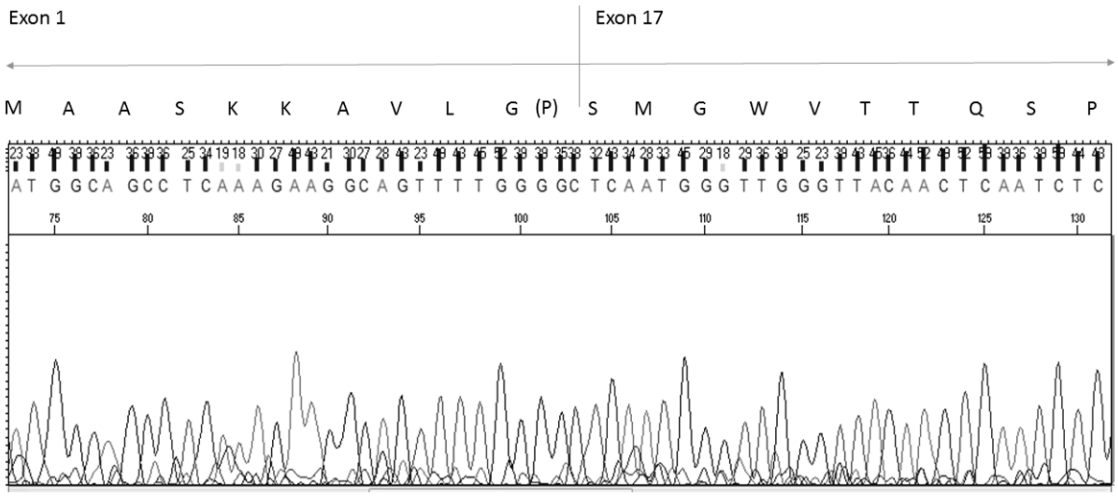

Figure 4.1 Sequence data of a glycerol kinase knock out clone

Sequencing chromatogram was captured using Sequencher sequence analysis software. The five nucleotides (e.g. GGGCT) highlighted in black showed the joint location of exon 1 and exon 17.

Author Contribution: Sequencing reactions were performed by Laragen sequencing services. C.H. performed CRISPR work and analyzed the sequencing data.

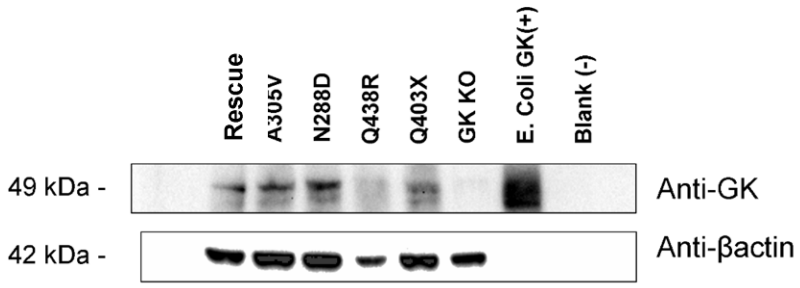

Figure 4.2A Western blot analysis of the GKD mutants in HEK293T *GK* knockout cells.

Western blot analysis of wild type rescue (lane 1), GKD mutants (A305V, N288D, Q438R, and Q403X) (lane 2-5) and *GK* knockout cells(*GK*KO) (lane 6). GKD mutant cells and WT rescue cells were made by infecting *GK* KO with lentiviruses. *E. coli* GK is used as a positive control (lane 7) and PBS was used as a blank control (lane 8). Blot was probed with anti-βactin as internal control.

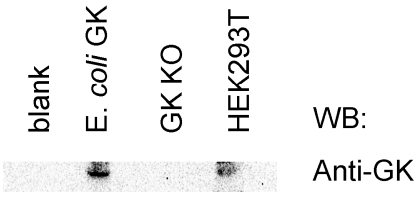

Figure 4.2B Western blot analysis of HEK293T parental cells

GK knock out cells (*GK* KO) were derived from HEK293T parental cells

Author Contribution: C.H. performed the tissue culture experiments, isolated protein extracts, and performed the Western blot.

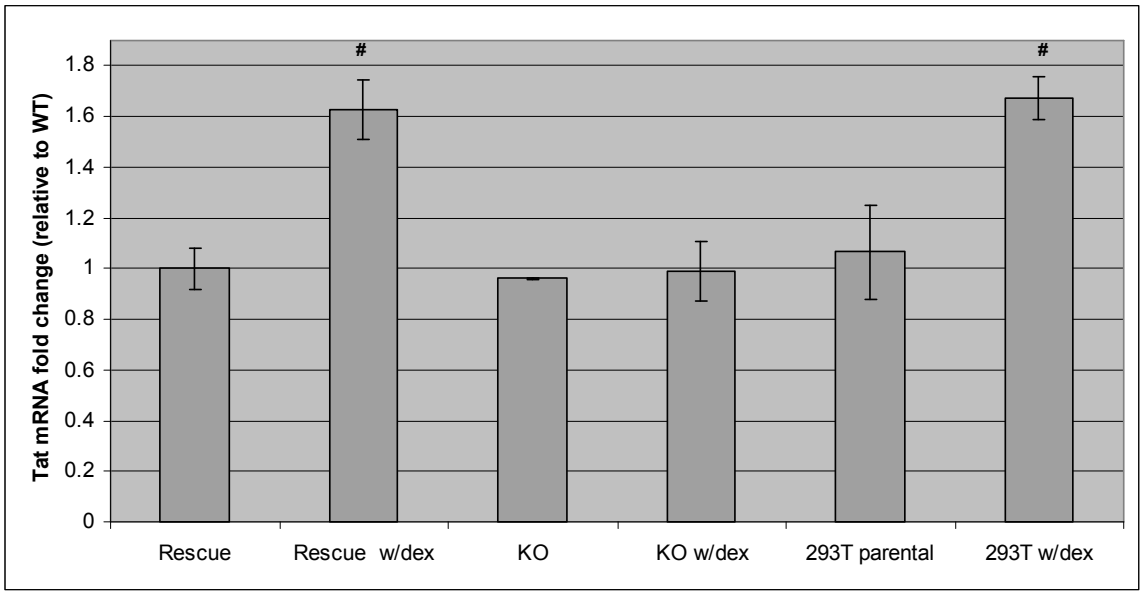

Figure 4.3A Quantification of ASTP activity, *TAT*, expression by quantitative real time PCR in knock out cells. Data shows gene expression levels for *GK* knockout cell line (KO), rescued GK (Rescue), or 293T parental cell line with (w/dex) or without dexamethasone. #$p<0.05$ compared to WT.
Author Contribution: C.H. performed all quantitative RT-PCR experiments.

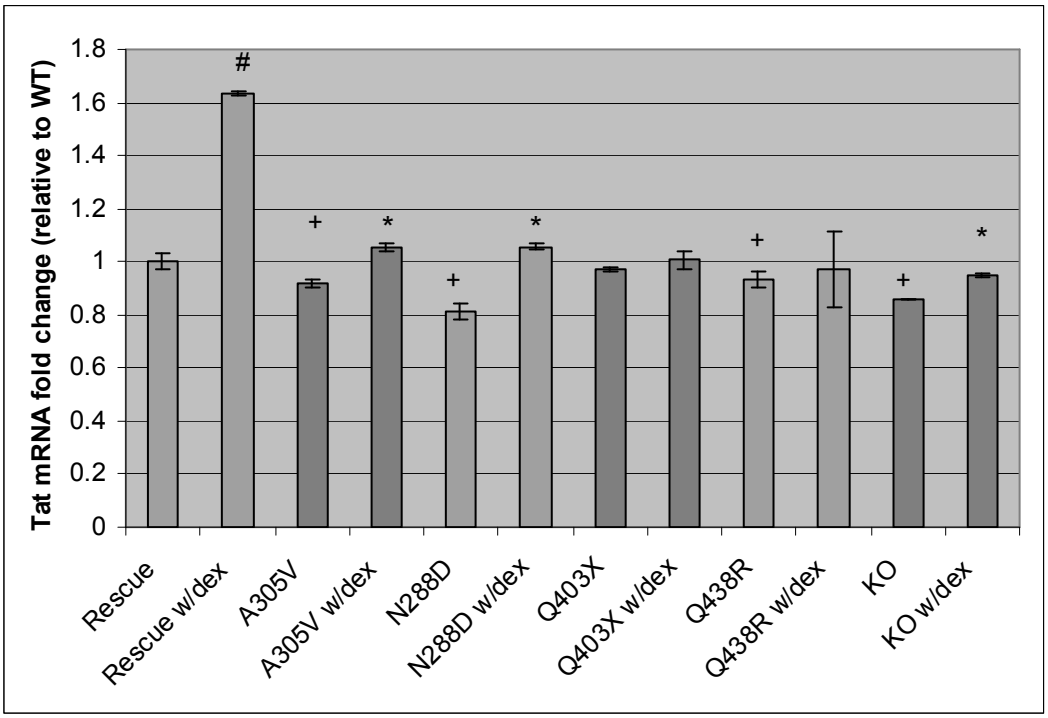

Figure 4.3B Quantification of ASTP activity, *TAT*, expression by quantitative real time PCR. Gene expression levels for GKD mutants (A305V, N288D, Q403X, and Q438R)) and *GK* knockout cell line (KO) compared to rescue with wildtype GK (Rescue) with (w/dex) or without dexamethasone. (#) $p<0.05$ Rescue vs Rescue w/dex. (*) $p<0.05$ mutant samples with dexamethasone compared to same mutant. (+) $p<0.05$ samples w/o dexamethasone compared to rescue

Author Contribution: C.H. performed all quantitative RT-PCR experiments.

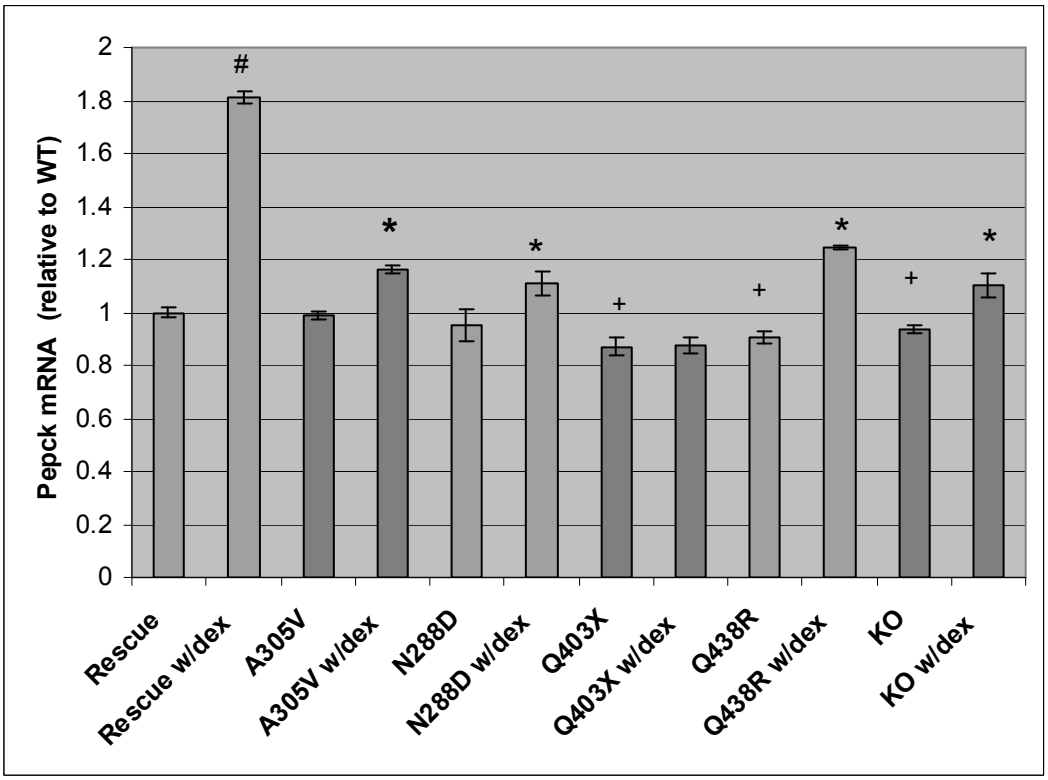

Figure 4.3C Quantification of ASTP activity, *PEPCK*, expression by quantitative real time PCR. Gene expression levels for GKD mutants (A305V, N288D, Q403X, and Q438R)) and GK knockout cell line (KO) compared to the rescue with wildtype GK (Rescue) with (w/dex) or without dexamethasone. (#) $p<0.05$ Rescue vs Rescue w/dex. (*) $p<0.05$ samples with dexamethasone compared to WT w/dex. (+) $p<0.05$ samples w/o dexamethasone compared to rescue

Author Contribution: C.H. performed all quantitative RT-PCR experiments.

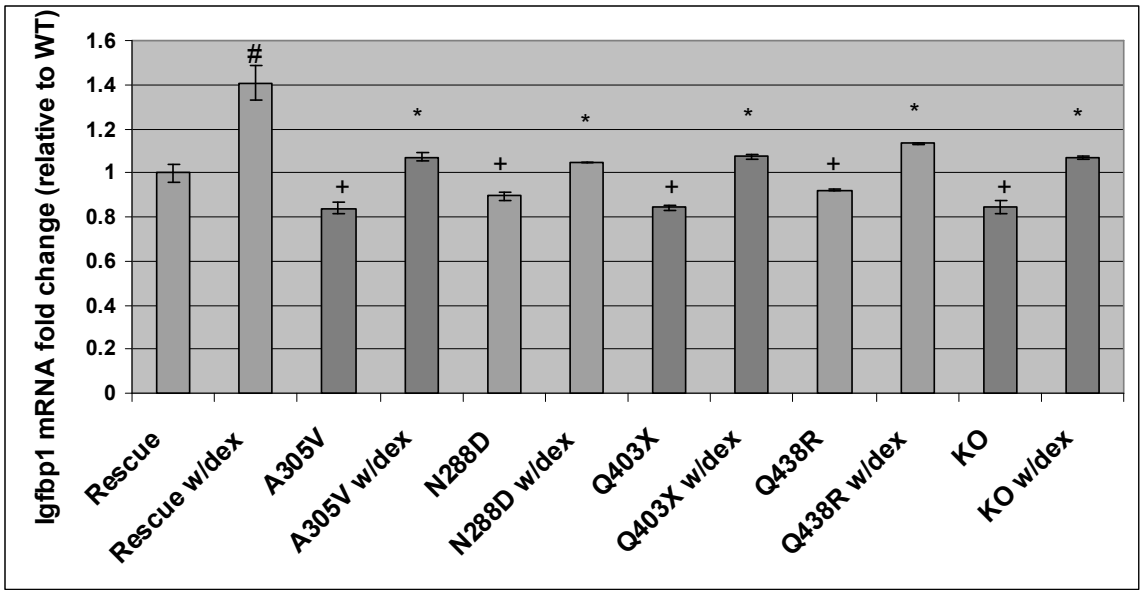

Figure 4.4A GR-responsive gene insulin growth factor binding protein 1(*Igfbp1*) expressions of GK mutants. Gene expression levels for GKD mutants (A305V, N288D, Q403X, and Q438R)) and GK knockout cell line (KO) compared to the rescue with wildtype GK (Rescue) with (w/dex) or without dexamethasone. (#) $p<0.05$ WT vs WT.dex. (*) $p<0.05$ mutant samples with dexamethasone compared to same mutant. (+) $p<0.05$ samples w/o dexamethasone compared to WT

Author Contribution: C.H. performed all quantitative RT-PCR experiments.

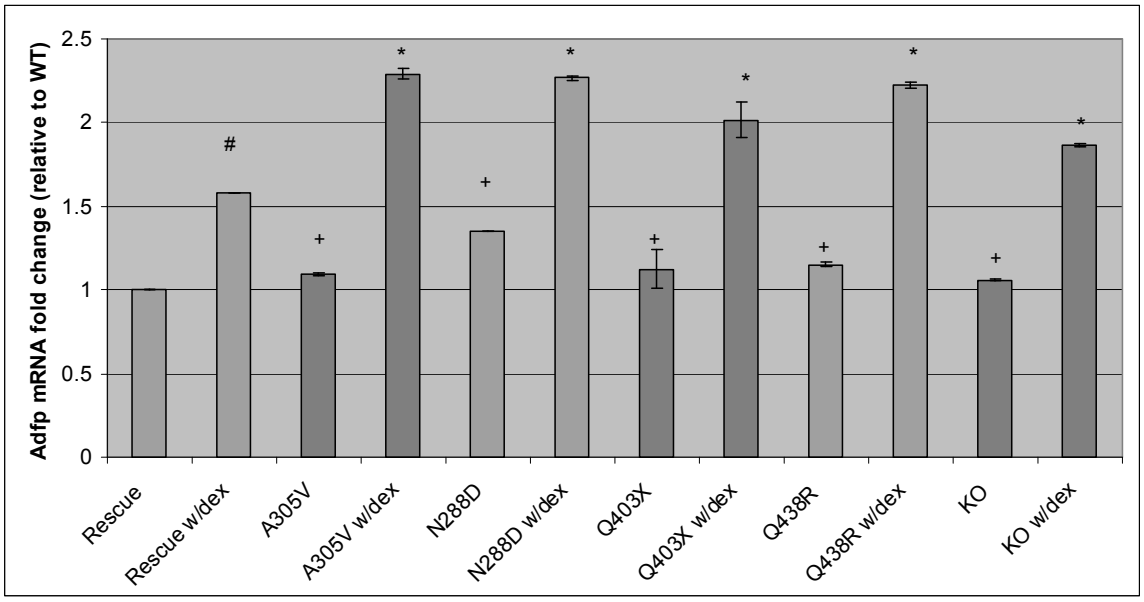

Figure 4.4B GR-responsive gene adipose differentiation-related protein (*Adfp*) expressions of GK mutants. Gene expression levels for GKD mutants (A305V, N288D, Q403X, and Q438R)) and GK knockout cell line (KO) compared to the rescue with wildtype GK (Rescue) with (w/dex) or without dexamethasone. (#) $p<0.05$ WT vs WT.dex. (*) $p<0.05$ mutant samples with dexamethasone compared to same mutant. (+) $p<0.05$ samples w/o dexamethasone compared to WT

Author Contribution: C.H. performed all quantitative RT-PCR experiments.

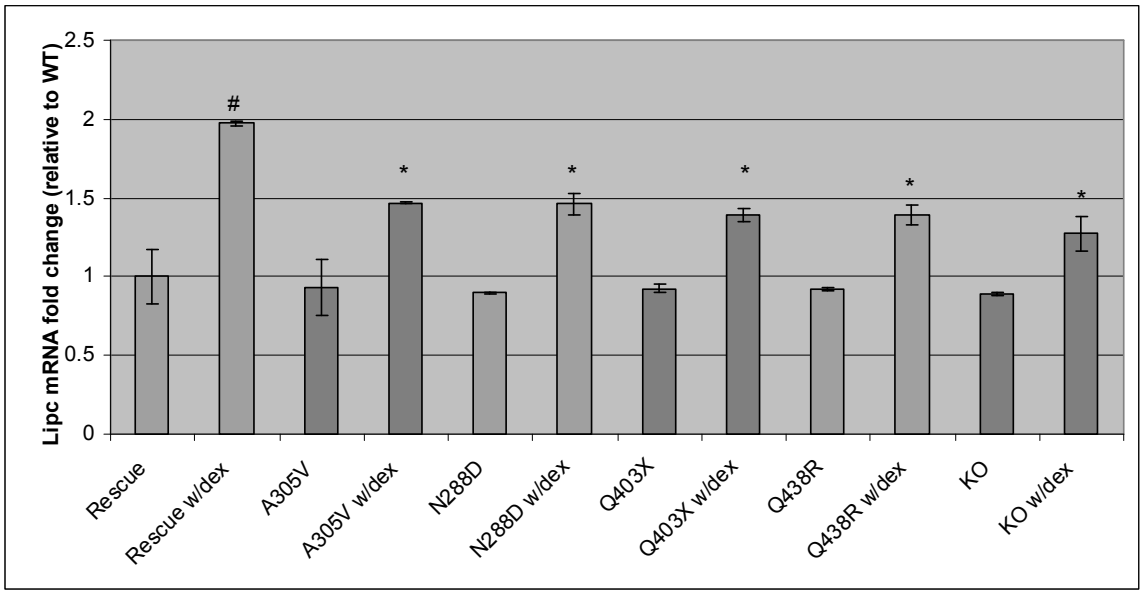

Figure 4.4C GR-responsive gene lipase (*Lipc*) expressions in response to GK mutations. Gene expression levels of GK mutants (A305V, N288D, Q403X, and Q438R)) and GK knockout cell line (KO) compared to the rescue with wildtype GK (Rescue) with (w/dex) or without dexamethasone. (#) $p<0.05$ WT vs WT.dex. (*) $p<0.05$ samples with dexamethasone compared to WT.dex. (+) $p<0.05$ samples w/o dexamethasone compared to WT

Author Contribution: C.H. performed all quantitative RT-PCR experiments.

Table 4.1 Glycerol kinase enzymatic activity and ASTP activity of the GKD mutants

Enzymatic activity levels are measured in the units of count per minute (CPM) by a scintillation counting instrument. GK activity values are expressed as percentage of GK activity in mutant cells relative to GK activity in rescue. ASTP activity is reported as the difference in the mRNA levels of a gene in response to dexamethasone treatment (e.g. a value of 1.63 means 63% increase in mRNA level in response to DEX).

	GK activity (%)	GK activity published by Dipple *et al*. [9] (%)	ASTP activity (*TAT*)	ASTP (*PEPCK*)	ASTP (*IGFBP1*)	ASTP (*ADFP*)	ASTP (*LIPC*)
Rescue	100	100	1.63±0.02	1.81±0.02	1.41±0.01	1.58±0.01	1.97±0.01
HEK293T	98±0.01	NA	1.6±0.02	1.79±0.02	1.40±0.03	1.61±0.02	2.01±0.02
N288D	4.32±0.12	5.53	1.29±0.01	1.16±0.04	1.17±0.02	1.67±0.01	1.62±0.02
A305V	7.34±0.09	5.81	1.14±0.00	1.17±0.00	1.27±0.06	2.09±0.04	1.57±0.05
Q403X	6.04±0.00	NA	1.03±0.11	1.00±0.04	1.27±0.01	1.79±0.03	1.50±0.02
Q438R	5.44±0.03	5.83	1.04±0.01	1.37±0.01	1.23±0.06	1.93±0.01	1.51±0.02
KO	0.110±0.06	NA	1.03±0.01	1.13±0.01	1.26±0.00	1.76±0.01	1.43±0.01

Author Contribution: C.H. performed GK enzymatic activity assay and the qRT-PCR for the ASTP assays.

Chapter 5

Protein-Protein Interaction Between Glycerol Kinase and Glucocorticoid Receptor

Abstract

Glycerol kinase (GK) is a moonlighting protein with multifunctional roles unrelated to its main functions. These alternative roles of GK can potentially regulate transcriptional and translational activities with metabolic properties. Since there is currently no satisfactory explanation of the pathogenesis of glycerol kinase deficiency (GKD) based on its enzymatic activity, we hypothesized that the moonlighting roles of GK are important contributors to the phenotypes observed in individuals with GKD. Of particular interest, we emphasized the protein-protein interaction of GK and glucocorticoid receptor (GR). Biochemical analysis using dot blots and immunoprecipitation/western blots confirmed that GK is the ATP-stimulated translocation promoter (ASTP) which translocates wR complex to the nucleus where it can be involved in transcriptional activation. Using a combined bioinformatics and mutagenesis approach, we show that the LXXLL motif of GK is critical for the ASTP activity of GK. Mutations were created in the LXXLL of GK that resulted in differential gene expression of many GR target genes, including *TAT* and *PEPCK*. Our data suggested that the altered expression of these GR responsive genes may play a significant factor in affecting the phenotype observed in individuals with GKD.

Introduction

Glycerol kinase (GK) is an enzyme that catalyzes the phosphorylation of glycerol, a reaction important for glycolysis or gluconeogenesis in central carbon metabolism and the formation of triglycerides for fat storage in lipid metabolism. Aside from its enzymatic function, GK is a moonlighting enzyme that performs other cellular activities

[1]. Moonlighting enzymes are defined as proteins with at least two different functions within a single polypeptide chain. These functions can be unrelated to its main functions and can occur within or outside of the cell [2]. In fact, many glycolytic enzymes are known to be moonlighting enzymes that are capable of regulating transcriptional and translational activities of the biological systems. GK's enzymatic functions are well defined, but the importance of its moonlighting functions is not well understood [2].

Many of GK's moonlighting functions have been proposed from previous studies. GK has been shown to interact with histones, which are proteins important in DNA folding[3]. GK's other protein-protein interactions include interacting with voltage-dependent anion-selective channel protein called porins at the surface of the outer mitochondrial membrane [4]. Moreover, GK is an ATP-stimulated translocation promoter (ASTP) [5] that promotes the translocation of activated glucocorticoid-glucocorticoid receptor (GR) complex to the nucleus for transcriptional activation of GR-responsive genes. We hypothesized that the disruption of these interaction may potentially have significant effect on the phenotypes of glycerol kinase deficiency (GKD). In this chapter, we concentrate on the protein-protein interaction between GK and GR, the ASTP interaction. Specifically, we aimed to investigate the interactions of GK and GR and the downstream effects of glucocorticoid responsive gene expression.

Previous GK studies have shown that GKD may be affected by moonlighting activities of GK [6,7, 8, 9, 10]. First of all, in the isolated form of GKD (iGKD), there is a lack of genotype and phenotype correlation, which means that family members with same mutation can present with different phenotypes [7]. For example, there was a case where only one of the two nonidentical twins, with the same GKD nonsense mutation Q403X,

have been found with symptomatic symptoms [8]. Also, recent studies showed that individuals with the specific N288D mutation in *GK*, resulting in GKD, revealed a link between GK and obesity [8]. Individuals with GKD mutations only have residual amount of phosphorylation activity. Since adipogenesis, obesity and type II diabetes mellitus are involved in many mechanisms of the metabolic pathways, we strongly believe that at least one of GK's moonlighting functions contributes to the phenotype of GKD. In another metabolic study at our laboratory, H4IIE rat hepatoma cells with *GK* over-expression showed altered fluxes in the carbon metabolism, especially in the pentose phosphate pathway and lipid synthesis [9]. Many other biological pathways and relating genes were significantly altered including insulin signaling genes and steroid biosynthesis genes [6, 10]. We hypothesized that the changes in gene expression and altered metabolic fluxes through these pathways are results of differential GK enzymatic activity and ASTP activity.

Glucocorticoid Receptor

Glucocorticoids are steroid hormones, secreted by the adrenal cortex, that are mainly used as immune suppressant and anti-inflammatory agent. They bind to the glucocorticoid receptor (GR), which is a member of the nuclear receptor superfamily of ligand-activated transcription factors. When glucocorticoids are absent, GR forms a protein complex with heat shock protein 70 and HSP 90 in the cytoplasm [11, 12, 13]. When glucocorticoids are available, they travel to the plasma membrane and bind with GR [14]. This leads to dissociation of GR from its chaperone proteins and translocation of the activated GR to the nucleus [15, 16, 17]. When the activated GR complex reaches

the nucleus, it can bind to DNA as a monomer or as a dimer to palindromic glucocorticoid response elements (GREs) and modulate transcription of glucocorticoid responsive genes [18, 19].

The mechanisms following the translocation of GR to nucleus are quite complex. Activated GR activates or represss transcription by interacting with different transcriptional regulators. In other words, GR directly binds the DNA and either interacts positively with transcription factors [20] leading to up-regulation of target gene expression or negatively by interfering with TFs leading to down-regulation of target gene expression. The repression system has been classified as mechanisms of anti-inflammatory actions [21]. There can be multiple signaling pathways acting on the glucocorticoid response units, including GRE and relating transcription factor binding sites, which can change the net effect of the GR target gene expression.

GR has been shown to directly interact with other proteins, including transcription factors and coactivators, for the activation of specific target genes, in different cell types. For example, GR-Stat5 protein-protein interactions have been confirmed to preferentially affect gene sets involved in postnatal growth and maturation in hepatocytes [22, 23, 24]. Another protein-protein interaction study concluded that the regulation of breast cancer growth inhibition can be monitored when GR interacts with estrogen receptor alpha (ERα), which is mediated by activator protein 1 (AP1) [25]. Other GST pull-down experiments also confirmed a formation of a multiprotein complex between activated GR, Raf-1 and 14-3-3 that leads to transcriptional regulation of cell cycle and cell differentiation [26]. In summary, GR can dynamically bind to selected proteins to affect different downstream mechanisms in a given cell types.

GR Isoforms

In addition to the actions of different GREs that get diversify GR signaling, GR has many isoforms, generated by alternative splicing and alternative translation initiation sites. Each isoform can provide different functions in cellular systems, which includes embryonic development, nervous system, muscular skeletal systems, and immune system. Post-translational modifications of GR include phosphorylation, acetylation, ubiquitnation, and SUMOylation allows for more variety of functional properties in cells [27]. For instance, GRs are known to undergo SUMOylation to regulate organization of chromatin structure and protein stability [28].

There are two main isoforms of GR (alpha and beta) in humans, generated by alternative splicing mechanics [29]. hGRα isoform binds to glucocorticoids in the cytosol and translocates to the nucleus, while recruiting coregulators to promote transcriptional events. hGRβ, on the other hand, stays in the nucleus and acts as a natural inhibitor of hGRα. hGRβ has the responsibility to regulate genes that are not regulated by the alpha isoform[29]. For this reason, hGRα is the most studied isoform due to its ability to translocate outside and within the nucleus. GRα isoforms can undergo alternative translation initiation, thereby generating eight more isoforms of GR with truncated N termini (e.g. GRα-A, GRα-B, GRα-C1, GRα-C2). Although they all have glucocorticoid-binding affinities and interactions with GREs, they can potentially bind to different coactivators that give fine-tuning of GR signaling in a given cell type under given physiological conditions [30].

One of the main objectives in this study was to confirm the existence of ASTP activity in GK. Also, we aimed to determine the mechanism behind the protein-protein

interaction of GK and GR. Furthermore, we wanted to understand the downstream factors affected as a result of the interaction. In order to meet these goals, we took an approach of using bioinformatics and biochemical strategies. By using immunoprecipitation and blotting techniques, we isolated pure GK and GR proteins using antibodies and studied the binding affinity of the proteins *in vitro*. We used multiple sequence alignment to predict possible modes of interaction between GK and GR. We verified the hypothesis by generating GK mutants and examining the interaction criteria of GK and GR using the newly developed GK knock out cell line (from Chapter 4).

Methods/Materials

Protein Lysate Preparations

H4IIE rat hepatoma cells overexpressing glycerol kinase were incubated with 100nm dexamethasone prior to harvest. Cells were then homogenized in 100ul of buffer containing 1%KCl, 1mM EDTA supplemented with 1 cOmplete protease inhibitor cocktail tablet (Roche Diagnostics, Germany) using a Sonicator. Protein lysate concentrations were measured by Bradford protein assay [31]. *In vitro* translated proteins of mutant GK were made using TNT Quick Coupled Transcription/ Translation Systems (Promega, Madison, WI) per manufacturer's instructions. Proteins were purified using immunoprecipitation procedures.

Immunoprecipitation (IP)

Prior to application of antibodies, 70ul of agarose protein A beads were washed with IP wash buffer containing 50ml PBS with 0.05% NP40 and 0.02% NaN3. Beads

were then precleared with 200ug of protein lysates for 30 min at 4 °C. Beads were then incubated with respective antibodies (GK antibody Ab70029 (Abcam, Cambridge, MA) or GR antibody sc-8992 (Santa Cruz Biotechnology, Dallas, TX) at 4 °C overnight. Precleared lysate was then incubated with antibody-coated beads at 4 °C overnight. After several stringent washes with IP wash buffer and SACI buffer containing 0.5% NP40, 10mM Tris Base pH8.0, 150mM NaCl, and 0.05% sodium azide. Protein-coated beads were then incubated with low pH 100nM glycine pH 2.5 to elute proteins. 1mM Tris-HCl pH9.0 buffer was used to neutralize the pH. Immunoprecipated proteins were used for dot blot and western blot assays.

Dot Blot Immunoassay

Dot blotting was performed using Bio-Dot microfiltration apparatus, per manufacturer's instructions (Bio-Rad, Hercules, CA). Using the microfiltration apparatus, purified GK proteins were transferred to a nitrocellulose membrane by gravity flow, followed by filtration of blocking solution containing nonfat dry milk in TBS. The nitrocellulose membrane was then retrieved from the microfiltration apparatus before it was rinsed in blocking solution containing GR proteins at 4 °C overnight. After several washes of the membrane, membrane was incubated with GR primary antibodies were incubated overnight at 4°C at the concentration of 1:1000, followed by secondary antibodies for 1 hour at room temperature. Immunoreactive bands were visualized by ECL plus kit (Amersham Biosciences, Piscataway, NJ), as per manufacturer's protocol, using ChemiDoc XRS+ Imaging system (Bio rad, Hercules, CA). Nuclear extracts (sc-2138, Santa Cruz Biotechnology, Dallas, Tx) were used on the membrane as the positive

control and *E. coli* GK proteins (Product 49955, Sigma Aldrich, St. Louis, MO) were used on the membrane as negative control.

Western Blotting

Cells were harvested using a cell scraper a confluent plate of cells in 1% KCl/EDTA buffer supplemented with protease inhibitor. Proteins were extracted from cells by sonication. And protein concentration was determined by BCA assay [31]. 100ug of protein were separated on a 4-12% Bis-Tris NuPage gel (Life Technologies, Grand Island, NY) and electroblotted onto a polyvinylidene difluoride (PVDF) membranes at 100 volts for an hour. The membranes were blocked in 0.01M PBS, 0.05% Tween 20 buffer (PBST) containing 10% blotto overnight at 4 ˚C. Primary antibodies were incubated overnight at 4˚C at a concentration of 1:1000, followed by secondary antibodies for 1 hour at room temperature. Immunoreactive bands were visualized by ECL plus kit (Amersham Biosciences, Piscataway, NJ), per manufacturer's protocol. All membranes were subjected to stripping using 1M NaOH for 10 min at room temperature, reblocked, and reprobed for B-actin (Invitrogen, Carlsbad, CA) at a concentration of 1:3000 overnight at 4˚C, and secondary antibody, goat anti-rabbit HRP, at a concentration of 1:5000 for 1 hour at room temperature and developed as previously described using Amersham ECL Plus Westeren Blotting Detection Kit (GE Healthcare Bio-Sciences, Pittsburgh, PA).

Bioinformatics Characterization of Glycerol Kinase

Full length glycerol kinase amino acid sequences (e.g. human, mouse, rat, orangutan, pig, *Drosophila melanogaster*, xenopus, *E. coli*, *E. fergusonii*, *P. syringae*) were retrieved from NCBI database. Characteristics domains or motifs were identified using the PROSITE profile database. (http://prosite.expasy.org/scanprosite/). Multiple sequence alignment were analyzed using ClustalW program (http://www.ebi.ac.uk/Tools/msa/clustalw2/).

HEK293T Cell Culture

HEK-293T were grown at 37 ˚C in a humidified atmosphere containing 5% CO2 in Dulbecco's modified Eagle's medium (DMEM), containing 10% fetal bovine serum (FBS) and 1% penicillin-streptomycin solution (PS) [32]. Prior to stable transfection on day 0, cells were seeded at one hundred thousand cells in a 12-well plate. For lentiviral transfection, cells are seeded at five million cells in a 10cm plate. Transfection can be performed above 75% confluency.

Construction of the Human GK Knockout Cell Line

The knockout cell line is generated using the type II CRISPR nuclease system developed by Cong et al. [33]. Two Cas9 target sites are located in exon 1 and exon 17 of human *GK*. A pX330-*GK* expression vector was constructed by ligating the cDNA encoding one of the target sequences between the two BbsI sites of the pX330 vector. Consequently, two expression vectors were made to allow for two Cas9 cleaving events in exon 1 and exon 17 of *GK*. The expression vectors (pX330-GKex1 and pX330GKex17)

(1ug of each vector) are co-transfected with 100ng of puromycin into the HEK-293T cells using Lipofectamine 200 transfection reagent as per the manufacturer's protocol (Life Technologies, Grand Island, NY). Screening of transfected cells were performed by dilution screening technique of single cell clone assisted by incubating cells in puromycin at working concentration of 5ug/ml [34]. PCR and Sanger sequencing were performed (Laragen Inc., Los Angeles, CA) to verify the cleaving/ repair sites for each clone.

Generation of the LXXLL Mutants

The LXXLL mutants are created using site directed mutagenesis using pRRL-GK plasmid as the backbone, where each leucine residue is replaced with alanine (*e.g.* AXXLL, LXXAL, LXXLA). Transfection procedures are identical to that of the GKD mutants, described in the previous chapter.

Lentiviral Transfection of *GK* Mutants

GK knock out cells were seeded in 6 well plates and were infected at 50% confluence using multiplicity of infection (MOI) of 10 for each well. Virus supernatants were applied to cells in Dulbecco's modified Eagle's medium DMEM containing 10% FBS and 10ug/ml polybrene in a final volume of 1ml. Cells were incubated with viral supernatant overnight and virus-containing media was replaced with DMEM containing 10% FBS on the following day. Flow cytometry was used at initial testings to access the efficiency of infection. Cells were grown to confluence before harvesting for experiments.

RNA Isolation and cDNA Synthesis

Total RNA was isolated from cell lines using the GeneJET RNA purification kit (Thermo Scientific, Pittsburgh, PA) per manufacturer's instructions. RNA was further purified using Turbo DNA-free DNase treatment (Life Technologies, Grand Island, NY). Purified RNA was visualized on agarose gel and its concentration was quantified using a NanoDrop spectrophotometer (NanoDrop Technologies, Wilmington, DE). cDNA was synthesized using Superscript III First-Strand systems (Life Technologies, Grand Island, NY) per manufacturer's instructions with random hexamers as primers. cDNA samples were diluted to an optimized concentration of 1ng/uL.

Quantitative Real Time PCR (qRT-PCR)

All assays were carried out using PerfeCTa SYBR Green FastMix (Quanta Biosciences, Gaithersburg, MD) with QuantiTect (Qiagen, Valencia, CA) primer assays. Cells were treated with 100nM dexamethasone [35] for 24 hours, after which RNA was isolated. Genes assayed included glucocorticoid receptor (*GR*) responsive genes [tyrosine aminotransferase (*TAT*), and phosphoenolpyruvate carboxykinase (*PEPCK*)], adipogenic genes [fatty acid binding protein 4 (*FABP4/aP2*) and CCAAT enhancer-binding protein (*C/EBPα*)], non-GR responsive gene cadherin-15 (*CDH15*), and lastly endogenous control beta-actin (*ACTB*). 1ng of cDNA was loaded into each reaction, which was detected using ABI prism 7500 Sequence detection system. Each sample was assayed in duplicates and each reaction was replicated as least once. Fold changes for each of the genes were determined using the $2^{(-\text{Delta Delta CT})}$ method [36].

GK Enzymatic Assay.

A radiochemical assay described previously [37] was used to determine the GK enzymatic activity. Each mutant was assayed in duplicate with 4ug of total cellular protein (for HEK-293T cells) for 20 minutes. For each assay, the scintillation count was plotted against the amount of protein, and the counts per minute (CPM) was proportional to relative GK enzymatic activity.

Results

To confirm the existence of GK-GR binding, human GK and GR proteins were made using *in vitro* translation of rabbit reticulocyte lysates. The proteins were purified by immunoprecipitation prior to blotting. The human GK proteins were absorbed onto a nitrocellulose membrane at an increasing concentration of 1ug to 10 ug. The membrane was then rinsed with a buffer solution containing GR proteins. GR antibodies were applied to the membrane to confirm binding of GR to the immobilized GK. Dot blot results confirmed that there was binding affinity between GK and GR as increased amount of signal was observed when more GK proteins were dotted onto the membrane (Fig. 5.1).

We alternatively confirmed GK and GR as binding partners using immuno-precipitation analysis. Using cell lysate harvested from H4IIE *GK*-overexpressing liver cells, the blots showed that the GK antibody (Fig. 5.2A) detected GK proteins at 49kDa and the GR antibody (Figure 5.2B) detected GR isoforms alpha and beta. Western blots analysis also detected both GK and GR eluted from the immunoprecipitation processes (Figs. 5.2 C and D). Specifically, immunoprecipitation of liver cell lysates using GK

antibody followed by anti-GR immunoblotting confirmed interacting proteins as GR at 95kDa. Conversely, when GR antibody was added in the immunoprecipitation followed by application of the latter GK antibody in western blotting, GK was detected at 49kDa. These results confirmed that the GK-GR complex exists.

To investigate the mechanisms of this protein-protein interaction, a multiple sequence alignment analysis was performed. Reference sequences of GK in multiple species, from different bacterial species to mammalian species, were gathered. In the sequence alignment(Fig.5.3), the regions where mammalian GK sequences are significantly different from the bacterial GK sequences are probable interacting domains of GK and GR due to the understanding that bacterial GK do not exhibit ASTP activity [38]. Among those results, one of the functional motifs, called the LXXLL functional motif, was the most favorable candidate. GK has one LXXLL motif (at amino acid residues 154 to 158), a motif that has been reported to preferentially bind to ligand-binding domains of the nuclear receptors like GR [39]. Based on this alignment analysis, we sought to examine whether the LXXLL motif in GK is important for the GK-GR interactions.

To determine whether the LXXLL motif in GK is critical for the GK-GR interaction, we incorporated the mutagenesis strategy, reported from previous chapter, into this study. At amino acid residues 154 to 158 of GK where LXXLL motif is located, we created site-directed mutations, in which we replaced each leucine residue of the motif to alanine. We created a total of three mutants for each of the Leucine residues. The conversion of an amino acid into alanine can theoretically preserve the overall secondary structure and the proper folding of the protein. Although these mutations are not found in

any individuals with GKD, this analysis further strengthens our hypothesis that GK interacts with GR.

In summary, we generated LXXLL mutants (e.g. AXXLL, LXXAL, LXXLA) of human GK by site-directed mutagenesis. *E. coli* , which does not have nucleus and therefore lacks ASTP activity, is used as a negative control for our experiments [38]. Alternatively, I created a synthetic *E. coli* GK control, by performing a sequential conversion of single mutations from LXXLL of hGK to create VXXIL of *E. coli*. During the mutagenesis process, we also obtained an intermediate LXXLL version of the *E. coli* GK, VXXLL. After purifying all the mutant proteins using *in vitro* translation and IP, we conducted a dot blot experiment of those mutant GK proteins (e.g. AXXLL, LXXAL, LXXLA, VXXLL, VXXIL). Our results showed that mutants had reduced amount of signal compared to normal GK proteins, indicating that mutant proteins do not bind to GR as efficiently (Fig. 5.4). Minimal signals were detected in all 5 LXXLL mutants, showing little to no binding affinity of those mutants to normal GR proteins. As expected, both VXXIL *E. coli* controls had the least amount of signal among all mutants.

In order to study the LXXLL mutations in cell culture, we generated lentiviruses with ability to infect our newly made GK KO cell lineso that they are able to express the LXXLL mutations. These LXXLL mutants were assessed based on GK phosphorylation activity and ASTP activities. GK enzymatic activity was determined using a radiolabel assay [37]. Our results from the GK enzymatic assay suggested that all mutants retained their ability to phosphorylate glycerol, despite their differences in the LXXLL motif (Table 1). Next, ASTP activity were measured by quantifying the level of mRNA in GR responsive genes, including *TAT* and *PEPCK*, in qRT-PCR analysis. Cell were either

incubated with or without dexamethasone prior to harvest, which would activate the glucocorticoid receptors. Analysis of GR responsive genes *TAT* and *PEPCK* mRNA by qRT-PCR analysis with RNA isolated from cells showed that wild type cells, with normal human GK expression, had increased expression of about 1.6 fold and 1.8 fold in *TAT* and *PEPCK*, respectively, in response to glucocorticoid receptor activation (Fig. 5.5, Fig. 5.6, and Table 5.1). AXXLL, LXXAL, and LXXLA mutants have only a 1.08-fold, 1.10-fold, and 1.08-fold increase, respectively, in *TAT* expression in response to dexamethasone treatment (Table 5.1). The results suggest that LXXLL mutant cells had significantly lower ASTP activity compared to normal cells, based on the decrease in GR responsive gene expression in response to dexamethasone treatment.

Discussion

ASTP activity was first proposed by Okamoto *et al.* [4], who demonstrated a macromolecule with the ability to enhanced the translocation of activated glucocorticoid receptor complex to nucleus in the presence of ATP. The ATP-stimulated translocation promoter was purified from cytosol of rat liver by DEAE-cellulose column chromatography and was found to have a molecular weight of about 93 kDa. They also sequenced this protein, which appeared to have an open reading frame of 524 amino acids with a molecular weight of 57kDa. The rat ASTP amino acid sequence was 99% identical with murine Gyk and 95% with human GK. Okamoto's initial findings that there is a protein-protein interaction between GK and GR. We alternatively proved that GK-GR interaction existed. Blotting experiments showed that GR proteins have binding affinity with GK proteins. First, dot blot experiments showed their binding affinity

between the two proteins. Secondly, it was shown that these two proteins are binding partners in an IP-Western experiment. Next, we investigated the binding domains in GK and GR that allowed for binding of the proteins. Although this *in vitro* experiment suggested that binding may not require the presence of ATP, we expected that ATP are required for functional activity in cells.

Two sets of IP-Western experiments were performed in this study. First, IP was carried out using GR antibody to identify potential partners of GR and GK was subsequently identified on the Western blot. We confirmed the results alternatively by initially using GK antibody in the IP to capture partners of GK and then identifying GR on the western. Our results identified interacting proteins with size slightly less than 95kDa, which could potentially be the size of an alternative splicing variant of the GR α isoforms (95kDa)) [27]. GR α isoforms are known to be the most active isoforms in binding with promoters of GR-responsive genes, compared to other isoforms [29].

The observed bands on the blot was analyzed in a mass spectrometry analysis in order to further confirm the presence of the GK-GR protein complex. Unfortunately, the mass spectrometry instrument was not able to detect the proteins. We hypothesized that lack of detection could be due to the dynamic aspects of the interaction as well as the low abundance of captured protein complexes. GR is a multi-functional protein known to be involved in many cellular functions, whether it functions in embryonic development, nervous system, muscular skeletal systems and/or immune system. The receptors must be continuously interacting with many different molecules to perform their respective functions. With that in mind, the mechanism of interactions in GR could take place in short time scales, and therefore difficult to capture the GK-GR protein complex.

In the LXXLL mutation analysis, we hypothesized that LXXLL mutants would have reduced or minimal ASTP activity. Our results indeed showed that all mutant proteins have less binding affinity for GR, suggesting that LXXLL motif is important for GK and GR binding. VXXIL synthetic control, in particular, had lowest amount of signal, which supported the hypothesis because we had previous confirmed *E. coli* do not exhibit ASTP activity [38]. These results agreed with a previous study using similar mutations of hGR (e.g. AXXLL and LXXAA) were created and showed that AXXLL mutant retained the same transactivation activity of GR while the LXXAA had complete disruption of GR transactivation activity [39].

GK enzymatic analysis on the LXXLL mutants showed that mutants retained its phosphorylation properties despite the single amino acid change in a functional motif (Table 5.1). This was not a surprise because the conversion of leucine to alanine theoretically would not affect the overall conformation of the protein. On the other hand, quantitative real time PCR analysis showed that LXXLL mutants had reduction in gene expression of GR-responsive genes (*TAT* and *PEPCK*) in response GR activation, hence less ASTP activity, compared to normal cells (Fig. 5.5, 5.6 and Table 5.1). The overall mutagenesis results showed that mutation of this motif only affect the ASTP activity of GK, but not its phosphorylation activity. The mutations of the LXXLL motif disrupted GK's binding with GR. LXXLL motif in GK is critical for the interaction with GR.

In conclusion, we captured the protein-protein interaction of GK and GR. We confirmed that changing LXXLL motif in GK has significant effect on the ASTP activity of GK, but not its enzymatic activity. Mutation of this motif, particularly the first, the fourth, and fifth position, can hinder the binding of GK and GR.

References

1. Sriram, G., Martinez, J.A., McCabe, E.R., Liao, J.C., and Dipple, K.M. (2005). Single-gene disorders: what role could moonlighting enzymes play? American journal of human genetics *76*, 911-924.

2. Jeffery, C.J. (2014). An introduction to protein moonlighting. Biochemical Society transactions *42*, 1679-1683.

3. Okamoto, K., Isohashi, F., Ueda, K., and Sakamoto, Y. (1989). Properties of an adenosine triphosphate-stimulated factor that enhances the nuclear binding of activated glucocorticoid-receptor complex: binding to histone-agarose. Endocrinology *124*, 675-680.

4. Okamoto, K., Isohashi, F., Horiuchi, M., and Sakamoto, Y. (1984). An ATP-stimulated factor that enhances the nuclear binding of "activated" receptor-glucocorticoid complex. Biochemical and biophysical research communications *121*, 940-945.

5. Ostlund, A.K., Gohring, U., Krause, J., and Brdiczka, D. (1983). The binding of glycerol kinase to the outer membrane of rat liver mitochondria: its importance in metabolic regulation. Biochemical medicine *30*, 231-245.

6. Blomquist, H.K., Dahl, N., Gustafsson, L., Hellerud, C., Holme, E., Holmgren, G., Matsson, L., and von Zweigbergk, M. (1996). Glycerol kinase deficiency in two brothers with and without clinical manifestations. Clinical genetics *50*, 375-379.

7. Dipple, K.M., Zhang, Y.H., Huang, B.L., McCabe, L.L., Dallongeville, J., Inokuchi, T., Kimura, M., Marx, H.J., Roederer, G.O., Shih, V., Yamaguchi, S., Yoshida, I., McCabe, E.R.(2001). Glycerol kinase deficiency: evidence for complexity in a single gene disorder. Human genetics *109*, 55-62.

8. Sriram, G., Parr, L.S., Rahib, L., Liao, J.C., and Dipple, K.M. (2010). Moonlighting function of glycerol kinase causes systems-level changes in rat hepatoma cells. Metabolic engineering *12*, 332-340.

9. MacLennan, N.K., Rahib, L., Shin, C., Fang, Z., Horvath, S., Dean, J., Liao, J.C., McCabe, E.R., and Dipple, K.M. (2006). Targeted disruption of glycerol kinase gene in mice: expression analysis in liver shows alterations in network partners related to glycerol kinase activity. Human molecular genetics *15*, 405-415.

10. Rahib, L., MacLennan, N.K., Horvath, S., Liao, J.C., and Dipple, K.M. (2007). Glycerol kinase deficiency alters expression of genes involved in lipid metabolism, carbohydrate metabolism, and insulin signaling. European journal of human genetics : EJHG *15*, 646-657.

11. Diehl, E.E., and Schmidt, T.J. (1993). Heat shock protein 70 is associated in substoichiometric amounts with the rat hepatic glucocorticoid receptor. Biochemistry *32*, 13510-13515.

12. Dalman, F.C., Scherrer, L.C., Taylor, L.P., Akil, H., and Pratt, W.B. (1991). Localization of the 90-kDa heat shock protein-binding site within the hormone-binding domain of the glucocorticoid receptor by peptide competition. The Journal of biological chemistry *266*, 3482-3490.

13. Sanchez, E.R., Toft, D.O., Schlesinger, M.J., and Pratt, W.B. (1985). Evidence that the 90-kDa phosphoprotein associated with the untransformed L-cell glucocorticoid receptor is a murine heat shock protein. The Journal of biological chemistry *260*, 12398-12401.

14. Okamoto, K., Isohashi, F., Horiuchi, M., and Sakamoto, Y. (1982). Three forms of macromolecular translocation inhibitor of the nuclear binding of "activated" receptor-glucocorticoid complex and their interaction with ATP. Biochemical and biophysical research communications *108*, 1655-1660.

15. Goidl, J.A., Cake, M.H., Dolan, K.P., Parchman, L.G., and Litwack, G. (1977). Activation of the rat liver glucocorticoid--receptor complex. Biochemistry *16*, 2125-2130.

16. Moudgil, V.K., and John, J.K. (1980). ATP-dependent activation of glucocorticoid receptor from rat liver cytosol. The Biochemical journal *190*, 799-808.

17. Markovic, R.D., and Litwack, G. (1980). Activation of liver and kidney glucocorticoid-receptor complexes occurs in vivo. Archives of biochemistry and biophysics *202*, 374-379.

18. Chalepakis, G., Schauer, M., Cao, X.A., and Beato, M. (1990). Efficient binding of glucocorticoid receptor to its responsive element requires a dimer and DNA flanking sequences. DNA and cell biology *9*, 355-368.

19. Nordeen, S.K., Suh, B.J., Kuhnel, B., and Hutchison, C.A., 3rd (1990). Structural determinants of a glucocorticoid receptor recognition element. Molecular endocrinology *4*, 1866-1873.

20. Drobeniuc, J., Greene-Montfort, T., Le, N.T., Mixson-Hayden, T.R., Ganova-Raeva, L., Dong, C., Novak, R.T., Sharapov, U.M., Tohme, R.A., Teshale, E.*, et al.* (2013). Laboratory-based surveillance for hepatitis E virus infection, United States, 2005-2012. Emerging infectious diseases *19*, 218-222.

21. Barnes, P.J. (1998). Anti-inflammatory actions of glucocorticoids: molecular mechanisms. Clinical science *94*, 557-572.

22. Lechner, J., Welte, T., and Doppler, W. (1997). Mechanism of interaction between the glucocorticoid receptor and Stat5: role of DNA-binding. Immunobiology *198*, 112-123.

23. Doppler, W., Windegger, M., Soratroi, C., Tomasi, J., Lechner, J., Rusconi, S., Cato, A.C., Almlof, T., Liden, J., Okret, S.*, et al.* (2001). Expression level-dependent contribution of glucocorticoid receptor domains for functional interaction with STAT5. Molecular and cellular biology *21*, 3266-3279.

24. Engblom, D., Kornfeld, J.W., Schwake, L., Tronche, F., Reimann, A., Beug, H., Hennighausen, L., Moriggl, R., and Schutz, G. (2007). Direct glucocorticoid receptor-Stat5 interaction in hepatocytes controls body size and maturation-related gene expression. Genes & development *21*, 1157-1162.

25. Karmakar, S., Jin, Y., and Nagaich, A.K. (2013). Interaction of glucocorticoid receptor (GR) with estrogen receptor (ER) alpha and activator protein 1 (AP1) in dexamethasone-mediated interference of ERalpha activity. The Journal of biological chemistry *288*, 24020-24034.

26. Widen, C., Zilliacus, J., Gustafsson, J.A., and Wikstrom, A.C. (2000). Glucocorticoid receptor interaction with 14-3-3 and Raf-1, a proposed mechanism for cross-talk of two signal transduction pathways. The Journal of biological chemistry *275*, 39296-39301.

27. Duma, D., Jewell, C.M., and Cidlowski, J.A. (2006). Multiple glucocorticoid receptor isoforms and mechanisms of post-translational modification. The Journal of steroid biochemistry and molecular biology *102*, 11-21.

28. Le Drean, Y., Mincheneau, N., Le Goff, P., and Michel, D. (2002). Potentiation of glucocorticoid receptor transcriptional activity by sumoylation. Endocrinology *143*, 3482-3489.

29. Lu, N.Z., and Cidlowski, J.A. (2004). The origin and functions of multiple human glucocorticoid receptor isoforms. Annals of the New York Academy of Sciences *1024*, 102-123.

30. Bledsoe, R.K., Montana, V.G., Stanley, T.B., Delves, C.J., Apolito, C.J., McKee, D.D., Consler, T.G., Parks, D.J., Stewart, E.L., Willson, T.M.*, et al.* (2002). Crystal structure of the glucocorticoid receptor ligand binding domain reveals a novel mode of receptor dimerization and coactivator recognition. Cell *110*, 93-105.

31. Bradford, M.M. (1976). A rapid and sensitive method for the quantitation of microgram quantities of protein utilizing the principle of protein-dye binding. Analytical biochemistry *72*, 248-254.

32. Zhu, X., Xu, Y., Yu, S., Lu, L., Ding, M., Cheng, J., Song, G., Gao, X., Yao, L., Fan, D., Meng, S., Zhang, X., Hu, S., Tian, Y. (2014). An efficient genotyping method for genome-modified animals and human cells generated with CRISPR/Cas9 system. Scientific reports *4*, 6420.

33. Cong, L., Ran, F.A., Cox, D., Lin, S., Barretto, R., Habib, N., Hsu, P.D., Wu, X., Jiang, W., Marraffini, L.A., Zhang, F. (2013). Multiplex genome engineering using CRISPR/Cas systems. Science *339*, 819-823.

34. Lacalle, R.A., Pulido, D., Vara, J., Zalacain, M., and Jimenez, A. (1989). Molecular analysis of the pac gene encoding a puromycin N-acetyl transferase from Streptomyces alboniger. Gene *79*, 375-380.

35. Rubin, C.T., Capilla, E., Luu, Y.K., Busa, B., Crawford, H., Nolan, D.J., Mittal, V., Rosen, C.J., Pessin, J.E., and Judex, S. (2007). Adipogenesis is inhibited by brief, daily exposure to high-frequency, extremely low-magnitude mechanical signals. Proceedings of the National Academy of Sciences of the United States of America *104*, 17879-17884.

36. Livak, K.J., and Schmittgen, T.D. (2001). Analysis of relative gene expression data using real-time quantitative PCR and the 2(-Delta Delta C(T)) Method. Methods *25*, 402-408.

37. McCabe, E.R., Fennessey, P.V., Guggenheim, M.A., Miles, B.S., Bullen, W.W., Sceats, D.J., and Goodman, S.I. (1977). Human glycerol kinase deficiency with hyperglycerolemia and glyceroluria. Biochemical and biophysical research communications *78*, 1327-1333.

38. Parr, L. (2010). The role of glycerol kinase in adipogenesis, in Department of Human Genetics. 2010, University of California, Los Angeles: Los Angeles

39. Dong, D.D., Jewell, C.M., Bienstock, R.J., and Cidlowski, J.A. (2006). Functional analysis of the LXXLL motifs of the human glucocorticoid receptor: association with altered ligand affinity. The Journal of steroid biochemistry and molecular biology *101*, 106-117.

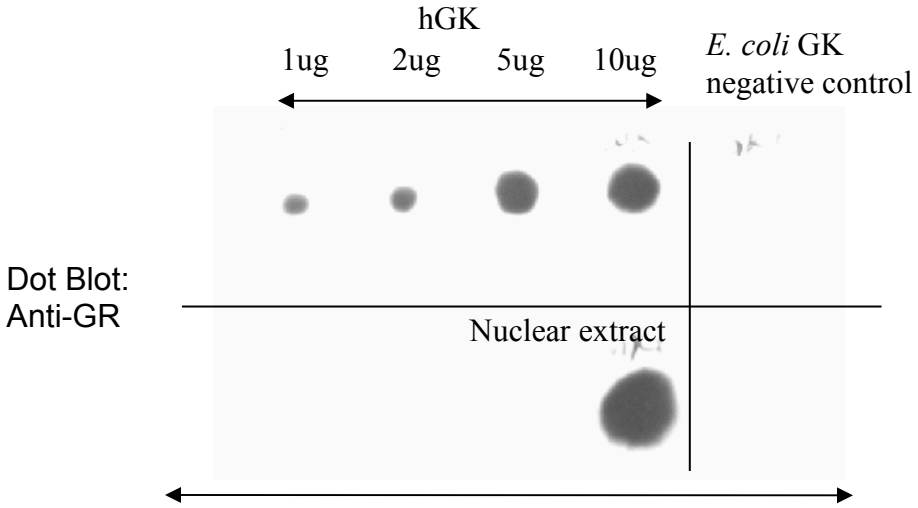

Figure 5.1 Dot blot analysis confirming the binding affinity of GK and GR

hGK was immobilized onto a nitrocellulose membrane. Prior to application of anti-GRantibodies, membrane was rinsed in buffer containing purified GR proteins.

Author Contribution: C.H. performed the dot blot experiment.

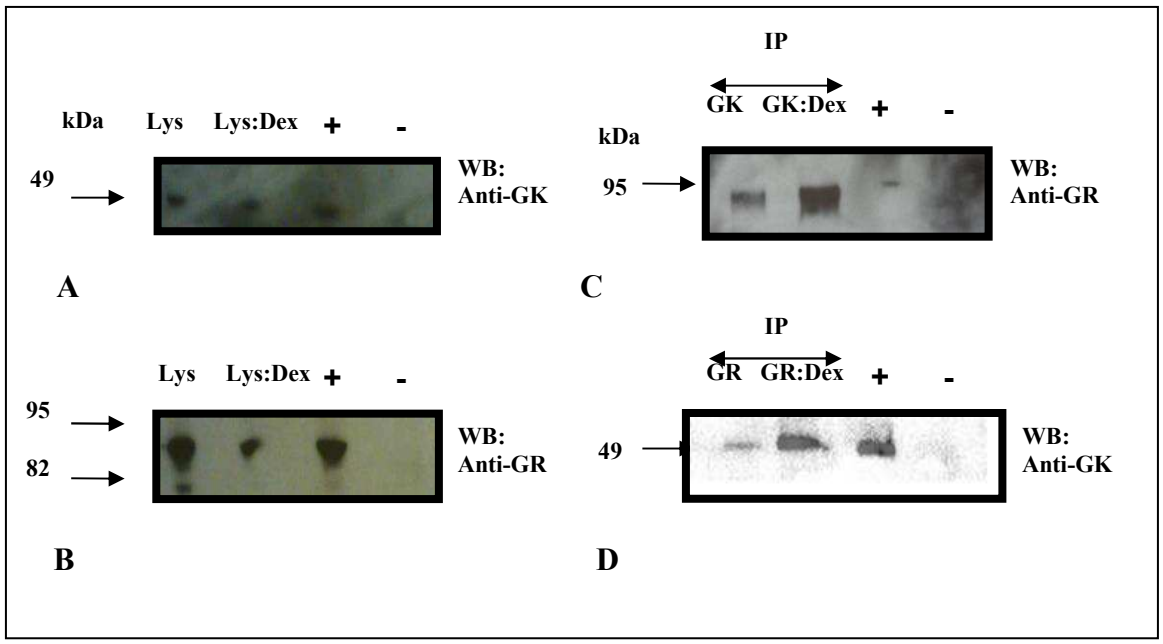

Figure 5.2 Immunoprecipitation and western blot analyses of GK/GR protein-protein interaction

A) Immunoblot of GK in H4IIE rat hepatoma cells pre-treated with synthetic glucocorticoids dexamethasone (Dex). Cell lysates (Lys) were either incubated with or without Dex prior to harvested and were loaded onto an SDS-PAGE gel. Anti-GK antibodies (dilution of 1:1000) were used to detect GK proteins in the cell lysate.

B) Immunoblot of GR in H4IIE rat hepatoma cells pre-treated with synthetic glucocorticoids dexamethasone (Dex). Cell lysates (Lys) were either incubated with or without Dex prior to harvested and were loaded onto an SDS-PAGE gel. Anti-GK antibodies (dilution of 1:1000)were used to detect GR proteins in the cell lysate.

C) Interaction of GK and GR determined by immunoprecipitation of GK in H4IIE rat hepatoma cells treated with dexamethasone. Anti-GK antibodies were added to cell lysates in the immunoprecipitation reactions to capture all binding partners of GK in cells, the product of the immunoprecipitation reaction was loaded onto an SDS-PAGE gel and probed with Anti-GR antibodies (dilution of 1:1000).

D) Interaction of GK and GR determined by immunoprecipitation of GR in H4IIE rat hepatoma cells treated with dexamethasone. Anti-GR antibodies were added to cell lysates in the immunoprecipitation reactions to capture all binding partners of GK in cells, the product of the immunoprecipitation reaction was loaded onto an SDS-PAGE gel and probed with Anti-GK antibodies (dilution of 1:1000).

Author Contribution: C.H. performed the immunoprecipitation and Western blot.

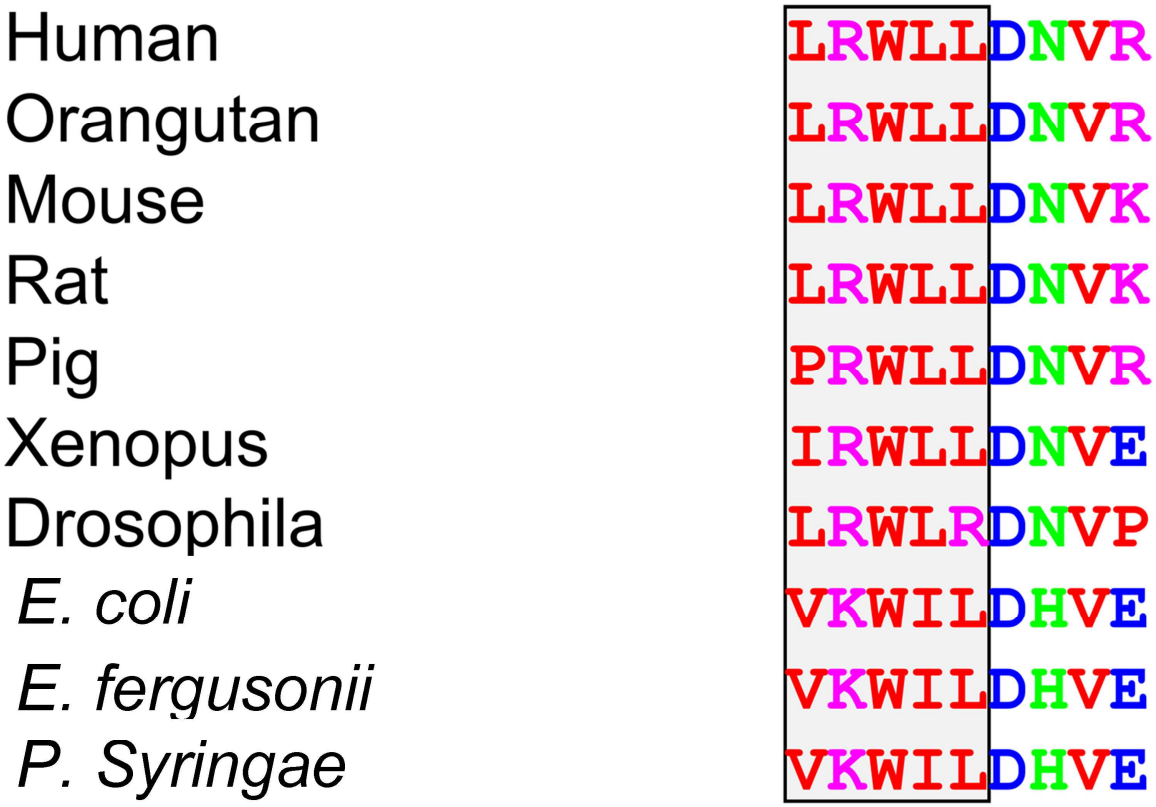

Figure 5.3 Multiple sequence alignment showing LXXLL motif of GK in various species

The full length glycerol kinase amino acid sequences (e.g. human, mouse, rat, orangutan, pig, *drosophila melanogaster*, xenopus, *E. coli*, *E. fergusonii*, *P. syringae*) were compared using multiple sequencing alignment tool ClustalW.

Author Contribution: C.H. performed the multiple sequence alignment analysis.

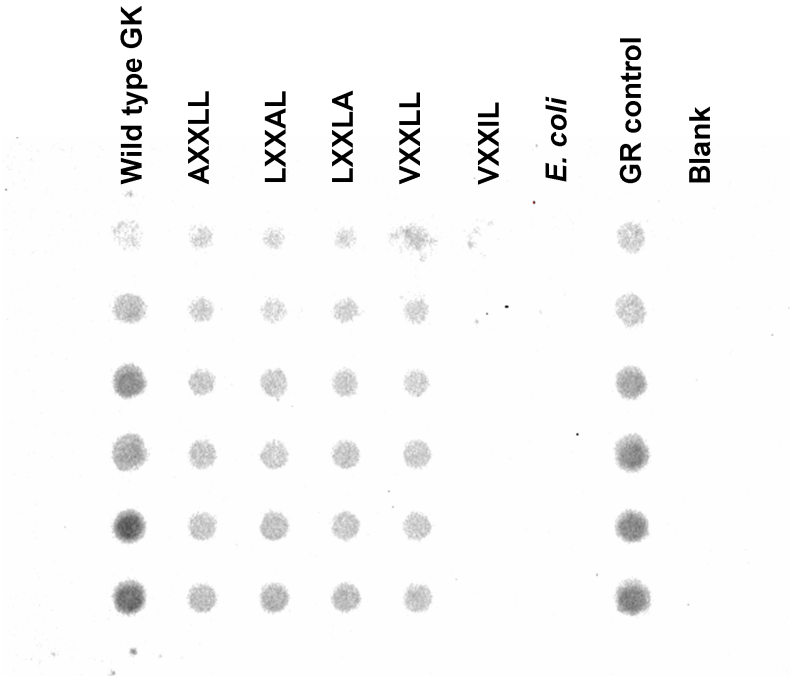

Figure 5.4 Dot blot analysis of LXXLL mutants

In vitro translated proteins (1ug, 2ug, 3ug, 4ug, 5ug, 6ug) were blotted onto the nitrocellulose membrane. LXXLL mutants (AXXLL,LXXAL, LXXLA, VXXLL, VXXIL) were compared against WT. GR control was used as positive control and *E. coli* GK and blank (PBS) were used as negative control.

Author Contribution: C.H. performed the dot blot experiment.

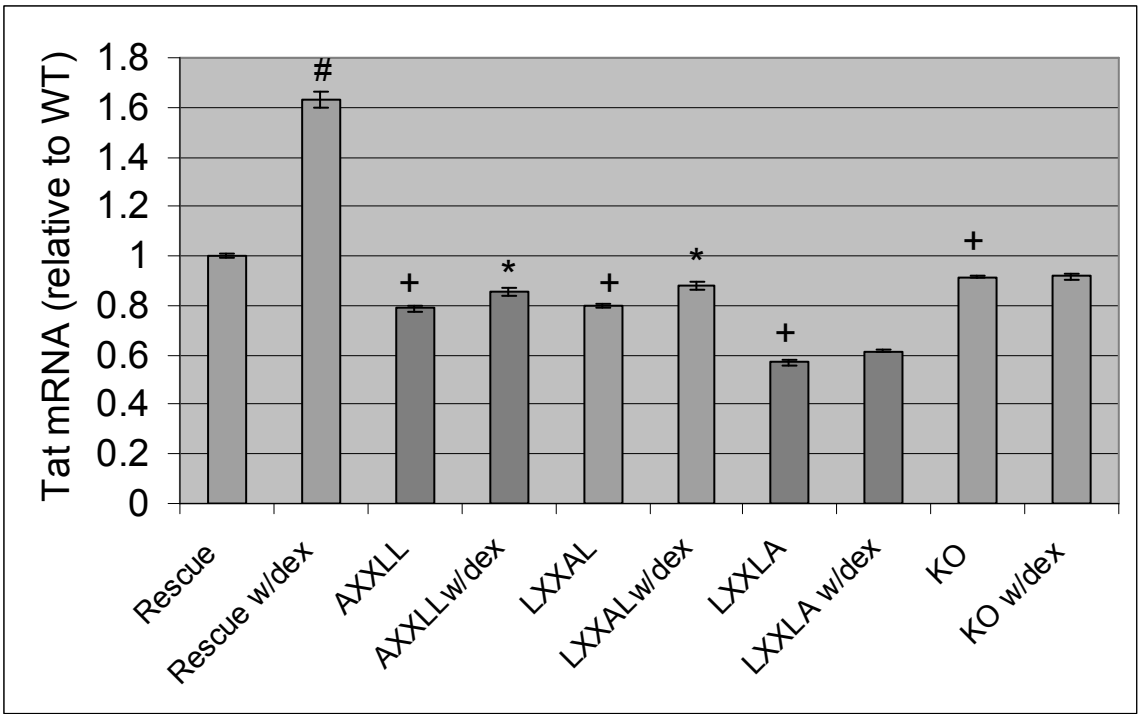

Figure 5.5 LXXAL and LXXLA mutant have reduced fold difference of *TAT* expression as a result of dexamethasone treatment, corresponding to decrease in ASTP activity. # $p<0.05$ WT vs WT w/dex

* $p<0.05$ mutant samples with dexamethasone compared to same sample without dexamethasone

+ $p<0.05$ samples w/o dexamethasone compared to WT

Author Contribution: C.H. performed the quantitative RT-PCR experiments.

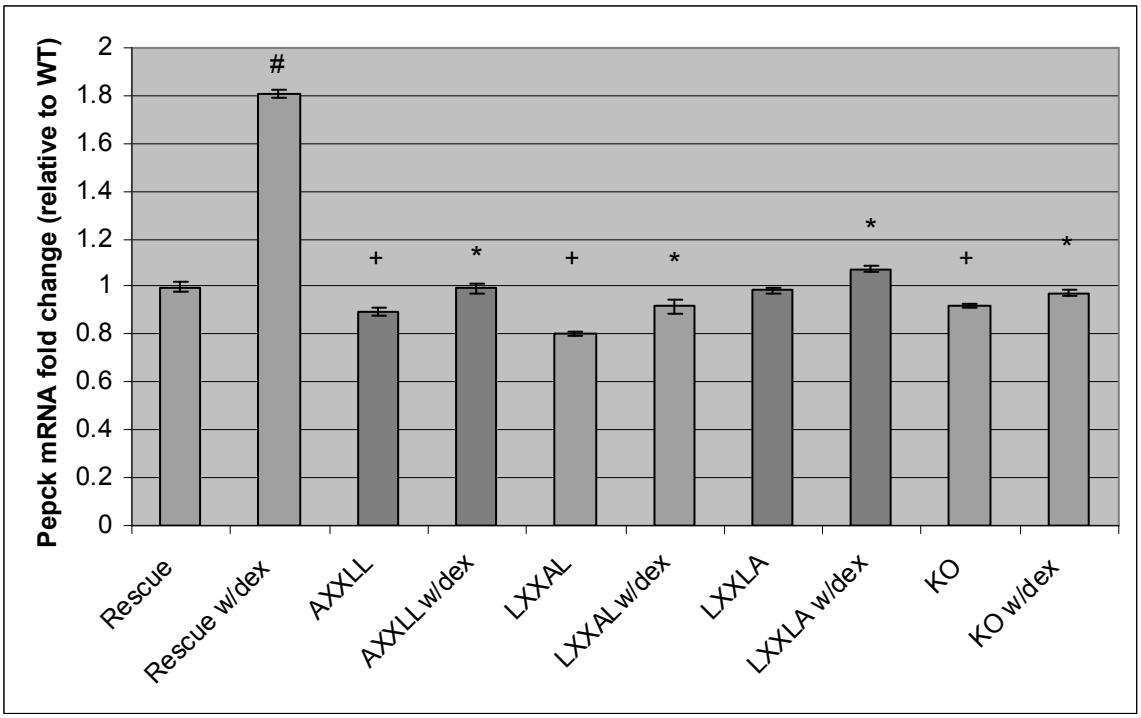

Figure 5.6 Reduced mRNA levels of *PEPCK* in LXXLL mutants as a result of dexamethasone treatment, corresponding to decrease in ASTP activity. # $p<0.05$ WT vs WT.dex

* $p<0.05$ mutant samples with dexamethasone compared to same sample without dexamethasone

+ $p<0.05$ samples w/o dexamethasone compared to WT

Author Contribution: C.H. performed the quantitative RT-PCR experiments.

Table 5.1 Glycerol kinase enzymatic activity and ASTP activity of the LXXLL mutants

Enzymatic activity levels are measured in the units of count per minute (CPM) by a scintillation counting instrument. GK activity values are expressed as percentage of GK activity in mutant cells relative to GK activity in rescue. ASTP activity is reported as the difference in the mRNA levels of a gene in response to dexamethasone treatment (e.g. a value of 1.63 means 63% increase in mRNA level in response to DEX).

	GK activity (%)	ASTP activity(*TAT*)	ASTP activity (*PEPCK*)
Rescue (human GK)	100%	1.63±0.02	1.81±0.02
HEK293T parental cells	98±0.01%	1.60±0.02	1.79±0.02
AXXLL	98.24±0.12%	1.08±0.01	1.10±0.01
LXXAL	96.42±2.01%	1.10±0.01	1.14±0.01
LXXLA	92.35±0.03%	1.08±0.03	1.09±0.03
KO	0.10±0.06%	1.02±0.02	1.13±0.01

Author Contribution: C.H. performed the GK enzymatic activity assay and the qRT-PCR for the ASTP assays.

Chapter Six

Summary and Discussion of

Understanding the Moonlighting Functions of Glycerol Kinase

General Discussion

This dissertation examines both enzymatic and moonlighting roles of glycerol kinase in relation to glycerol kinase deficiency (GKD), using newly developed study models developed in our laboratory.

Chapter two discusses the characterization of our transgenic mouse strain with overexpression of glycerol kinase in liver. Our transgenic mice had increased fat deposition in liver and adipose tissues due to the overexpression. Analysis of the metabolites in blood plasma leads to conclusion that the transgenic mice have high risk of developing obesity and type II diabetes mellitus. This chapter is a version of Ho C, Badjatiya A, Dipple K. Mice With Enhanced Glycerol Kinase Expression Have High Risk For Developing Obesity and Type II Diabetes Mellitus (Manuscript In Preparation).

Chapter three introduces a mathematical model that can predict glucose uptake rate of biological systems based on their insulin signal transduction gene expression activities. We demonstrated the ability to apply microarray gene expression data of glycerol kinase knock out mice into the mathematical model to predict their insulin sensitivity. Our simulation suggested that the knock out mice have reduced GLUT4 translocation accompanied with reduced glucose uptake rate, implying that they are susceptible to insulin resistance. This chapter is a reprint from Molecular Genetics and Metabolism, with permission from journal: Ho C, Rahib L, Liao J, Sriram G, Dipple K. Mathematical Modeling of the Insulin Signal Transduction Pathway for Prediction of Insulin Sensitivity from Expression Data, Mol Genet Metab. 114(1):66-72, 2015.

Chapter four describes the generation of a new knock out model in our laboratory. A human GK knock out kidney cell line was established using CRISPR/Cas9 technology.

Lentiviruses were used to transfer variation of GK genes into these knock out cells. As a result, many mutants carrying GKD were produced and compared against each other based on GK enzymatic and ASTP levels. The enzymatic assay results are consistent with previous tests done in human studies.

Chapter five emphasizes the protein-protein interactions of GK and glucocorticoid receptor. Using a combination of bioinformatics and biochemical techniques, we confirmed that the LXXLL motif in GK is responsible for GK-GR binding. We applied the lentivirus mutagenesis approach to create LXXLL mutants and showed that LXXLL motif in GK is critical for the binding to GR and activation of GR responsive genes, but it does not affect GK phosphorylative properties. Differential gene expressions of adipogenic and insulin signaling genes were among the GR direct targets downstream affected by the GK-GR interaction.

To summarize the key findings of the thesis dissertation, many study models (e.g. mathematical model, mouse model, and cell culture model) were developed to examine the moonlighting functions of GK. We showed in the diet study that GK is involved in fat deposition and adipogenesis, and its overexpression increases risk of obesity and T2DM in mice. Our mathematical model predicted that GK knock out mice have reduced glucose uptake and reduced insulin sensitivity, based on differential gene expression of key genes in the insulin signal transduction pathway. Lastly, cell culture studies showed that protein-protein interaction of GK and GR is critical for regulation of GR responsive genes. Overall these studies confirmed that GK is involved in increased risk of obesity, and T2DM. This appears to occur through increased adipogenesis andrequires both GK enzymatic and ASTP activity.